AN ELECTRON DIFFRACTION STUDY OF THE DEVELOPMENT OF PREFERRED ORIENTATIONS IN VACUUM-CONDENSED DEPOSITS.

By

KANDARPA KUMAR KAKATI

THESIS SUBMITTED FOR THE DEGREE OF DOCTOR OF PHILOSOPHY OF THE UNIVERSITY OF LONDON.

APPLIED PHYSICS AND CHEMISTRY OF SURFACES LABORATORY,
DEPARTMENT OF CHEMICAL ENGINEERING AND CHEMICAL TECHNOLOGY,
IMPERIAL COLLEGE OF SCIENCE AND TECHNOLOGY,
LONDON, S.W.7.

FEBRUARY, 1969.

ACKNOWLEDGEMENTS.

I am extremely grateful to Dr. H. Wilman, D.Sc., F.Inst.P, Reader in Applied Chemical Physics, Imperial College, London, for kindly giving me the opportunity to carry out this work and for his constant and abiding interest in it, his most valuable suggestions and guidance throughout the course of this research investigation.

I am also grateful to the Ministry of Education, State Government of Assam, India, for providing me with a maintenance allowance which enabled me to devote my full time to carry out this investigation.

I also thank my friends and well-wishers for their inspirations in the completion of this work.

Thanks are also due to Dr.A.E.B.Presland and Mr.P.Marlow for kindly supplying the electron-micrographs.

ABSTRACT.

The surface orientations of the deposits of spec-pure gold, silver, copper, zinc and cadmium condensed in vacuum on stainless-steel and glass substrates at room temperatures were investigated by the grazing incidence electron-diffraction technique.

Au, Ag and Cu were deposited (at ~30A/sec. for Au and Ag and ~20A/sec. for Cu) within the range of 10^{-3} to 10^{-8} torr of residual air. Zn and Cd were deposited at pressures down to 10^{-5} torr and 10^{-3} respectively at rates up to ~1000 A/sec.

In all the metals, the surface orientations showed systematic variation in relation to thickness and pressure of the residual air.

For Au, Ag and Cu, at all pressures, thin deposits showed random orientation but with increasing film thickness, this was followed by (111) orientation due to the strong development of octahedral faces, further followed by (110) in Ag or (211) in Au and Cu due to the twinning of the crystals on the {111} planes.

The film thickness at which a change to a different orientation occurred, was maximum at a certain pressure, which was related to the chemical reactivity of the metal with the residual gases (especially oxygen and water vapour)

present in the system.

Thin deposits of Zn and Cd showed (001) orientation at high rates of deposition, which was mostly followed by (100), (101) and (112). In some rare cases of Zn deposits, (135), (114) and orientation intermediate between (101) and (112) were observed. These orientations were again caused by development of faces and more rapid growth of crystals oriented with such a face most nearly normal to the vapour stream.

When the vapour was incident obliquely, the tilt of the orientation axis in the case of Au and Cu showed systematic variation with the film thickness at pressures higher than 10^{-5} torr for gold and 10^{-6} for copper. At lower pressures no appreciable tilt was observed.

Thin deposits of Zn and Cd (a few hundred A) did not show any tilt of the orientation axis, although thicker ones showed such tilt accompanied by asymmetrical distribution of arc positions and/or intensity, and strong development of faces.

CONTENTS.

Page

SECTION 1.

INTRODUCTION

1.1. General Introduction:

In the present work, the crystal growth and structure of one-degree oriented thin metal films, prepared by the condensation of the metal vapour on glass and polished stainless-steel substrates have been investigated. In the last few years interest in the study of the thin metal films formed by different processes has increased considerably. The usefulness of thin metal films in industry and research has also much increased. In the fields of semiconductors, superconductors, magnetics and in space-research applications, thin metal films are significantly important today. In a thin film, since one dimension is greatly reduced, the surface effects should be significant in causing slip on a larger fraction of the slip planes, and the study of the mechanical properties of some films has reached a stage where it may throw light on the theory of work hardening of crystals and mechanism of fatigue.

In the growth phenomena of a thin film the deposition parameters such as rate of deposition, thickness, nature of substrates, residual air pressure, etc. have significant roles. It is extremely difficult to control

all these parameters closely during the growth of the film. However, attempts have been made to establish the relationship between the structure of a film and the deposition parameters under which it was prepared. The progress has been made possible due to the improved experimental set up for preparing the specimen and then its subsequent examination by electron diffraction. Thomson's (1927) photographic technique has led to the extensive use of high energy electrons as a means of investigating the atomic structure of matter in thin films. Owing to the scattering and absorption of electrons by matter being very much greater than that of X-rays, even films only a few atoms thick can give clear diffraction patterns, and the immediate surface regions of massive materials can be studied without the diffraction pattern being confused by features contributed by the underlying material. The method of electron diffraction is thus an ideal one for the study of some of the fundamental problems of crystal growth in surface layers. Various workers have applied the technique of electron diffraction to the study of the structure of films deposited on solid or liquid substrates, molecular structure, catalysis, friction, wear and lubrication, anodic process, photo-electric processes, chemical reaction, etc.

Neutron diffraction and electron microscopy have also reached a very high standard of precision in studying growth and structure of thin films. The ion-field emission microscope, in some cases allows us to observe directly the surface arrangement and movement of individual atoms during the crystal growth.

In the present work, however, reflection electron diffraction technique has been adopted to study the surface structure of the metal films of spectroscopically pure gold, silver, copper, zinc, and cadmium. This was . . because electron diffraction gives much the most definite and detailed information as to the chemical nature of the materials present and their crystalline form, orientation, crystal habit and twinning, while also providing general information as to the degree of surface roughness on the atomic scale.

The penetration of the 50-60 KV. electron beam in the primary beam direction is only a few thousand angstroms even when the atomic weight of the material is low (C, Si, O, Al, etc.). For such electron beams at grazing incidence the penetration along the normal to the surface under consideration is thus only 50 to 100 A, even in materials of low atomic weight. The penetration is further reduced to a few angstroms only in a denser material, especially if

the surface is atomically smooth, e.g. a highly polished surface.

The principal methods of preparation of thin solid films on metallic and non-metallic substrates are: (1) condensation from the vapour in vacuum; (2) electro-deposition; (3) chemical precipitation; (4) explosion of metal wires in an inert gas; (5) cathodic sputtering and (6) thermal decomposition. In the present work, the vapour-condensation technique has been adopted throughout. Vapour condensation is normally carried out at reduced pressures and it is possible to evaporate a wide range of metals and compounds in vacuum.

Most of the works so far carried out on the structure of thin films have been the investigation of the growth phenomena or the initial nucleation, without much relation to the deposition parameters. In spite of much progress in the experimental techniques and numbers of papers being published every day, there is not yet any unifying quantitative theory of film growth and the relationship between deposition parameters, film structure and physical properties. In the present work, attempts have been made to throw more light on the relation between the film structure and the various deposition parameters.

1.2. Condensation, Nucleation and Growth of Thin Films:

1.2(a). Theory of Nucleation and Condensation:

Most of the studies on the nucleation and growth of thin metal films have been made by examining the deposits prepared by condensation from vapour in vacuum. Such a deposit is built up essentially atom by atom. The crystals grow from initially small nuclei formed by atoms meeting at isolated nucleation sites on the substrate. A sheet of atoms is first built up which expands sideways till another sheet begins to grow on its surface.

Wood (1916) showed that the initiation of nucleation and growth of a metal film in vacuum depends upon a critical density of the vapour beam, below which, at any particular substrate temperature, no condensed film could be formed. Conversely, there is a critical substrate temperature for a given vapour stream density, above which no deposits can be obtained. In other words, the critical density of the vapour stream is a function of the substrate temperature. Many early workers like Knudsen (1909), Langmuir (1917), Semenoff and Chariton (1924), Estermann (1925) and Cockcroft (1928) have supported the above theory from their experimental findings. They all observed that the critical density of the vapour stream is different from metal

to metal and has widely varied values for different substrate temperatures.

The observations are best explained by the more recent idea of condensation and re-evaporation of metal atoms, where the vapour atoms are supposed to have an average lifetime on the surface of the substrate. This idea replaces the classical theory of reflection of the atoms from the substrate surface.

Volmer (1921) observed that the growth rate of a film cannot exceed a certain maximum value - which is reached when every atom incident on a substrate is condensed. From his experiments with mercury condensed on a cooled surface he was able to show that the velocity of growth of a crystal in a certain direction is much greater than in other directions. He postulated that when an atom or molecule strikes a face of a crystal, it is bound with an energy which is less than the equivalent energy of the molecular or atomic heat of evaporation. He further concluded that such an atom is only adsorbed on the surface of the substrate and can migrate towards the edges thus leading to the growth of extended facets. Such an atom cannot re-evaporate again because it is bound by the energy given off in the heat of adsorption.

Estermann (1923) provided support for this theory

by condensing silver onto polished quartz at room temperature and observing that when the average thickness of the deposit was less than that of the corresponding monolayer, the film consisted of scattered crystallites instead of being homogeneous. This phenomenon can only be interpreted as due to migration of the silver atoms (incident uniformly on the quartz surface) until they meet and adhere to another silver atom to form a less mobile aggregate.

A very successful theory of nucleation was put forward by Frenkel (1924). According to this theory, vapour atoms after arriving at the surface move over it during their lifetime on the substrate, at the end of which they re-evaporate. The activation energy of an atom for its surface migration is much less than its evaporation energy. However, if the average lifetime of such an atom incident on the substrate surface is sufficiently long for another atom to collide with it, then an atom-pair can be formed and the average lifetime of the 'doublet' is increased. Consequently, the energy required to re-evaporate the pair is also considerably increased. Such an atom-pair may become a stable nucleus of condensation. The probability of the average lifetime of the atoms on a substrate will be more and hence condensation more likely, the more intense the force binding the atoms to the substrate and the lower the substrate temperature. Further, the greater is the number of atoms

reaching the substrate/unit area in a given interval of time, the greater will be the probability of nuclei of condensation being formed.

The above phenomenon can be observed with some hexagonal metals like Zn, Cd, etc. with the substrates at room temperature. The forces between the condensed atoms and those of the substrate are very weak in these cases. The same thing may be expected with other metals of higher melting point also when the substrate is at a raised temperature.

Semenov (1930) proposed another condensation mechanism, according to which atoms of the condensing metal, migrating on the substrate, can be regarded as a two-dimensional vapour passing at the 'saturation point' into a two-dimensional liquid (vapour → liquid), which constitutes the basis for further condensation.

Picard and Duffendack (1943) and Levinstein (1949) observed isolated crystals of cadmium and zinc which later acted as nuclei for other atoms. Levinstein (1949) concluded that the kinetic energy of the vapour particles has no influence upon the condensation process. This he attributed to the random nature of collisions and the inelastic collisions of the vapour atoms with the substrate.

From his velocity spectrum experiments with Sb, Au and Bi, it was found that for low velocity regions the aggregates were larger in size due to larger nuclei of condensation, while the phenomenon for the high velocity region was the reverse.

Sennett and Scott (1950) concluded from their experiments on silver deposited on formvar at different rates (from 0.15 A/sec to 90 A/sec) that deposition rates influence the initial stages of condensation.

Sennett, McLauchlan and Scott (1952) evaporated zinc and cadmium within an electron microscope and observed that particles often as large as 200 A appeared on the substrate instantaneously. This was in contrast to what gold and silver exhibited.

The analysis of numerous experimental results (Rozenberg, 1952; Konozenka, 1954) on Zn, Cd, Sn and other condensates suggests that according to the nature of the metal and the conditions of condensation, the condensation of metals may proceed by either 'vapour→crystal' or 'vapour liquid' mechanism.

Pashley (1956) has remarked about two possibilities of nucleation, viz., 'gradual nucleation' and 'spontaneous nucleation'. In the 'gradual nucleation' mechanism the deposit atoms are mobile over the substrate until they lose

sufficient thermal energy and become trapped on the surface either at a random lattice site or at some preferred place such as a hole, edge or step. The trapped atom acts as a preferential point for the trapping of other incoming atoms, so that a nucleus which may be very often oriented, is built up. In the case of 'spontaneous nucleation', crystallisation occurs via an intermediate stage, which could be one of an amorphous or liquid state. When the amount of the deposit material is increased to a certain value, a crystallisation process occurs and nuclei are spontaneously formed.

Palatnik and Komnik (1959) suggested that the mechanism of condensation of metals in vacuum is determined by the existence of two critical temperatures, T_1 and T_2. The temperature of the substrate T_1 corresponds to the passage of the condensation mechanism from vapour→ crystal to vapour→ liquid type. In terms of the kinetics of formation of the condensate one can assume that the condensation of the metal occurs by the creation and growth of liquid on crystalline two-dimensional nuclei. The decisive factor is the process of formation of nuclei which takes place at the initial stage, when the atoms of the condensing metal adsorbed on the substrate represent a two-dimensional vapour. Further rapid growth of the nuclei

is ensured by a considerable overcooling and supersaturation of the vapour. The temperature T_2 is the critical condensation temperature above which the condensation of the metal can occur only as a result of the effect of impurities present on the surface of the neutral substrate. They made these observations from experiments with Bi.

Hirth and Pound (1963, 1964) reviewed the treatment of Frenkel as follows. The atoms or molecules incident from the vapour stream are adsorbed on the substrate and rapidly reach thermal equilibrium. These 'adatoms' diffuse on the substrate and interact to form polyatomic clusters or embryos through thermal fluctuations in local concentration. In a supersaturated system some clusters will grow and form embryos of a critical size which condense out as stable nuclei. There is a critical supersaturation above which the nucleation rate is very large and below which it is very small.

Melmed (1965) has reported about nucleation and growth of copper on tungsten from the vapour phase, in the temperature range from -195°C to 750°C for a limited range of rates of deposition. Nucleation occurs in patches, rather than homogeneously, the sites of nucleation varying with substrate temperature. He concludes that the impinging copper atoms have sufficient energy to diffuse a short

distance (about 50 A) on the substrate and thus agglomerate to form small nucleii.

In addition to the above, very many workers [Ptushinskii (1958), Moazed and Pound (1960), Chirigos et al (1957), Mayer and Gohre (1963), Gunther (1957), Fray and Nielsen (1961), Matthews (1961), Bryant et al (1959), etc.] have published quite a number of papers on the nucleation and condensation theories. Only a short and brief account has, however, been presented here on this topic.

1.2(b). Atomic Mobility, Island Structure and the Initial Growth Process:

Evidence of the atomic mobility of condensed atoms:

As already described above, Volmer's (1921) work first made it clear that atoms or molecules can often migrate considerable distances after their condensation on a substrate. The migrated atoms prolong the faces of a growing crystal as the deposition process proceeds.

The evidence of atomic mobility of very thin films at temperatures far below the melting point of the metal were also noticed by early workers such as Estermann (1925), Cockcroft (1928), Andrade and Martindale (1936), Ditchburn (1933), etc.

Andrade and Martindale (1936) found that when

sputtered silver and gold deposits were heated, aggregation took place at about 280°C and at below 400°C respectively. According to them, this shows that the atoms of the film must be freely mobile at temperatures very far removed from the melting point. The fact that during the earlier stages there was little sign of any decrease of intensity of colour in the film, as seen by transmitted light, indicated that only the surface layers were concerned and that atoms moved in from distances which were many times the linear dimensions of the aggregates. Eventually small octahedra were visible in the optical microscope.

The mobility is dependent on the melting point of the metal. The lowest temperatures for which it was observed with mercury (-50°C) and cadmium (-120°C) (Volmer, 1921; Estermann, 1925), were much lower than that found by Andrade and Martindale for silver and gold.

Mayer (1955) stated that although the surface mobility of the atoms depends on the one hand upon the energy of condensation and the thermal energy corresponding to the substrate temperature, it also depends on the forces between the deposited atom and the substrate.

Campbell (1962) observed that the mobility of the gold atoms varied considerably when condensed on to different substrates. He deposited gold in vacuo on single crystal

LiF, freshly cleaved mica, carbon film, glass and single crystal silicon and found that mobility was least on carbon film and greatest on LiF.

Observations of "island" structure of thin deposits:

Picard and Duffendack (1943) from their electron microscope investigations of the nature of metallic films (Al, Au, Zn, Cd, Cu, Mg) prepared by vacuum ($\backsim 10^{-6}$ torr) condensation on collodion substrates observed that these deposits at the initial stage showed surfaces made up of agglomerates ("islands") with channels between them. The films of aluminium condensed on a liquid-air cooled surface exhibited no new characteristics.

Similarly they found that gold and copper films initially consisted of isolated patches, which on thickening showed disappearance of the interstices.

Zinc condensed at room temperature showed large blank spaces with occasional crystals of the metal, clusters of crystals and irregular particles resembling droplets. They observed splotchy surface of the Zn deposits even on the surface of the glass of the apparatus. Zinc condensed on collodion cooled with liquid air in the vacuum of the electron microscope, still showed isolated crystals, and so did cadmium and magnesium.

Levinstein (1949) observed that the rate of deposition affects the grain size of the deposit. When antimony was evaporated rapidly, small isolated patches or islands were formed which at first exhibited amorphous structure. With slower rate of evaporation, larger islands with more stability were obtained, and they were crystalline in nature.

He explained the dependence of the antimony particle size on the rate of evaporation by introducing two basic assumptions to Frenkel's concept of surface mobility, viz., that (1) the number of atoms in motion on the surface is proportional to the number of atoms arriving at the surface per unit time, and (2) atoms or molecules will move over the surface until they suffer a collision with other atoms or molecules and thereby lose their mobility.

He stated that after the start of condensation there will be a few atomic groups on the substrate. Further newly arrived atoms will either collide with these aggregates, thereby increasing their size, or collide with each other forming new nuclei and increasing the number of such patches. If the rate of arrival of the atoms on the substrate is high, the latter possibility is higher, since the probability of collisions between the migrating atoms is greater than that between atoms and already existing

aggregates. Thus, many small nuclei are formed. On the other hand, if the rate of arrival of the atoms is low, they will more frequently collide with the already existing aggregates, thereby extending the size of these.

As mentioned earlier, Sennett and Scott (1950) observed on thin silver films (50 to 175 A thick) condensed on formvar at room temperature, well separated aggregates which increase in size with increasing thickness and finally join and merge together leaving only a few cracks which in turn are finally obliterated.

Saikia (1961) while depositing tin on glass substrates in vacuum at room temperature, observed the appearance of such isolated patches at the initial stage.

Matthews and Wronski (1962) deposited tin in vacuo on SiO films at 150°C, and the electron micrographs showed discrete crystallites of mean radius from 25 to 200 A. These particles were spherical or oblate spheroids in shape as indicated by the circular images in the micrographs.

Campbell (1962) showed from his investigations of lithium fluoride deposited upon carbon films that for a constant rate of deposition, the size of the islands in the initial stages of growth increases with thickness up to a certain point above which the size decreases. Although the effect was very much pronounced with lower rates of

deposition, the phenomenon could not be observed when he tried to repeat the experiment for gold films deposited on carbon substrates. He further observed that fast deposition rates gave rise to smaller island formation.

Preece, Stoddart and Wilman (1967) and Preece and Wilman (1966, 1968), investigating the structure of tin films condensed on glass at room temperature at 10^{-8} torr of air and in oxygen at 10^{-5} torr, observed that at 10^{-8} torr the deposits were electrically discontinuous until the thickness exceeded about 2000 A, whereas deposits prepared at 10^{-5} torr of oxygen were electrically continuous even at 200 A. The electron micrographs of these deposits condensed at 10^{-8} torr of air revealed discontinuous surface structures with discrete island formation.

The first appearance of the initial nuclei:

Was (1939) while condensing gold on glass at liquid air temperature at less than 10^{-6} torr of air found that the deposits were amorphous but crystallised on warming to room temp., if the thicknesses did not exceed 50 A.

Schultz (1952) found that deposits of alkali halides gave observable electron diffraction patterns for average thicknesses as low as 2 A. The linear size of the nuclei at this stage was at least 100 A.

The sudden appearance of nuclei of finite size

were observed by Newman and Pashley(1955) for copper films condensed on smooth (111) faces of silver single-crystals substrates at room temperature and also by Newman(1957) for the growth of tin on a (111) face of a silver single crystal at room temperature. Newman observed nucleation to occur at an average thickness of about 10A.

Bassett, Menter and Pashley(1959) observed gold films condensed on cleavage surfaces of rocksalt at ~300°C that the initial stages of film growth often involved the formation of three-dimensional nuclei, even when the thickness of the deposit was less than one atomic diameter.

Bassett, Newman and Pashley(1959) concluded that the earliest observable stage of growth of a metallic film condensed from the vapour is in general the formation of discrete nuclei. These can occur when the total amount of deposit is insufficient to form a continuous monatomic layer. They supplemented Frenkel's theory by adding that once a sufficiently stable and high density of initial nuclei is formed on the substrate, further deposition gives rise to growth in three ways: (1) by direct deposition on to the nuclei; (2) by interchange of atoms between neighbouring nuclei causing large nuclei to grow at the expense of smaller nuclei; and (3) by physical growing together of the neighbouring nuclei.

As mentioned earlier, Campbell(1962) observed from the fractional areas covered by the gold films deposited on carbon substrates that nuclei of finite size (50-100A) suddenly appear.

Pashley, Stowell, Jacobs and Law (1964) supported

qualitatively the above views. They observed that in the condensation of gold on MoS_2 (001) cleavage faces at 400°C, a sudden burst of nuclei of fairly uniform size was seen and no further nucleation occurred until a much later stage of growth. The smallest nuclei detected had diameters of 20-30 A and at the least deposition rates (rates not mentioned), sufficient material was deposited within a fraction of a second in order to allow nuclei of this size to be formed at this observed average separation of about 500 A. They held that the growth of the nuclei was three-dimensional and that their growth parallel to the substrate was greater than that normal to it.

Ogawa, Ino, Kato and Ota (1966) observed diffraction patterns from gold films of mean thickness 1 A, prepared on potassium chloride (001) cleavage faces at about 300°C.

Ino and Ogawa (1966) obtained diffraction patterns from Pd 10 A thick condensed on KCl at 300°C, and of Ni 10 A thick condensed on NaCl cleavage face at 200°C.

Ino (1966) observed multiple-twinned particles in the earliest stage of gold films (5 A) condensed on a (001) face of NaCl at 300°C at 10-50 A/min. He also pointed out that the multiple-twinned particles are already formed before the beginning of appreciable coalescence of

nuclei. This, he suggested, indicated that the multiple-twinned particles do not result from the coalescence but are formed by the twinning in themselves.

The location where the nuclei are formed:

Bassett (1958) observed that when gold was deposited in vacuum on the cleavage surface of rocksalt at about 400°C, nucleation started at the step edges even when the average thickness of the deposit was only monatomic. Gold atoms had a certain mobility on the surface after arrival. Nucleation apparently occurred more readily along the edges of steps and gave rise to a smaller spacing between nuclei than on other parts of the substrate. The sizes of these nuclei were less than those formed on the flat parts of the crystal substrate. He determined the size of the nuclei along the step edges to be from 25 A to 10 A for a film thickness of 3 A. For the same film on the flat areas the crystal nuclei ranged down in size from about 60 A. It was also observed that the nuclei formed along the terminal step of a cleavage "staircase" (i.e. the step adjoining a flat region of a crystal) were intermediate in size between nuclei formed on the flat crystal and in the centre of the cleavage step. Bassett explained it as due to the fact that the mobility of the gold atoms on the crystal surface permits this terminal step to draw upon mobile material on the flat

surface on one side of the step.

From the consideration of the wandering steps on the crystal surface Bassett could measure the distance that the gold atoms could migrate on the crystal surface. When two such steps were separated by a distance greater than some critical distance, gold nuclei were formed having density and size corresponding to the flat regions of the crystal. As the steps got closer together than about 150-200 A all the arriving gold atoms were able to migrate towards the sites of nucleation along the step edges.

Independently, Sella, Conjeaud and Trillat (1958, 1959) found that gold condensed on cleavage faces of KCl, NaCl and KBr, (at about 400°C), formed crystal nuclei on the cleavage edges, slip lines, dislocations and the other faults on the surfaces of these crystals. They did not observe such "decorations" while depositing at room temperature, which was due to the relatively lower mobility of the crystal nuclei at room temperature.

The size and form of the crystal nuclei:

As mentioned earlier, Schultz (1952), found that on a 2 A thick deposit of alkali halides on alkali halides the linear size of the nuclei was at least 100 A.

Newman and Pashley (1955) condensed silver bromide and copper in vacuum ($\sim 10^{-4}$ torr) on to (111) surfaces of

silver single crystals at room temperature. They observed that the copper nuclei were plate-like and were formed on the surface of the silver. The measurement of the nuclear size was uncertain because of refraction effects. They also observed that the silver bromide nuclei have no well-defined shape and were partially embedded in the metallic silver. They stated that the deposits grew as oriented three-dimensional nuclei. As the deposit thickness was increased (thickness not stated) the size of the nuclei remained almost unchanged and the number of the nuclei increased.

Bassett, Menter and Pashley (1959); like previous workers, found in their investigations of growth phenomena on crystalline substrates that the initial stages of growth very often involve the formation of three-dimensional nuclei even when the average thickness of the deposit is less than one atomic diameter. The deposit of rhodium formed on a {111} silver crystal surface had well oriented nuclei with a triangular outline which was probably pyramidal.

Bassett (1960), examining the growth of silver deposits on to MoS_2 cleavage faces at raised temperature found that nuclei approximately 100 A in diameter were initially observed and growth then occurred laterally.

Pashley and Stowell (1966) recently made some interesting studies on the nucleation and growth of gold

and silver films deposited in vacuo on MoS_2 cleavage surface at about 400°C. They observed that these metal deposits are initially in the form of separate crystalline nuclei distributed over the substrate surface. These nuclei can be 10 A in diameter or even less when first observed and their density is commonly in the range 10^{10}-$10^{12}/cm^2$. Further deposition leads to an increase in size of the nuclei or islands and then further increase in size is accompanied by a decrease in numbers.

Matthews (1967) observed that information about the shape of nuclei can be obtained from the images of stacking faults on their twins that extend through some of the larger nuclei. According to him nuclei greater than 100 A or so in diameter usually have facets parallel to low-energy surfaces.

Coalescence of islands during deposition:

As mentioned already, the initial three-dimensional islands or nuclei grow in size with the addition of more material and gradually they coalesce, thus making a continuous film.

Mention has already been made to Scott and Sennett (1950) who observed the coalescence phenomenon of island structures of silver deposits on formvar.

Sella, Conjeaud and Trillat (1958, 1959) also

noticed such growth process in gold nuclei condensed on KCl, NaCl and KBr at 400°C.

Bassett (1961) made direct observation of such a growth process in silver deposits condensed in vacuo on MoS_2 cleavage faces at raised temperatures. Nuclei about 100 A in diameter were initially observed which then grew laterally. As the islands grew the nuclei joined together with sufficient relative rotation not to introduce detectable imperfections at the joining interfaces.

The coalescence of the nuclei were also studied in detail by Pashley and Stowell (1962), Pashley, Stowell, Jacobs and Law (1964), Poppa (1964), Jacobs, Pashley and Stowell (1966), etc. in recent years.

Pashley, Stowell, Jacobs and Law (1964) investigated the behaviour of gold films during deposition onto MoS_2 at 400°C inside an electron microscope. The adjacent nuclei grow until they appear to touch and then coalesce very rapidly in a liquid-like manner, i.e. as if there were a surface tension and high mobility of atoms. The event takes place in less than 0.1 sec. for small nuclei. They also noticed that nuclei having well-defined crystallographic shapes before coalescence became rounded during the event.

They observed that the liquid-like character of

the coalescence leads to enlargements of the uncovered areas of the substrate, with the result that the secondary nuclei later form between the islands. This effect becomes noticeable when the primary islands have grown to about 1000 A and continues until the final hole-free film is formed. A secondary nucleus grows until it touches a neighbour and if this happens to be a much larger island, the secondary nuclei may coalesce very rapidly and may become completely incorporated in the large islands. They also observed that the islands become elongated and join to form a continuous network structure in which the deposit material is separated by long irregular and narrow "channels" of width 50-200 A. As the deposition continues, re-nucleation occurs in these "channels" and these are bridged at some points and fill in rapidly in a liquid-like manner.

Pashley and Stowell (1966) in their investigations of gold deposits on MoS_2 (mentioned earlier), further reported that the islands join to form a continuous network structure, and the structure which occurs immediately before a continuous hole-free film is formed consists of a continuous film containing a maze of irregularly-shaped and terminating channels about 100-300 A across.

They arrived at the following conclusions:-

(1) Appreciable mass transfer of already deposited

material occurs by the surface migration of the deposit atoms over existing deposit islands and this gives rise to the so-called liquid-like coalescence behaviour.

(2) Considerable recrystallisation or grain-growth occurs as the film growth proceeds, and this can have an important influence on the orientations and grain size of the deposits.

(3) Lattice defects are introduced into the growing film to accommodate the rotational and translational displacement misfits that exist between coalescing islands.

Matthews (1966, 1967) has also expressed almost similar views. He further observed that nuclei of nickel, palladium and platinum (deposited in vacuo (10^{-8} to 10^{-9} torr)) on NaCl cleavage faces at 360°C, coalesced to form continuous films at a much earlier stage of film growth than did nuclei of gold, silver or copper under identical conditions. He noticed marked early coalescence in nickel deposits, which completely covered the rocksalt surface before their thickness reached 200 A.

1.3. A General Outline of the Main Factors Affecting the Structure and Orientation of Thin Films Condensed in Vacuum:

Atoms arriving from the source on a substrate surface aggregate together to arrange themselves in a manner depending upon a number of factors or parameters. These are mainly (1) the nature of the substrate (amorphous, polycrystalline, single crystal; degree of roughness, degree of cleanliness, etc); (2) the temperature of the substrate; (3) rate of deposition; (4) pressure and nature of the residual gas in the vacuum; (5) thickness of the deposits; (6) obliquity of the vapour stream; (7) annealing, etc.

All these parameters can influence the structure and orientation of the crystal nuclei in the initial growth process and at the surface of a deposit. The effects of the individual factors are of great interest, and such individual effects on crystal growth can be studied while keeping the other variables constant - which is by no means an easy task.

The effects of these parameters on the structure and orientation of deposits are outlined below under separate headings.

1.3(a). The Effect of the Nature of the Substrate - Epitaxy:

It was realised by early workers that the atomic arrangements in an amorphous substrate do not affect the orientation of the crystal growth. On the other hand, it has also been realised for a long time that the growth of metal films is greatly affected by an "active substrate", i.e. one in which the atoms are arranged in a regular periodic lattice. At a raised temperature the crystals deposited on such a single-crystalline substrate grow parallel to one another in one or more definite orientations with one or more particular lattice rows parallel to a well-defined crystallographic direction of the substrate surface. Such a phenomenon is known as "epitaxy" and the corresponding growth as "epitaxial growth".

Several reviews have been published on this topic by many workers, and here only a short account will be presented.

The lattice-dimension relationships required for epitaxy to occur:

Barker (1908) concluded that for epitaxial overgrowth of crystals on an isomorphous crystalline substrate, the molecular volumes of the two must not be too dissimilar.

Royer (1928) from his studies of epitaxial growth of alkali halides and other crystals from solutions concluded that at the interface between the substrate and the deposit crystals there must be a two-dimensional network almost identical in axial dimensions (within a difference of 15%).

This early theory of Royer can, however, be regarded as not too significant. In this laboratory, Acharya (1948) showed that a misfit of as much as 90% occurs in the epitaxy of Sb_2O_3 on (111) Sb, and Elleman (1949) observed about 50% misfit in Ag_2S on Ag.

Wilman's (1950, 1951) observations on crystal groupings led him to the conclusion that stable preferred orientation relationships (including epitaxy) between two crystals involve essentially only a correspondence of x lattice spacings of one lattice to y spacings of the other lattice (x and y, small integers) in one or more directions at the interface. It appears to be not necessarily a 1:1 relation that need be involved.

Schultz (1952) similarly showed that epitaxial growth can occur for misfits in the range from -39% for LiF on KBr to +90% for CsI on LiF, where the percentage of misfit is $\frac{b - a}{a} \times 100$ (a and b are the lattice parameters of the substrate and the epitaxially grown film respectively).

Bassett, Menter and Pashley (1959) recorded misfits

up to 90% in epitaxial growth and they found no strong indication of "pseudomorphism".

The effect of the type of bonding:

Royer (1928) pointed out that the binding nature of the constituents of the deposit and the substrate must be of the same type to favour epitaxial growth.

This rule is not always important as it was shown by Kirchner and Lassen (1935) and Bruck (1936) that metallic single-crystal films can be grown successfully on ionic crystals.

Royer (1936) himself later concluded that it was a similarity in spacing of one pair of parallel lattice rows rather than a lattice network which was of importance in favouring epitaxy.

Willems (1943, 1944, 1948) made extensive studies of epitaxial growth of many organic materials and observed that the dipole vector of the polar materials tends to coincide with the long axis of linear molecules or to be parallel to the plane of planar molecules.

Recently Bicknell et al (1966) pointed out that in each of the epitaxial relationships observed on the growth of silicon on alumina, there is always a coincidence of certain symmetry elements normal to the surface. They suggested that when no definite type of bonding arrangement

(Nodler and Cadoff, 1965) appears possible, the epitaxial arrangement is determined by the two-dimensional symmetry of the surface, the substrate in the effect transferring the symmetry to the epitaxial layer.

Pseudomorphism in epitaxy:

A further early concept in epitaxial growth was that of "pseudomorphism" (Finch and Quarrell, 1933, 1934) which considered that in the early stages of growth of an oriented layer, the deposit crystal lattice is constrained to fit that of the substrate in their common contact plane. They observed that aluminium deposited on crystalline platinum sometimes showed a remarkable change in structure from f.c.c. to f.c.tetragonal lattice. They concluded that when aluminium vapour is deposited on f.c.c. platinum, the platinum atoms exerted attractive forces on the aluminium atoms arriving to form the first plane, thus causing them to take up positions in the lattice similar to those which would have been occupied by the platinum atoms had the vapour been of this metal. The fact that a sufficiently thick aluminium layer did not exhibit any change from its normal f.c.c. structure, showed that the effect of the above-mentioned pseudomorphic strain upon the surface layers disappeared with sufficient film thickness.

Subsequent work made it clear that this effect is

difficult to detect and that the crystal structure of the deposit has spacings which agree fairly closely with that of the deposit material in the bulk. Nevertheless, the concept is widely accepted and forms the basis of many theoretical works on epitaxy.

Frank and Van der Merwe (1949) developed a theory of epitaxy which also assumes the initial formation of a pseudomorphic layer. They postulated that the atoms of a deposit are regularly arranged in the potential trough of the substrate surface and thus form a two-dimensional pseudomorphic lattice as suggested by Finch and Quarrell (1933, 1934).

Smollett and Blackman (1951) postulated that the atoms of the deposit are regularly arranged in potential wells of the substrate and thus form a two-dimensional 'pseudomorphic' lattice. This arrangement can often be fulfilled with a low misfit between the surface lattice of the substrate and a particular low-index crystal plane of the film material.

Factors which determine the type of epitaxial orientation:

Wilman (1940) suggested from his observations of the growth of some of the silver halides on silver that a preferred two-degree orientation of crystals grown on a single-crystal substrate depends fundamentally on their being

a similarity of spacing (with a difference less than 15%) in at least one row of closely spaced atoms in each lattice. Thus, in the initial deposition of atoms on the substrate such an atom row of the deposit lattice would naturally tend to be built up most readily and parallel to the corresponding row of the substrate, since a single atom of the deposit would tend to occupy a potential trough of the substrate. Further addition of atoms at the side of such a row would then most likely take place so that a small crystal would be formed with one of its planes of closest atomic packing oriented parallel to the mean substrate surface. Or, if a densely populated plane occurred in which atom-rows in one direction could simultaneously fit in with the periodicity of the substrate lattice, then the plane containing this and the former atom-row would probably tend to grow parallel to the substrate surface.

Seifert (1935, 1953) emphasised that the local atomic matching of the deposit and substrate structure must enter into the first nucleation of the epitaxial growth.

Elleman and Wilman (1949) emphasised that epitaxy must be initiated by local matching of atomic arrangement by the deposit nucleus on the substrate and that lattice relationships arise only as a secondary feature as growth proceeds. The orientations observed in the case of the

growth of $PbCl_2$ on PbS conform to the general observation that when strong epitaxial orientation occurs there are at least one or more lattice row types which are parallel to the substrate and overgrowth crystals with nearly equal lattice spacings along parallel directions.

Drabble (1949) considered epitaxial growth from the point of view of co-ordination. He pointed out that in various cases where the orientation is such that large misfits occur, the deposit orientation corresponds to the build-up of the deposit on the substrate, so that the atoms or ions have their normal co-ordination with their nearest neighbours in the substrate surface.

According to Wilman (1951) the epitaxial growth is determined by the tendency of the atoms (or ions or molecules) on arrival on thesubstrate to be held in the potential troughs which exist in a periodic array on a flat substrate crystal face, though the deposit atoms have on arrival an initial kinetic energy and they retain on the average a certain mobility over the substrate, depending upon the nature of the deposit and substrate and temperature of the surface. He further stated that the orientation is determined by the arrangement of the first layer or so of the deposit atoms or molecules in positions of lowest attainable potential energy on the substrate.

According to Turnbull and Vonnegut (1952) the nucleation theory for epitaxial growth is that the critical nucleus of minimum Gibbs' free energy of formation will be the one in which the actual lattice parameters of the stable crystalline phase has changed such that the resulting mismatch between the nucleus and the substrate will be smaller than the misfit, resulting in a lower value of the crystal-substrate interfacial energy.

Disorientations in epitaxial growth:

Evans and Wilman (1950) pointed out that there is often a disorientation of the deposit crystals. They showed, however, that this can sometimes be recognised as consisting of a range of rotation about a main lattice row, which they thought probably due to epitaxial misfit causing stress and slip.

After thin epitaxial films have been isolated from the substrate, the transmission electron diffraction patterns often show a rotational disorientation which is attributable to partial breaking of the film followed by bending about a densely populated lattice row (Goche and Wilman, 1939; Elleman and Wilman, 1948, 1949; Wilman, 1949).

The effect of residual air pressure in the vacuum:

Murr and Inman (1966) from their work on

epitaxial growth of gold, silver, nickel and aluminium on NaCl substrate arrived at the following conclusions:

(1) The pressure of the air in the evaporation unit has a significant effect on the epitaxial growth of these metals.

(2) The epitaxy of f.c.c. metals is enhanced by high evaporation rates.

(3) The epitaxy and the effective grain size of these metals is enhanced by lowering the nominal vapour pressure before deposition on to the NaCl substrate.

(4) The structure of the vapour-deposited f.c.c. metals is altered with film thickness.

(5) Film growth is influenced by the condition of the substrate surface with reference to adsorbed impurities and the vapour environment surrounding the substrate.

1.3(b). The Effect of the Temperature of the Substrate :

In addition to the nature of the substrate, another important factor influencing the film structure is its temperature.

Inert substrates:

On a cool enough inert substrate like cellulose, carbon or a smooth glass surface, the crystal size in thin deposits is small (50-100 Å) and orientation weak or absent.

If the temperature of the substrate is raised above the room temperature during the condensation of the vapour atoms, the crystals formed are larger in size and at a sufficiently raised temperature, tend to grow in a more or less strongly developed preferred orientation.

When the temperature of the substrate is raised, the atoms arriving on it become more mobile. Further, the vibration amplitude of the surface atoms in the substrate is increased due to gain in energy and this facilitates easy migration of the vapour atoms. Thus, the deposit atoms can move to positions of low potential energy on the substrate and at the same time aggregate together in close packed sheets so that densely-populated planes tend to grow parallel to the substrate surface.

Dixit (1933) suggested that the kind of orientation developed in metal deposits might be expected to depend on the temperature of the substrate. He attempted to formulate a theory based on the concept of the initial thin deposit layer of atoms behaving in effect as a two-dimensional gas. His experimental evidence provided no clear support for the above expectations.

Umanskii and Krylov (1936) observed that iron deposited on glass showed (111) orientation only when the substrate was sufficiently heated by the radiation from the evaporator.

Bannon and Coogan (1949) like Burgers and Dippel (1934) observed (111) orientation in the upper regions of calcium fluoride deposited on different kinds of glass at 25°C, but they also found that when the temperature was raised to 110°C a (110) orientation was observed instead of (111).

Schultz's (1949) results with alkali halides showing development of strong orientation with increasing thickness of the deposit were explained by Holland (1958) by the fact that the thicker deposits would reach higher temperatures due to the heat radiation from the vapour source (as Evans and Wilman (1952) had indicated). Schultz found that MgF_2 films below 1000 A were amorphous but became crystalline for higher thickness. Similarly CdF_2 films showed (111) orientation when the temperature of the glass substrate was raised to $\sim$100°C.

Evans and Wilman (1952) condensed Cu, Ag, Au, Ni, Fe, Pd on glass substrates and found that the crystals first formed are small ($\sim$50 A dia.) but their size increase at the surface as the deposition proceeds. They also observed development of preferred orientation associated with facet formation in the upper parts of the deposits more than 500 - 1000 A thick. This they explained was due to the increase in mobility caused by the rise in temperature of the deposit

by the incoming heat radiation from the source.

Although Murbach and Wilman's (1953) copper strip substrates reached about 100-150°C during deposition of Ni and Fe, it was later clarified by Wilman (1955) that the surface temperature reached during deposition was much higher, higher in fact than the normal recrstallising temperature of the deposit metal.

Herbstein (1957) deposited silver on silica substrates maintained at 20°, 340°, 416°, 595° and 710°C. There was no sign of orientation in the deposits made at the three lower temperatures. The one at 595°C consisted of large crystals of which a small proportion exhibited one-dimensional orientation about the [111] axis. The deposits made at 710°C showed predominantly (111) together with (100) and (110).

Buckel (1959) reported amorphous form of Bi when condensed on an amorphous substrate at 2°K, whereas films of Cu, Al, Pb, Tl, Hg, Zn, Sn, etc. condensed at liquid He temperature showed crystalline structure.

Via and Thun (1961) reported mixed (110) and (100) orientations for germanium deposits on borosilicate glass at 400 and 450°C. At higher temperatures the (100) orientation faded out and at about 600°C, (110) became predominant.

Saikia (1961) deposited tetragonal tin on glass and observed (100) orientation for a film of 320 A thick when the substrate temperature was 104°C. Stronger (100) orientation was observed in deposits condensed at 164°C and 207°C substrate temperatures. He also observed random orientation of the Sn deposits when the substrate temperature was about 254°C.

Dutta (1968) condensed several silver films on glass substrates maintained at 100° to 160°C during deposition. He, however, did not observe any significant change either in structure or in orientation of the deposits, from those prepared at room temperature. This might have been due to the fact that initial substrate temperatures were considerably less than the temperature of of recrystallisation of silver (~200°C).

Active substrates:

It has been realised that epitaxial growth does not occur on all single-crystal substrates at room temperature. When condensation is on a substrate at raised temperature, the mobility of the atoms on the substrate is increased and at a certain temperature a second-degree orientation (epitaxial growth) develops. The initial stage then consists of atom rows of the deposit crystals being formed parallel to a densely-populated row in the substrate at the interface, of similar density of atomic population.

Finch and Quarrell as early as 1933 reported that sputtered platinum film employed as substrates for the reception of vapourized metals (Mg, Zn, Al) possessed a completely unoriented structure when the heating of the substrate was not sufficient. But when the receiver became sufficiently heated due to the incoming radiation from the source, the deposit crystals showed preferred orientations.

Finch and Ikin (1934) also observed preferred orientations of sputtered Pt when they were prepared under high current conditions causing heating of the substrate.

Lassen (1934) found that metal deposits on a rocksalt cleavage face at below 150°C were random, but above it there was complete orientation, i.e. epitaxy.

Bruck (1936) and Rudiger (1937) observed the existence of a critical temperature of the active substrates, above which the deposit metals exhibited epitaxial growth.

Finch and Wilman (1937) noticed that silver grew epitaxially on potassium bromide cleavage face when warmed sufficiently.

Kirchner and Lassen (1935), Finch and Wilman (1937), Goche and Wilman (1939) obtained Kikuchi-line patterns by reflection from epitaxial silver films condensed on NaCl cleavage faces, which indicate highly accurate alignment and large size of the mosaic crystals formed at raised substrate temperatures.

Shirai (1943a,b) observed that the epitaxial orientation of iron and chromium on NaCl and KCl varied with the temperature of the substrates.

Elleman (1948) in this laboratory observed that if a rocksalt cleavage surface substrate is heated in vacuo at 500°C for an hour and then cooled to room temperature silver deposits then prepared on it showed parallel orientation along with {111} twinning. This result was similar to that normally observed with a freshly cleaved face heated to 150°C during deposition. He also observed random orientation of Ag deposits when deposited at room temperature on NaCl cleaved in air. He suggested that this effect may be due either to the removing of an adsorbed air or moisture layer, or to the annealing of the crystal, thus perfecting its surface. This promotes mobility of the deposit atoms on such a substrate and thus favours the oriented growth of the deposit crystals.

Kehoe (1957) deposited copper, silver and gold on the cleavage surfaces of alkali halides at various temperatures (from 20° to 385°C). He showed that the character of the crystallisation at some temperatures depends markedly on the deposit thickness. With experiments on Cu condensed on NaCl he found that at 160°C and below, the orientation tends to improve with thickness but at higher

temperatures randomly oriented crystals occur during further deposition on an initially perfectly orientated Cu deposit. In the case of copper, orientation was first observed at 90°C and the growth characteristics were almost identical at 130°C. In the case of silver, initial orientation was observed at about 50°C.

He also agreed with Gottche (1956) that for each metal-substrate pair two substrate temperatures can be defined: T_o, below which the deposit is completely random, and T_{min}, above which the orientation is complete, i.e. epitaxial.

Sloope and Tiller (1961) investigated the relationship of rate of deposition, deposition temperature and thickness to the formation of thin single-crystal Ag films on NaCl cleavage face. They thought that a critical temperature above which epitaxy occurs, such as Rudiger(1937) found, does not exist, but that the minimum temperature of deposition is dependent on the rate of deposition. Likewise, structural characteristics of the films are quite dependent on the formation conditions.

1.3(c). <u>The Effect of the Thickness of the Deposit</u>:

To investigate by electron diffraction the variation of deposit structure with increasing thickness, it is in general necessary to use the method of grazing

incidence. Here, the diffraction patterns are obtained from the surface region of the deposit 10 to 200A deep, depending on the angle of incidence, surface roughness and atomic weight of the material. In transmission, on the other hand, the diffraction is obtained from the whole thickness of the deposit until this becomes too large for coherent scattering to be obtained (5000 A for very light materials and only a few hundred A for heavy materials).

The variation of orientation of deposits with thickness has been observed by many workers in this laboratory and elsewhere. The observations of Burgers and Dippel (1934), Nelson (1937), Levinstein (1949), Evans and Wilman (1952) etc. have been mentioned elsewhere. Other results were also provided by Schulz (1949) who found that thin films of LiF and NaCl of less than 100 A thickness (on amorphous substrate) showed almost random orientation with a small amount of (100) texture. As the thickness was increased to 500 A or more, there was a change in orientations to (111) for LiF and (110) for NaCl.

Ramos (1961) (see also Ramos and Wilman, 1962), also studied systematically the orientation of alkali halides deposits on glass as a function of thickness. They found that NaCl, KCl and KBr developed (111) orientation at about 1000 A, which became sharper and azimuthally limited at higher thicknesses up to 10,000 A, but then a change to a (211) type of orientation (with the same limited azimuthal

range) occurred in the further growth.

Saikia (1961) found an appreciable change in the nature of the orientations of Sn deposits on NaCl cleavage face and amorphous substrates with increasing thickness of films.

Preece (1966) (also Preece and Wilman, 1967), noted a change in the kind of orientation of Sn films condensed at 10^{-8} and 10^{-5} torr of air and oxygen respectively, on glass at room temperature, when the thickness varied between 500 to 5000 Å.

Dutta (1968) observed a well-defined sequence of orientations of silver deposits with increase of thickness. His results showed systematic progressive changes in orientation at the deposit surface, from random to (111), (111) + {111} twinning, (110) and (211) orientations, as the deposit thickness increased. This sequence of orientations was the same for all deposits at all residual air pressures P between 7 $x10^{-6}$ and 7 $x10^{-3}$ torr, but the thickness at which each transition occurred decreased nearly rectilinearly with increase in log p. It was concluded that the initial random layer was associated with low mobility of the silver atoms at room temperature, but that the mobility increased as deposition proceeded, and led to development of octahedral faces in the crystals, and hence

to preferential growth of the crystals having such a face most nearly normal to the vapour stream. Evidently increase in the air pressure favoured more rapid development of octahedral faces on the growing silver crystals. The (111)-oriented crystals then developed additional {111} twinning, and the final (110) and (211) orientations were concluded to arise by secondary twinning, favoured however by presence of (110) or (211) faces at this stage of growth.

1.3(d). Effect of the Obliquity of the Vapour Stream:

The structure and orientation of thin metal films are also affected by the direction of the incident vapour beam on the substrate. Many workers have reported the influence of the vapour beam obliquity on the structure and texture of these films. A short review will be presented here.

Burgers and Dippel (1934) first observed in calcium fluoride deposits that in the upper regions of deposits over 600 Å thick, orientation is developed, with its axis normal to the substrate when the vapour stream was incident normally on the substrate, but slightly inclined towards the vapour stream where the vapour stream was incident obliquely.

Beeching (1936) reported that the [100] orientation axis in aluminium films was tilted by 15°, for

a vapour stream incidence of 45°. Nelson (1937) found that for iron films the [111] axis was inclined to the normal at a region where the vapour stream was incident obliquely.

Evans and Wilman (1952) (see also Murbach and Wilman, 1953) have also provided further evidence regarding the variation of the tilt of the orientation axis with vapour obliquity.

Burgers and Dippel (1934), Thomson and Cochrane (1939) and Thomson (1948) explained the influence of the direction of the vapour stream by supposing that the crystals grew by atoms arriving on a face, moving over it until they came to the edge and thus prolonging the face. Such plane crystal faces normal to the vapour stream will then receive more atoms per unit area on these faces and will grow faster than the others, where similar faces are inclined to the vapour stream. Planes parallel to the surface have the advantage that they can grow laterally in all directions. Thomson (1948) concluded that the partial tilt of the orientation axis is due to a compromise between these two opposing tendencies.

Evans (1950) and Evans and Wilman (1952) carried out a detailed investigation of the effects of an inclined vapour stream over a wide range of angle of incidence for substances of differing structures and properties,

particularly of iron, lead sulphide and zinc.

For iron deposits they observed that the tilt of the [111] axis increased with increasing angle of incidence of the vapour stream, up to a region where the angle of incidence was about 30°. The tilt, however, then fell off with further increase of the angle of incidence, being only 5° at $i = 70^{\circ}$.

For PbS deposits, they found that the tilt of the [100] axis was small, increasing with i up to $i = 20^{\circ}$, and remained constant ($\sim 8^{\circ}$) over a range from $i = 24^{\circ}$ to $i = 60^{\circ}$.

Evans and Wilman (1952) explained these results on the basis of fine-scale roughness of the deposit surface and the increasing mobility of the deposit atoms. Although the glass substrates have a remarkably smooth surface, on the atomic scale, the surfaces of all such amorphous substrates are rather undulatory. During the evaporation of the metal in a sufficiently good vacuum, the metal atoms travel in straight lines from the source and some of them are deposited on the substrate. If a metal is used which does not migrate after deposition, the thickness will be greatest on that part of the surface which faces the oncoming atoms, and there may even be regions of the substrate that will be shielded so as to receive little or no metal.

When the vapour stream strikes the surface at

normal incidence, all parts of the surface are almost equally favoured for deposition; the crystals grow with a particular orientation axis normal to the surface. However, when the vapour beam is incident obliquely to the surface, parts of the surface receive a lower density of atoms owing to their obliquity, or even are shadowed by mounds on the surface, resulting in the portions of mounds facing the vapour stream receiving the greatest portion of the deposited metal. Moreover, the atoms of metals like iron do not migrate initially, at room temperature, to such an extent as to fill up the depressions of the wavy surface.

Evans and Wilman (1952) suggested that when the deposit surface becomes hot enough by the progressive heating by radiation coming from the source, and the kinetic energy of the deposited atoms, the crystallites developed preferentially on these portions of the surface will tend to be oriented with a certain lattice plane as boundary face, parallel to the local elements of the surface, so that the net effect is a partial tilt of the mean orientation axis towards the vapour stream. This explanation could also account for the decrease in the angle of tilt with increased angle of incidence of the vapour stream. When the vapour stream is very much inclined towards the surface, only the extreme tips of the mounds will be in position to receive

the vapour so that the orientation axis will, necessarily, be less inclined to the normal of the mean surface. The film will be thinner in these regions of the specimen as a whole, which correspond to greater obliquity, due to the greater distance from the source of atoms.

Herbstein (1957) observed that the orientation of Ag films on amorphous substrates at above 300°C was such that a lattice plane was parallel to the substrate surface irrespective of the angle of incidence of the vapour stream.

Saikia (1961) found a tilt of the [110] orientation axis of silver deposits prepared at room temperature. He observed the maximum tilt as 19.5° for $i = 56^{\circ}$ of the vapour stream.

Ramos and Wilman (1962) and Sancho, Ramos and Bru (1966) observed (111) orientation in thicker deposits from their work on alkali halides and that the [111] axis of orientation showed increase in the angle of tilt δ as i was increased but they noted that for all the cases $\delta < i$ when $i \neq 0^{\circ}$. Much thicker deposits (>10,000 A) showed (112) orientation, and when it was first observed, the orientation axis showed a tilt of a few degrees in a direction opposite to that of the vapour stream. With increasing thickness the tilt of the [112] axis became positive, i.e. inclined towards the vapour stream.

Palatnik and Fedorenko (1967) examined transverse sections of vacuum-deposited Be films and they concluded that the degree of perfection of the orientation is determined mainly by the angle of incidence of the vapour stream and the substrate temperature. The optimum values of i for the growth of (001) and (100) perfect orientations lie between 15° and 30°, and the optimum temperature in the former case was within 160-210°C and in the latter 340-370°C.

Dutta (1968) has shown the variation of δ with i for silver specimens of 5500 A (prepared at $\sim 7 \times 10^{-5}$ torr of residual air), 7000 A (prepared at 7×10^{-4} torr), 12000 A (at 7×10^{-5} torr) and 16720 A (at 7×10^{-5} torr) thick. The (i, δ) plots show straight lines through the origin in each of the cases. He observed that the tilt δ has larger values when the orientation is of the (110) type than in the case of (111) for the same values of i, at oblique incidence of the vapour stream. For the 16,720 A thick silver specimen, he reported prominent (110) orientation together with (211) cubic and (100) hexagonal orientations, for $i = 0$; for $i = 45^{\circ}$, the pattern showed predominantly (110) orientation. The tilt of the orientation axis at $i = 45^{\circ}$ was 30°.

1.3(e). The Effect of the Rate of Deposition:

The rate of deposition of the metal also has considerable influence on the growth, nucleation, grain-size and orientation of thin films.

Elleman and Wilman (1948) while studying growth of PbS deposits on rocksalt substrates in vacuo, came to an almost generalised conclusion that the atoms had a certain degree of mobility over the surface before losing most of their kinetic energy. Thus, sooner or later, they meet other atoms and aggregate to form small nuclei. The greater is the number of atoms incident on unit area per unit time, the larger will be the number of these nuclei. The higher the rate of arrival of the atoms per unit area, the greater is the number of atoms bombarding each nucleus per second, and if the rate of arrival is high enough, not all the atoms will reach the lowest potential troughs, and this hinders the development of the orientation which would be imposed by the substrate and result in a correspondingly weaker orientation or even a completely random crystal deposition. They observed strong orientation of PbS deposits even at temperatures of about 150°C when a relatively higher rate of deposition (~40 A/sec) was used.

Levinstein (1949) states that zinc and cadmium films could not be formed at all at low rates of evaporation.

When the rate of evaporation was high, films could be formed readily. For intermediate rates of evaporation isolated zinc and cadmium crystals could be observed, which might eventually behave as nuclei for further growth. He also deposited antimony at different rates and observed that large patches of slowly condensed antimony produce a diffuse diffraction pattern, while the smaller patches of rapidly evaporated antimony produce a sharp ring pattern. However, the effects observed for antimony could not be used to generalise for all metals. The amorphous state has never been observed for most metals condensed on substrates at room temperature. The variation of the patch-size with the rate of deposition has been discussed in §1.2.(b).

Sennett and Scott (1950), and Hass and Scott (1949), also observed the influence of the rate of deposition on the grain size in the deposit.

Thun (1963) stated that at very low rates of deposition the nucleation rate is low and the long mean free time of the mobile surface atoms permits a preferential growth of the crystalline surfaces representing the lowest free energy. The resulting films prepared by low rates of deposition exhibit roughness and a relatively loose distribution of "islands". With increasing rates, the film density and smoothness improves up to a point where atoms are

increasingly buried in random sites by successively arriving atoms. This involves considerably higher activation energy, and the result is a decrease of the average crystal size and a considerable increase in the number of lattice faults.

Preece (1966) reported the variation of the surface orientation with the rates of deposition in tin deposits on glass substrates at room temperature. He observed a mixture of (100) and (001) orientations for a film about 250 Å thick (prepared at a residual air pressure of 1 $x10^{-5}$ torr) for all rates of deposition less than 70 Å/sec. Films of the same thickness prepared in the same vacuum but with higher rates of deposition showed mostly random orientation. Similarly, films of thicknesses between 1000-1500 Å (prepared at residual air pressure 1 $x10^{-5}$ torr) mostly showed (001) orientation for all rates of deposition below about 70 Å/sec, and at higher rates showed the same (001) orientation along with occasional (301). Preece concluded that such an influence of the rate of deposition on change of orientation was due to the increase of the surface mobility during the growth of the film.

1.3(f). <u>The Effect of Residual Air Pressure</u>:

The residual air in a vacuum chamber, where the specimens are prepared, may have important effects on the structure of the film. Gas molecules from the residual gas

atmosphere may be adsorbed in the film during the deposition process. The trapping of gas molecules mainly bound by Van der Waals forces results in porous, highly disordered films. The gas occlusion phenomenon primarily depends on (1) the adhesion to the substrate of the residual gas molecules and their desorption probability which increases with temperature, and (2) the $\frac{p}{r}$ ratio (see also Behrndt, 1962) which is the ratio of the number of gas molecules arriving at the substrate surface per unit area and time, to the corresponding number of film atoms for a given film material and substrate temperature.

Stahl (1949) obtained electron diffraction evidence that the initial thin layers of deposited metal often contain some oxide. He pointed out that oxidation may occur either while the metal vapour is in transit or during condensation. Taking the mean free path of Al atoms in air at 0.1 microns of Hg air pressure to be more than 100 cm, intense oxidation is unlikely to be due to gas-vapour collision in the space, which is generally a few cm. in length. The combination of vapour atoms with oxygen molecules on the substrate surface is more probable, in which case, the longer the period of condensation, the greater will be the number of gas molecules impinging on the substrate.

On the point of whether the gas may affect the film

during its formation or affects the individual atoms in transit from the source to the substrate, Levinstein (1949) observed that what takes place depends upon the pressure of the residual gas, that of the metal vapour and the degree to which the chemical reaction may take place between the two. He considered two extreme cases: When the residual gas is a metallic vapour which may form an intermediate compound with the metal evaporated, a reaction may take place at the film surface even when the pressure of the residual gas is low. In that case the type of film being condensed and the type of residual gas rather than its pressure are the determining factors. In an experiment to form a composite film of zinc and gold, he observed that when Zn was evaporated slowly from a filament no zinc film could be formed due to its quick re-evaporation. When gold was evaporated simultaneously, however, a film was formed which in electron diffraction examination appeared to be a compound. This behaviour was also pronounced when mercury vapour was present. Since the residual gas pressure was exteremly low, any reaction between residual gas and metallic vapour during the transit of the atoms is highly improbable.

The other extreme case considered by Levinstein is the case when a residual gas which does not react with the metallic vapour is used at high pressure. In this case the

vapour is not atomic but consists of a cloud of particles which seems to originate near the filament. The gas in this case affects the metallic beam in transit by producing collisions between the individual atoms before they reach the collector, so that the material reaching the collector consists of clumps of atoms. The most striking results showing such particulate deposits were observed when zinc and cadmium were evaporated at a pressure of 0.01 mm of Hg air pressure. A possible explanation was given by Levinstein (1949) on the basis of Frenkel's (1924) hypothesis. When zinc atoms arrive at the substrate, they remain on thesurface for only a short period and then re-evaporate before sufficient other zinc atoms arrive to make film formation possible. When the pressure of the residual gas is increased, collisions between individual metal atoms take place in the vicinity of the filament, thereby producing aggregates of atoms which have a much greater life time on the substrate than atoms. These aggregates act as nuclei for other atoms and thus make film formation possible.

Levinstein (1949) made some further observations:

(1) Metals which generally showed preferred orientation at high vacuum, showed no orientation when evaporated at about 0.1 mm. Hg air pressure (Sb, Bi, Te, Cd, Zn, Mg, Th, etc.).

(2) Metals which produced a sharp diffraction pattern when condensed in high vacuum, showed broadened rings when condensed at 0.1 mm.Hg air pressure (Au, Ag, Cu, Ni, Fe, Co, etc.).

(3) Metals which showed diffuse rings at low pressures continued to show diffuse rings at 0.1 mm.Hg air pressure (Ta, In, Si, Ge, etc.).

Bauer (1962) stated that if the growing surface during vacuum-deposition is struck by active residual gas atoms, the crystal habit in the deposit can be strongly influenced. He observed that if the interaction between residual gas and crystal was temperature dependent, i.e. if there was chemisorption at low temperatures and orientation at higher temperatures, then the habit will also be temperature dependent. He concluded that the orientation behaviour of reactive materials in active residual gases is hard to predict. He further observed that the reactive residual gases not only influence the habit, but also the nucleation behaviour.

Caswell (1961) showed that indium films deposited in a high vacuum had (010) orientation, while films heavily doped in a high partial pressure ($\sim 1 \times 10^{-4}$ torr) of oxygen showed random orientation. He stated that the presence of oxygen decreases the mobility of the atoms on the substrate.

Preece (1965), Preece, Wilman and Stoddart (1967) and Preece and Wilman (1967) in this laboratory, carried out experiments to study for the first time in systematic detail the effect of residual air pressure on the development of orientation of thin films of tin, condensed on glass substrates at room temperature. They showed that for a film 500 A thick, the orientation in the surface region depended on the residual air pressure. The orientation was (110) at an air pressure of 1 $x10^{-4}$ torr, which gradually changed to (001) at 1 $x10^{-5}$ torr. At $\sim$2 $x10^{-6}$ torr, it changed to a mixture of two orientations, viz., (100) + (001). There was no change in orientation when the pressure was 1 $x10^{-7}$ torr, but finally, when the pressure was still lowered to 4 $x10^{-8}$ torr, they observed pronounced (100) orientation. Preece concluded that this orientation was characteristic of tin in absence of gas adsorption, and that the other orientation changes were mainly due to the adsorption of oxygen on the deposit layers during condensation.

Dutta (1968), also in this laboratory, carried out systematic experiments to show the influence of the residual air pressure on the orientation of the silver deposits. A silver film 3000 A thick showed (211) + (110) f.c.cubic + (100) hexagonal structure at 7 $x10^{-3}$ torr, (111) f.c.cubic + {111} twinning at 7 $x10^{-4}$ torr, prominent (111) at 7 $x10^{-5}$

torr, and random orientation when the pressure of air is further reduced to 7 $x10^{-6}$ torr. In another series of experiments he showed that a silver film about 4500 A thick had (211) f.c.cubic + (100) hexagonal orientations at 7 $x10^{-3}$ torr, (110) f.c.cubic at 7 $x10^{-4}$ torr, (111) f.c. cubic at 7 $x10^{-5}$ torr and when the pressure is further reduced to 7 $x10^{-6}$ torr, there is no deviation in orientation from (111).

When the thickness of the silver film was increased to $\sim$7500 A, he observed one-degree f.c.cubic (110) orientation at pressures 7 $x10^{-4}$ torr and 7 $x10^{-5}$ torr, which changed to (111) + {111} twinning in deposits at 7 $x10^{-5}$ torr. At a still higher thickness of the film, $\sim$9000 A, he observed f.c.cubic (110) orientation at 7 $x10^{-5}$ and 7 $x10^{-6}$ torr.

Dutta's results showed the same sequence of orientations at the deposit surface (random, (111), (111) + {111} twinning, (110) + (211), as the thickness increased, at all pressures from 7 $x10^{-6}$ to 7 $x10^{-3}$ torr, except for additional presence of some hexagonal silver towards 10^{-2} torr. The thickness at which the transition from one orientation to the next occurred, <u>decreased</u> nearly rectilinearly with increasing logarithm of the residual air pressure. Increase in air pressure thus caused more rapid development of at first the octahedral faces on the crystals, and later the twinning.

1.3(g). The Effect of Annealing a Metal Film:

The structure and orientation of crystals in thin films are not only influenced by the substrate temperature during condensation, but can also be affected by annealing after formation of the film.

Early work of Andrade and Martindale (1936) showed the structural change in gold and silver films annealed after preparation. They observed the formation of small aggregates when films ~50 atoms thick were maintained at about 230°C for silver and at a higher temperature (below 400°C) for gold, for three hours. The growth of aggregates or such crystallites was accompanied by the formation of large, irregular, transparent areas, which they called "windows". When the temperature was raised further the deposits consisted of a thin uniform window with crystals scattered on it. They concluded that the aggregates were formed by the motion of the upper layers of the film only. They thought that the deposit atoms became mobile and that surface-tensional forces caused the formation of the spherical agglomerates. Later, flat faces of limited extent appeared on the larger crystals, so that the form was polyhedral.

McGee and Lubszynski (1939) heated Ag films condensed on mica to 700°C in air and found that if the layer is thick (thickness not mentioned) the effect of heating is

to cause a number of holes to appear. In the case of thinner films these holes increase in size until they merged into one another, leaving islands of silver completely separated.

Buckel (1959) noted that the condensation of a vapour on a substrate at very low temperature corresponds to a rapid quenching, because the atoms which hit the substrate lose their energy very quickly. He found that metals like Cu, Al, Pb, Tl, Hg, Zn, Sn, etc. were crystalline in nature when condensed even at the liquid helium temperature. After annealing to even room temperature (in the case of Hg, to 155°K) some of these deposits showed a thinning of the electron diffraction rings, due to annealing, which indicated increase in the crystal size.

Keith (1956) observed from X-ray diffraction studies that copper deposits condensed on glass at liquid-nitrogen temperature were amorphous but on warming to room temperature showed crystalline structure.

Saikia (1961), in this laboratory, made extensive electron diffraction investigations on the aggregation and annealing phenomena of tin films condensed on glass at room temperature. He observed that for tin deposits of thickness varying between 290 A to 7600 A, aggregation of the crystals took place when the deposits were heated in vacuo to

temperatures below the melting point of the bulk tin. The lowest temperature at which he observed the initiation of aggregation was around 184°C in a deposit about 290 A thick, and the lowest temperature at which the aggregation formed granular structures was about 200°C. In another specimen having a region of thickness of 640 A, he observed the breaking up of the film into separate islands on annealing it in vacuo at 220°C for nearly three minutes.

Saikia (1961) also reported change in orientation of Sn deposits after being annealed. In one experiment he observed (110) orientation to change to a strongly oblique (001) when heated in vacuo between 229° and 238°C. On further heating above the melting point (001) orientation changed to (100).

1.3(h). <u>The Effect of Substrate Cleanliness</u>:

This discussion must include a further very important parameter i.e. the cleanliness of the substrate and presence of any contaminants on it.

When the substrate contains impurities like isolated dust particles on it, these behave as nucleation centres for the evaporated material, and thus may influence the initial growth of the film. It is, therefore, extremely necessary to have a clean surface for deposition.

Impurities may be present on the substrate in many forms. The initial cleaning process may still leave

some residues on the surface, or, contamination from hydrocarbons (oils, greases, etc) from the pumping system may also be present. Both these effects may produce differences in the Van der Waals forces, as they are only operative over atomic distances, and these differences would give rise to variations in film characteristics. If the contaminants are present in the form of isolated islands, the film material may be nucleated preferentially at these impurities. Chemical cleaning may also leave etch pits on glass or other surfaces and these may also act as preferential nucleation sites.

Very many attempts have been made to obtain reproducible standard of cleanliness, especially in the case of glass substrates. Evans and Wilman (1952) suggested the use of nitric acid and propyl alcohol ~~and benzene~~, followed by rinsing with distilled water, for cleaning such substrates. This has been found very useful in all such works in this laboratory.

Hunt (1961) made use of the wetting angle of water on glass as a criterion for indicating cleanliness, but for thin film work, where local nucleation of particles is important, the method seems to be of not much use. The wetting angle is only affected by organic materials and colloidal particles make a negligible effect.

Weaver (1960) used the detergent "Teepol" to remove dirt and grease from glass surfaces, followed by a rinse with distilled water and final polishing with lens tissue. A mixture of chromic and sulphuric acid has also been suggested as a good cleaning agent, but while cleaning the substrate excellently, it also has been found to etch the glass.

The method of using ion bombardment inside the deposition chamber is often considered to cause pitting of the surface, and therefore causes erroneous nucleation sites. The method of ultrasonic vibration has also been claimed to be one of the efficient methods to obtain a highly clean glass surface.

A simple method used in this laboratory has been found to be very satisfactory for cleaning glass, even for sensitive deposit materials like zinc. In this method, the glass substrate is first washed in alochol, then immersed in a mixture of propyl alcohol and added nitric acid followed by thorough rinsing in distilled water and finally drying on clean filter paper as usual, but then further heating in air at 150°C for about 5 mins., and cooling to room temperature.

In the case of active substrates like cadmium chloride or mica, the cleanest possible surface has been obtained by cleaving them in vacuum by some mechanical means (see e.g. Ogawa, Ino, Kato and Ota (1966)).

1.4. Mechanism of the Development of Preferred Orientations in Vacuum-Condensed Deposits:

Various theories have been put forward to account for the development of preferred orientations in thin films. However, several different cases can be distinguished and a single theory cannot explain all cases of the development of orientations. The nucleation process and its dependence on substrate temperature, obliquity of the vapour stream, etc in some cases leads to the development of definite crystal orientations in the initial stage of growth of thin metal films. In other cases the films grow at first with random polycrystalline structure and only develop preferred orientation in the upper regions of thick deposits. In certain cases preferred orientations involve recrystallisation during or after the film deposition.

Volmer (1921) attributed the predominant growth of Zn crystals with (0001) faces normal to the vapour stream direction to the higher rate of lateral growth of such crystals along the (0001) plane. Volmer's theory was based on two initial assumptions viz., (1) supersaturation was sufficiently high to prevent two-dimensional nucleation in the initial stages, and (2), the rate of lateral extension of the faces was determined by the number of atoms striking them per unit area per unit time.

Dixit (1933) considered that the atoms in the early stage of condensation might behave like a two-dimensional gas. With the progress of condensation this might become supersaturated and two-dimensional crystallites be formed. He introduced the idea of a "two-dimensional vapour pressure" associated with this process and thought that the faces having the minimum "vapour pressure" were preferentially developed in contact with the substrate and concluded that these were the crystal faces having a dense population of atoms, i.e. in decreasing order, the (111), (100), (110) ... ... faces in the case of an f.c.c. lattice. However, his experimental evidence did not support this theory.

The results of Burgers and Dippel (1934) showed that in a material having a high melting point, such as CaF_2, condensed on a substrate at room temperature, randomly oriented deposits are obtained at first and preferred orientation begins at a later stage and is associated with development of plane faces on the growing crystals.

Evans and Wilman (1952) and Wilman (1952) made a detailed study of the nature of the orientations developed in Zn, Sb, Bi, Fe, Al, NaCl, NaF and PbS, and drew conclusions of the dependence of orientation on the degree of mobility of atoms of the material, deposit thickness, inclination of vapour stream and roughness of substrate and

deposit surfaces. They reported about two kinds of orientations, viz., (1) growth where initially a densely populated plane is preferentially developed parallel to the mean substrate surface, and (2), thin deposits having little or no orientation at the initial stage of growth, but one-degree orientation develops as the deposit thickness increases. According to them, materials of low melting points and high atomic mobility (Zn, Cd, Sb, Bi, NaCl) develop initially a densely populated plane parallel to the mean substrate surface, even when the vapour stream is oblique. They found that preferred growth of these crystals whose main faces are most nearly normal to the vapour stream, developed at the expense of the others as the deposit became thicker. In the case of the Zn films condensed on amorphous substrate they found that the films tend to grow with (112) orientation yet with occasional (001) habit leading to preferred azimuthal limitation where the vapour stream was incident obliquely, when the thickness was around 2000 A. They attributed the initial spread of orientation to the surface undulation, because the spread was largest on glass, less on rocksalt cleavage faces and least on mica cleavage surfaces. Further deposition gave rise to (112) oriented crystals having azimuthal orientations such that their (001) faces were most nearly normal to the inclined vapour

stream. In some of the Zn deposits (135) orientation was also observed. This was attributed to the modification of the initial (112) orientation during further growth due to the development of faces other than (112), evidently (101).

Evans and Wilman (1952) further found that materials with low mobility (Fe, Al, NaF, PbS, CaF_2) have little or no orientation in thin layers at room temperature. These materials showed a tendency to develop a preferred orientation with an oblique axis when the vapour stream was oblique. They concluded that the orientation orginated from the fine scale roughness of the deposit surface followed by progressive heating of the substrate and the growing deposit by the incident heat radiation and kinetic energy of the condensed material, so that the mobility of the atoms gradually increased.

Sachtler (1954) observed that in the early stage Ni films are randomly oriented when deposited at room temperature, but are found to develop orientation on heated substrates. He argued that in the early stage of deposition films are made up of unoriented crystals bounded by a number of crystallographic planes. The rate of growth of all the planes are not equal. Those having a faster growth have the direction of most rapid growth perpendicular to the substrate surface. For b.c.c. metals the $\langle 111 \rangle$

direction has been shown to be the fastest growth direction and for f.c.c. metals ⟨110⟩ .

Bauer (1961), however, seems to disagree with the above view. According to him, although the rate of growth for f.c.c. metals in the ⟨110⟩ direction is faster than along the ⟨111⟩ and ⟨100⟩ directions, there may be even higher growth rate in other directions.

According to Bauer (1956, 1961, 1963) some materials like the alkali halides develop orientation which varies with the deposit thickness. The "initial orientation" (I-O) developed in the thinnest stage of the deposit (or in the upper regions of relatively thin deposits) is representative of the lowest potential energy configuration of the atoms in the crystals relative to the substrate. At a later stage, the deposits show a transitional stage, following which the orientation changes progressively towards a stable texture. He concluded that the final orientation (II-O) exhibited by the upper regions of the thick deposits tended to show two-degree orientation when the vapour stream was incident obliquely. His observations were confined to the high supersaturation stage, i.e. under conditions where two-dimensional nucleation was not a growth rate-determining factor.

He concluded that in the initial stage, a preferred

crystallographic plane tends to develop parallel to the surface of the substrate. The later transition to the final two-degree orientation is due to the plane faces being developed on the crystals and hence most rapid growth of those crystals oriented with such a face normal to the vapour stream. His theory seems to have neglected the effect of the residual air pressure, which in fact has a significant role in the orientation phenomenon.

When the deposit atoms or molecules have sufficient mobility (i.e. at a high enough substrate temperature) the first deposit crystals may grow in a definite orientation. The nucleation process should thus have a pronounced effect on the nature and development of the preferred orientation in such vapour-condensed deposits. Reviews of epitaxy in deposits on single-crystal substrates have been given by Van der Merwe (1949), Seifert (1953), Pashley (1959), etc. On epitaxially inactive substrates, the nucleation process can similarly lead to crystal nuclei having a definite crystal face in contact with the substrate.

Walton (1962) considered the effect of the nucleation and supersaturation on the development of preferred orientation in thin metal films. He has interpreted two much used terms as follows: (1) "The smallest stable cluster" is the smallest cluster which has

a probability greater than one-half of growing. That is, it will on the average receive an atom from the two-dimensional gas of singly adsorbed atoms before an atom leaves the cluster. (2) "The critical nucleus" contains one atom less than the smallest stable cluster and its configuration is such that the addition of a single atom in the appropriate location will produce the smallest stable cluster. The critical nucleus has the probability of growing less than or equal to one-half.

It is possible to conceive of substrate temperatures which are so low that the critical nucleus is a single atom. At sufficiently high supersaturations (low substrate temperature and/or high rate of deposition), the nucleation of the deposit consists of the formation of pairs. Each time a pair is formed it does not, on the average, dissociate; and begins to grow as a part of the deposit. Since the pair is assumed to be stable, all other single bonds are stable and each time a single atom strikes the cluster it is trapped. This is a random process, and therefore the cluster cannot be expected to grow with a single orientation except in the special case where adsorption sites on the substrate coincide with the location of atoms in a crystallographic plane of the deposit.

If the supersaturation is lowered, a stage will be

reached at which a single bond is unstable, i.e. if an atom is attached to the cluster by a single bond, on the average, it will leave the cluster before another atom can arrive to replace it. At supersaturations below this, double bonds may still be stable. Thus an atom which joins the cluster in such a way that it is attached to two other atoms, will remain, while an atom which joins the cluster so that it is joined to one other atom, will leave. Therefore, an oriented structure can now be formed. Walton thus suggests that if the substrate temperature is low enough or the incidence rate high (supersaturation high), a single bond is stable and no preferred orientation can be expected. If the supersaturation is low enough for multiple bonds to be stable, an oriented deposit may result. Walton arrived at the following important conclusions.

(1) The epitaxial temperature is the substrate temperature at which a single bond becomes unstable. This temperature (T) is connected to the rate of deposition by the following relationship:

$$T = \frac{-(U_2 + Q_{ad})}{k.\ln(Ra^2/\gamma)}$$

where U_2 = binding energy of a single atom to the cluster,

Q_{ad} = binding energy of a single atom to the substrate,

a = distance between the adsorption sites,

ν = frequency of vibration,

R = rate of incidence of a vapour stream,

k = Boltzmann constant.

At a given substrate temperature a change from disoriented to an oriented structure is possible as the incidence rate is decreased and vice versa.

(2) Most of the observed orientations are such that closely packed lattice planes are prallel to the substrate and the order of preference for f.c.c. crystals is (111), (100) and (110). The critical nucleus for a (111) orientation is a pair when a double bond is stable, for a (100) it is three atoms, and for the (110) it is four atoms.

(3) Changes in orientation from a (111) to a (100) may be related to a change in the size of the critical nucleus accompanied by a change in its structure.

SECTION 2.

EXPERIMENTAL.

2.1. The Electron Diffraction Technique:

The electron diffraction camera (fig.1(a)) used for recording the electron diffraction patterns, is in general similar to that used and described by Finch and Wilman (1937), with the mercury diffusion pumps replaced by oil diffusion pumps. It essentially consists of two parts - the discharge tube and the main diffraction chamber. Electrons are emitted from a polished metal surface in a cold cathode discharge in the discharge tube. By supplying constant current to the discharge, a monochromatic beam of electrons is obtained, which is limited to a very fine beam by means of a pin-hole of about 0.1 mm diameter of a diaphragm made of nickel, mounted in the anode block. The beam can be further collimated by use of a number of diaphragms in the main body of the camera. The beam can be focussed to a point on the fluorescent screen by applying a coaxial magnetic field by a variable current in a coaxial focussing coil placed at 48-50 cm from the specimen. The focussed beam may be moved about by tilting the plane of the magnetic lens, and the beam of electrons is then allowed to pass through a very thin specimen film or fall at grazing incidence on a more massive specimen.

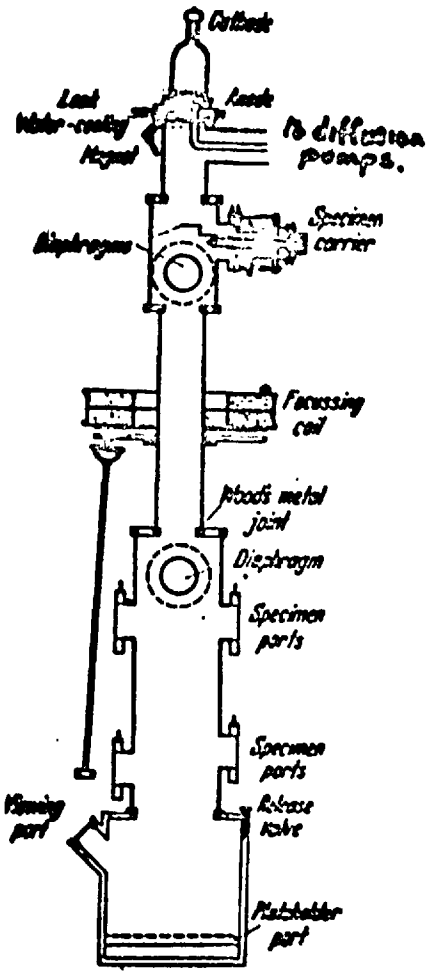

Fig.1(a) Electron Diffraction Camera.

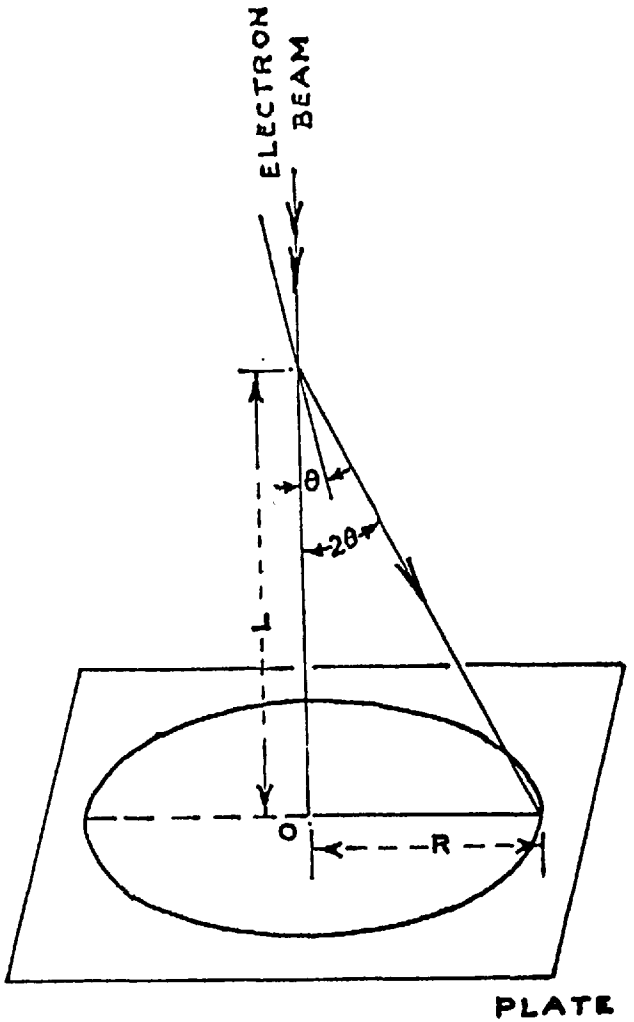

Fig. 1(b) Principle of Electron Diffraction.

The diffraction pattern is recorded on a photographic plate contained in a plate holder. The plate holder is specially designed to contain more than one plate, and is fitted with a fluorescent screen for visual purpose.

The electron accelerating voltage used in the present work was in the range 45-60 KV.

2.2. Interpretation of Electron Diffraction Patterns:

Methods of interpretation of electron diffraction patterns have been described by Thomson (1930), Finch, Quarrell and Wilman (1937), Thomson and Cochrane (1939), Laue (1944) and Pinsker (1949, 1953). More recently, very useful and convenient methods of interpreting the electron diffraction patterns from rotating crystals or one-degree-oriented polycrystalline specimens have been developed by Wilman (1952) in this laboratory. Methods of interpretation of Kikuchi-line patterns from single crystals have also been developed by Wilman (1948a,b), who has also given interpretation details for spot patterns from crystal groupings (Wilman 1950, 1951).

The electron diffraction patterns of diffuse maxima from molecular crystals were discovered by Finch & Wilman, 1937 and interpreted in this laboratory by Charlesby, Finch and Wilman (1939) and the maxima of intermediate diffuseness

due to thermal molecular oscillations were recognised by Charlesby and Wilman (1942).

A further special type of electron diffraction pattern is that associated with a continuous or discrete "directed disorientation", which is associated with stresses in epitaxial layers on single crystal substrates, due to the lattice misfits (Evans and Wilman, 1950; Goswami, 1950; Gharpurey, 1950; Kumar, 1953; Reddy and Wilman, 1959).

In the present experiments reflection electron diffraction technique is used to study polycrystalline deposits on inert substrates. These give either a continuous ring pattern from randomly oriented crystals or a spot (or arc) pattern on various ring positions from preferentially oriented crystals, and hence methods to interpret these two cases will be discussed here in detail.

2.2 (a). Interpretation of a Continuous Ring Pattern:

In considering the diffraction pattern from a polycrystalline specimen, the specimen can be regarded as equivalent to a single crystal rotated through the same range of orientation as exists in the specimen. So, if there are many crystals with random distribution in the path of the beam, a pattern of rings will result analogous to the X-ray powder pattern, diffracted beams arising whenever Bragg's law is saisfied. From the geometry of fig. 1(b)

it is seen that

$$R = L \tan 2\theta \qquad (2.1)$$

where, R = radius of the ring,

L = distance of the central spot from the point of incidence of the electron beam on the specimen,

θ = Bragg's angle of grazing incidence.

Again, from Bragg's law,

$$2 d \sin\theta = n\lambda \qquad (2.2)$$

where, d = spacing of the net planes,

n = order of reflection,

and λ = wavelength of the electron beam.

From equations (2.1) and (2.2) we get,

$$\frac{d}{n} \sim \frac{\lambda L}{R} \qquad (2.3)$$

for small values of θ. A multiplying factor $[1 + \frac{3}{8} \cdot \frac{R^2}{L^2} + \ldots \ldots]$ is used to give a still closer approximation.

The general equation relating the net-plane spacing d of any plane (hkl) with unit cell constants a, b, c and axial angles α, β, γ and the corresponding Miller indices h, k, l, is

$$\frac{1}{d^2} = \frac{1}{(1+\sum\cos^2\alpha + 2\cos\alpha\cos\beta\cos\gamma)} \times \left[\sum\frac{h^2\sin^2\alpha}{a^2} + \sum\frac{2hk}{ab}(\cos\alpha\cos\beta - \cos\gamma)\right] \qquad (2.4)$$

For highly symmetrical crystal systems, we have from equation (2.4):

$$\begin{aligned}
&\text{Cubic} && \frac{1}{d^2} = \frac{h^2+k^2+l^2}{a^2} \\
&\text{Tetragonal} && \frac{1}{d^2} = \frac{h^2+k^2}{a^2} + \frac{l^2}{c^2} \\
&\text{Orthorhombic} && \frac{1}{d^2} = \frac{h^2}{a^2} + \frac{k^2}{b^2} + \frac{l^2}{c^2} \\
&\text{Hexagonal} && \frac{1}{d^2} = \frac{4}{3a^2}\,(h^2 + k^2 + hk) + \frac{l^2}{c^2}
\end{aligned} \qquad (2.5)$$

Measuring the ring radius R from a diffraction pattern, the net-plane spacing d can be estimated, and values of h, k, l must then be assigned by trial and error or graphical methods, when λ, L and a, b, c are known.

The wavelength λ of the electron beam can be determined as follows:

The energy of an electron with charge e, mass m, velocity v and accelerated through a potential difference V is given by

$$eV = \frac{1}{2} mv^2 \qquad (2.6)$$

From De Broglie's equation,

$$\lambda = \frac{h}{mv} = \frac{h}{\sqrt{2\,m\,e\,V}} \qquad (2.7)$$

On substituting the appropriate values of h, m, e and V, the expression for the wavelength of the electron

becomes:

$$\lambda \simeq \sqrt{\frac{150}{V}} \text{ A} \qquad (2.8)$$

Considering the relativistic mass correction, equation (2.8) can be shown to become

$$\lambda = \frac{ho}{\sqrt{eV\ (eV + 2m_o e^2)}} \qquad (2.9)$$

where the symbols have their usual meanings.

Hence, applying a known potential difference V to an electron beam, its wavelength can be determined.

2.2(b). Interpretation of Arc or Spot Pattern from One-degree Oriented Specimens:

In such a specimen, the crystals have a certain type of lattice row [UVW] in common, but otherwise random orientation about this axis. Such a lattice row is called the orientation axis. Such a deposit will give an electron diffraction pattern equivalent to that which would be obtained by rotating a single crystal about the orientation axis or any axis parallel to it. The one-degree orientation is very rarely perfect and there is always a certain amount of spread of the orientations of the crystals away from the mean orientation axis. This, along with the undulating nature of the substrate causes the diffraction maxima to appear as arcs instead of spots.

The natural undisturbed orientation developed in most crystalline layers during deposition on inert substrates are best studied by the reflection method, where the electron beam strikes the surface at nearly grazing incidence. The pattern in this case is due to transmission through the projecting crystals which the electron beam traverses without appreciable loss of energy. Slightly more than half of the diffraction pattern is cut off by absorption in the opaque specimen.

The Laue-zone method of interpretation of rotating crystal patterns or one-degree oriented polycrystalline specimens was developed in general form by Wilman (1952). For the case of orientation of an (HKL) plane parallel to the substrate, it is necessary to determine U:V:W, where [UVW] is the lattice direction perpendicular to the (HKL) plane. The ratio U:V:W for the general triclinic case have been calculated by Wilman (1952), and from this, expressions for crystals of higher symmetry can be derived, for example

$$\begin{aligned}
&\text{Cubic :} && U:V:W = H:K:L \\
&\text{Orthorhombic:} && U:V:W = \frac{H}{a^2} : \frac{K}{b^2} : \frac{L}{c^2} \\
&\text{Tetragonal:} && U:V:W = H:K:L/\left(\frac{c}{a}\right)^2 \\
&\text{Hexagonal:} && U:V:W = (2H+K):(H+2K):\tfrac{3}{2}L/\left(\frac{c}{a}\right)^2
\end{aligned} \qquad (2.10)$$

A diagram is constructed showing the ring positions and also the layer lines or Laue-zones associated with the [UVW] lattice row. These layer lines are practically straight and normal to the projection of [UVW] lattice rows on the plate and are equidistant with spacing $\frac{\lambda L}{T_{uvw}}$, where L is the camera length, T_{uvw} is the lattice translation vector along the [UVW] direction. Any diffraction with indices hkl will lie at the intersection of the hkl ring with the corresponding h'th order layer line, where

$$h' = hU + kV + lW \qquad (2.11)$$

Such intersecting points satisfying the relation (2.11) are marked in the diagram, bearing in mind all the symmetrically equivalent planes {hkl} giving rise to diffractions on the ring position concerned.

If the one-degree orientation is very strong then the pattern consists of short well defined arcs or spots; if the orientation is weak then spots will spread into arcs along the rings. The angular spread of a spot along the ring radius is a measure of the strength of the orientation, i.e. it is a measure of the degree of exactness with which the crystallites tend to be oriented with a plane parallel to the surface.

2.3. Measurement of Diffraction Patterns and Identification of the Material:

We have $d = \frac{\lambda L}{R}$, so in order to determine d, λL and R are estimated. The ring radii R are measured by using a travelling microscope.

A calibrated sphere-gap voltmeter is used to measure the wavelength λ of the electron beam. The readings from the scale of the gap directly give the electron accelerating voltage in KV and by using equation (2.8), the corresponding value of λ can be determined.

The camera length L, which is the distance between the point on the specimen where the beam impinges and the photographic plate, is measured directly. In the present work this length varied between 45 cm and 48 cm.

When more accurate determination of λL is necessary, a pattern from a material of known lattice dimensions is simultaneously recorded along with that of the unknown material, from which λL can be determined.

For identifying purposes, the experimental pattern from the unknown substance may be compared with the data obtained from X-ray or electron diffraction powder patterns from known materials. For the X-ray powder pattern data there is available the card-index file of the American Society for Testing Materials. For a comparison, (a) the

values of R are plotted on a strip of paper using a logarithmic scale, and (b), a second plot is made of "d" values obtained from X-ray data for a relevant material on a similar but reversed logarithmic scale. The two plots may then be compared. If a correspondence is not obtained, plot (a) must be compared with plots similar to (b) of some other material which may possibly be present. Alternatively, one can make use of Hull-Davey charts to index the diffraction rings if the material is cubic, tetragonal or hexagonal, from which the lattice parameters of the material can often be determined, which may then lead to identification of the material.

2.4. Vacuum Apparatus for Preparation of Films by Condensation in Vacuum:

2.4(a). System to Produce a Residual Air Pressure of 10^{-3} to 10^{-4} torr.

In order to prepare specimens at such a relatively high pressure, an Edwards "Coating Unit Model 6E" was used. The system consisted of a Metrovac Rotary Vacuum pump, and a small oil diffusion pump of oil charge 11 cc. The system could produce a residual air pressure of approximately 10^{-3} torr in a bell-jar of dimensions 15 cm dia. x 30 cm long. The pressure was measured by using a "Speedivac" Penning type gauge head connected to an Edwards Pirani

Vacuum Gauge unit. A rubber gasket sealed the base of the bell-jar. At the base plate of the system, glass-metal seals were provided for electrical connections. Two copper electrodes of diameter 2 mm and of suitable lengths were used for further connecting these terminals to a tungsten heater filament containing the metal to be evaporated. The heater filament consisted of a coil of three turns of 0.012" dia. tungsten wire, the coil being 2 mm dia. x 4 mm long. A pyrex flat-bottomed dish, 12.5 cm dia. and 6.5 cm high, was used as a screen inside the bell-jar to prevent the metal vapour from going into the pumping lines. "Spec-pure" zinc and cadmium films were prepared in this system.

2.4(b). <u>System to Produce a Residual Air Pressure down to 10^{-6} torr</u>.

This system consisted of a Metrovac rotary backing pump, an Edwards F.203 oil diffusion pump using Apiezon "C" oil, and an Edwards "Speedivac" liquid nitrogen trap. The evaporation chamber was a pyrex tube 20 cm long and 7 cm in diameter. One end of the tube was sealed with picein wax to a brass annulus, which was soldered to the 2" diameter stainless-steel mouth of the ionization-gauge head (Edwards 1G2M). The other end, which was in the form of a ground flange, could be fitted on to the ground brass flange of the pumping system near the liquid nitrogen trap, with a neoprene "O" ring seal (fig.2).

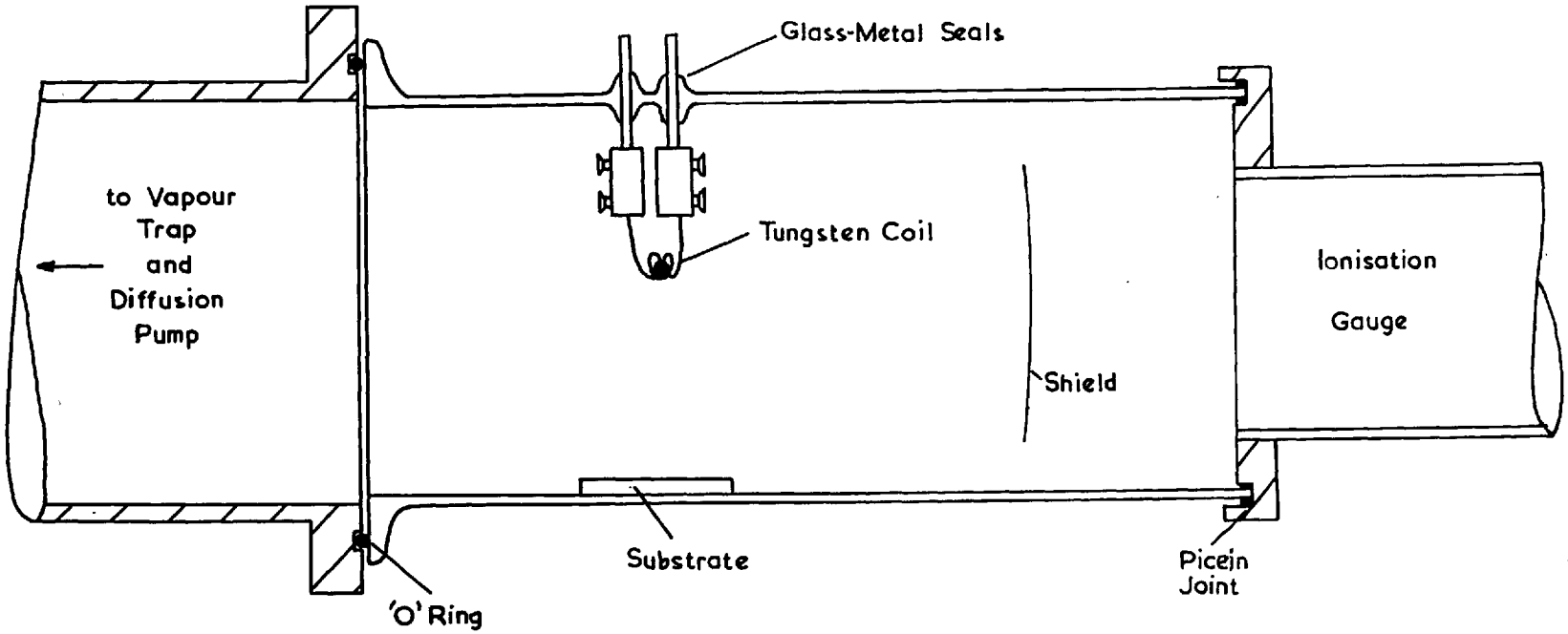

FIG. 2. THE EVAPORATION CHAMBER

Four tungsten electrodes were fused through the wall of the tube for electrical connections. A pyrex shield was used to prevent any metal vapour from entering the ionization gauge head during the evaporation of the metal. Further precautions were taken while evaporating Zn and Cd to protect the gauge head. Two brass annulus rings were properly (fixed on flat pieces) put one in front and the other at the back of the pyrex shield. The external and internal diameters of the rings were 6.5 cm and 3 cm respectively. This arrangement was found quite satisfactory.

The system could attain a pressure of 2 $x10^{-5}$ torr without use of liquid nitrogen within 90 minutes and 5 $x10^{-6}$ torr with use of liquid nitrogen after a further hour of pumping.

The tungsten heater filament coil was first pre-heated at a pressure of 10^{-4} torr. An amount of about 0.3 gm of the experimental metal was carefully introduced into the coil and a bead was made by melting it on the filament by passing a current of about 6 amp. at a pressure of 10^{-4} torr. A small quantity of the metal was always evaporated away in vacuum in order to remove any surface impurities.

The system was first used for making films of Zn

and Cd. In view of the high mobility of these metals, the whole system had to be thoroughly cleaned, and a new ionization gauge head (Edwards IG2M) fixed before further use of the system to prepare films of silver, gold and copper.

2.4(c). Ultra-High Vacuum System:

In order to prepare high-purity films it was necessary to reduce the number of residual gas molecules inside the evaporation chamber. For this purpose an Ultra-high vacuum system (type FQD 45) supplied by Vacuum Instruments and Products Ltd., was used. The getter-ion pumps and the stainless-steel body were made by Ferranti Ltd.

The vacuum system consisted of a pyrex bell-jar, 11½" diameter, 14½" high, sealed by a viton gasket to the flange of a cylindrical stainless-steel vessel of diameter 11½" x 20" high. The stainless-steel vessel was fitted with ten flanged ports for connecting a mass-spectrometer (type MS 10, AEI), an ionization gauge (Mullard 10G-12), electrical connections, thermocouples, and a rotatable axis (from Torvac Ltd) on which was mounted a shutter so as to make films stepwise of various thicknesses. Copper/ceramic seals for electrical lead-throughs and metal-valves were used throughout except for the seal on the bell-jar. When the pressure was to be reduced below 1 $x10^{-7}$ torr, the

bell-jar was replaced by a stainless steel top, sealed to the main body by a copper ring, using special steel clamps supplied for the purpose. The system was pumped by sorption, sublimation and getter-ion pumps.

The fore pumping was carried out by two sorption pumps used alternatively. Since a sorption pump relies for its pumping action upon the absorption of gas molecules by a chilled molecular sieve (aluminium calcium silicate) contained in the lower portion of the pump, the pumps were chilled by putting liquid nitrogen flasks around them for a sufficient period of time. The major constituents of the air viz., nitrogen, oxygen and argon, could be absorbed by these pumps and a pressure of 1 $x10^{-3}$ torr could be obtained. The pumping action by these pumps is reversible and after they were isolated by the all-metal valves from the main body, they were allowed to warm up to room temperature, to give off the adsorbed gas.

Titanium filaments (85% titanium, 15% molybdenum) were used for the sublimation pump. This pump operated by subliming titanium atoms from the resistance heated filament (at 45-55 amps) and depositing the titanium on the adjacent walls of the system, which then formed stable compounds by reacting with the active gases present within the system. There was no pumping speed for the noble gases and these were

removed by using the ion-pump. To run the sublimation pump efficiently, the rate of sublimation was so adjusted that a fresh layer of titanium was deposited as soon as the old one became inactive.

The Ferranti Getter-ion pump (FJD 141) provided a pumping speed of 140 litres/sec. at pressures lower than 10^{-4} torr. The system could attain a pressure of 1 $x10^{-6}$ torr with the bell-jar and 5 $x10^{-7}$ torr with the stainless-steel top without baking, within 5 to 6 hours. After baking the system overnight at a temperature of 150°C with the bell-jar and at 250°C with the stainless-steel top, the pressure could be reduced to 1 $x10^{-7}$ torr, and 1 $x10^{-8}$ torr respectively. Since the present work involved especially pressures down to that range only, further lower pressures were not tried, although it was claimed that the system could attain a pressure of 1 $x10^{-10}$ torr or even less.

Since titanium from the sublimation-pump unit was deposited over most of the stainless-steel chamber, it was considered desirable to mount a pyrex beaker 7 cm dia. and 6 cm high, round the region of the tungsten filament used for preparation of specimens, to shield the substrate from any trace of titanium. The open upper end of the beaker was shielded by an inverted pyrex crystallising dish, 15.5 cm diam. and 7 cm high, with its mouth at the level of the open

end of the beaker. These two glass shields were cleaned by acetone or propyl alcohol before each experiment.

The tungsten heating spirals were similar as described in § 2.4(a) except that the straight parts leading to the spiral were 5 cm long.

2.4(d). Preparation of Substrates.

Two kinds of substrates were used, viz. (1) glass substrates and (2) stainless-steel substrates. The glass substrates were portions of microscope slides of thickness 0.15 cm and having smooth polished surfaces, 0.5 cm x 3 cm. These were cleaned just before use by a solution of propyl alcohol and nitric acid. The chemical action was sufficient enough to degrease the substrates. When the reaction between alcohol and nitric acid subsided, the substrate was taken out, rinsed with distilled water and most of the water removed by touching the edge with a clean filter paper. A substrate so cleaned was immediately introduced into the deposition chamber.

The stainless steel substrates were prepared from 2.5 mm thick sheets of stainless steel, and were 0.5 cm broad and 3.5 cm long, or sometimes 0.4 cm broad and 1.5 cm long. These substrates were abraded with wet 0, 2/0, 3/0 and 4/0 emery paper in sequence to ensure a finely smooth surface. They were finally polished with "Bluebell" metal polish on

'Selvyt' cloth. The substrates were next cleaned by washing thoroughly with acetone or propyl alcohol. While for Ag, Au and Cu this was sufficient to make the substrates virtually grease-free, for the hexagonal metals Zn and Cd further care was necessary. Evans (1950) experienced splotchiness in deposition of zinc on glass substrates and he pointed out this as due to high reflectivity of Zn on even slightly contaminated glass surfaces. While in the present work the same trouble was also experienced with these hexagonal metals, yet it was observed occasionally that some deposits were found to be fairly continuous and uniform when the glass substrates were cleaned several times by repeating the process mentioned above. Much improvement was achieved when the polished stainless-steel substrates were degreased still more completely by heating them in air in a pyrex test tube to a temperature of 150°C. The substrate was then allowed to cool down to room temperature. An ordinary mercury-in-glass thermometer was used, well cleaned before use. With substrates polished, cleaned and degreased in this way, uniform and continuous deposits of the hexagonal metals were obtained almost in a hundred per cent of the cases.

The substrates were placed beneath the preheated vapour source at a distance varying from 1-3 cm from it with

one end directly under the source, so that the angle of incidence of the vapour stream could vary from 0^{o} at this end to about 45^{o} at the other.

2.5. Preparation of Specimens and Measurement of Rate of Deposition and Thickness of Films:

2.5(a). Preparation of Films of Zn and Cd:

Spectrographically standardised rods of these metals (approx. dimensions: 7 mm diameter and 10 cm long each) were supplied by Johnson Matthey Ltd., London, in well-protected covers. The supplier's reports on the estimates of the quantities of impurities are given below:

Materials supplied	Impurities	Estimate of Quantity Present (parts per million).
(1) Spec-pure zinc	Iron	5
	Silicon	1
	Cadmium, Bismuth Magnesium, Calcium	Each less than 1
(2) Spec-pure cadmium	Bismuth	1
	Iron	1
	Aluminium, Copper Calcium, Magnesium & Silver	Each less than 1

The beads of any of these metals were prepared following the procedure described in 2.4(a). A small quantity of the metal was melted in the loop of the heater-filament in vacuo at a residual air pressure of 5×10^{-3} torr

to 2 x10^{-4} torr. The heating current was about 4 amps, which was just sufficient to melt these metals. The distance between the source and the substrate in these experiments was 3 cms. Various rates of depositions starting from 30 A/sec up to 1000 A/sec were obtained by simply varying the heating current slightly. These metals gave serious difficulties in determining the thickness of their films. Since these hexagonal metals were highly mobile even at a pressure of 10^{-3} torr, and since the walls of the bell-jar (or the pyrex glass tube) reflected the metal vapour profusely towards the substrate thus causing a great deal of uncertainty in the film thickness estimation, it was extremely necessary to reduce the reflection of metal vapour from the surrounding walls. For this purpose, the pyrex flat-bottomed dish (cf.§2.4(a)) which contained the stainless-steel substrate, was baked for 12 hrs at a temperature of 150°C in a thermostat and then allowed to cool down to room temperature before introducing it into the evaporating chamber. The process was repeated for every experiment. This reduced the reflection of the hexagonal metal atoms from the walls of the immediate surroundings as indicated by bright uniform deposition on the inner walls of the flat-bottomed dish. However, the deposition chamber of the system described in §2.4(b) could

not be baked due to practical difficulties. In this case, only the pyrex shield and the brass annuli were baked and the rest had to be degreased by acetone several times. The utmost care was taken in each experiment not to touch anything inside the chamber by the fingers. Properly degreased stainless-steel tweezers were used for this purpose.

During the evaporation of these metals the pressure fell down by about a factor of six as was indicated from the pressure measurements before and after evaporation. This was due to the gettering action of the metal vapour atoms with the gas molacules in the system. It is admitted that the exact pressure during the deposition process was not known.

Zn was evaporated at pressures of 5×10^{-3} torr, 2×10^{-4} torr, and 1×10^{-5} torr; Cd was evaporated at a pressure of 5×10^{-3} torr only. The thickness of the films was varied over a wide range, from 150 A to about 10,000 A. After preparation of the films, 45 minutes to an hour was always allowed for the film to cool down to room temperature before letting in air to the system. The specimen was then quickly transferred to the diffraction camera for examination.

2.5(b). Preparation of Gold, Silver and Copper Films:

Spectroscopically standardised metals supplied by Johnson Matthey Ltd were used for the present work. Their estimates of the impurities in these metals are as follows:

Materials supplied	Impurities	Estimates of quantity present (parts per million)
Spec-pure silver rod	Iron	2
	Copper	1
	Magnesium, Manganese	Each less than 1
Spec-pure Copper rod	Nickel	3
	Iron	2
	Silver, Calcium, Magnesium, Silicon Manganese, Sodium	Each less than 1
Spec-pure Gold rod	Iron	3
	Silver	3
	Copper, Magnesium	Each less than 1

The general outline of the technique of preparation of films of these metals was as described in §2.5(a). Polished stainless-steel substrates were used, unless otherwise stated, for preparation of films of these metals. In view of the high melting points of these metals (1063°C for gold, 1083°C for copper and 960.5°C for silver) a current of 6 to 7.5 amps had to be passed through the heater filament in order to make the bead and to evaporate the metal. The distance between the bead and the substrate in

the cases of silver and copper was 3 cm, and 1 cm in the case of gold. Since the chemisorption on copper was comparatively higher than the other two metals, a copper bead had to be preheated for about 8 minutes by a current of 3-4 amps just before the deposition was started. The preheating for gold and silver was around 3 minutes. The filament preheating, bead making, etc. were carried out at a pressure of 1 $x10^{-4}$ torr in the system described in 2.4(b). Copper and gold films were prepared at a pressure in the range of 5 $x10^{-3}$ torr to 1 $x10^{-8}$ torr and silver films were prepared at pressures of 1 $x10^{-6}$ and 2 $x10^{-7}$ torr only. The rate of deposition used for gold and silver was 28 to 35 A/sec, and that for copper was 10 to 20 A/sec. For preparation of films of gold thicker than about 5000 A, glass substrates were used, since such films were found to peel off stainless-steel substrates. A few of the gold, silver and copper deposits were prepared simultaneously on glass and stainless-steel substrates to examine if there was any change of structure with the change of substrates. No difference was, however, obtained.

Since the U.H.V. system was to be very often baked and pumped by heating the titanium-molybdenum filaments within it, a considerably long period of time was always allowed to cool down the system to room temperature before

any deposition was carried out. A calibrated thermocouple junction was introduced within thesystem and the hot junction was kept just below the pyrex beaker containing the substrate, in order to record the temperature of the system in general and of the substrate in particular. Deposits of variable thicknesses could be prepared by controlling the rotatable shutter by hand from outside. Usually, three deposits were prepared at a time, one at the middle of the substrate to receive the vapour beam normally and the other two on either side of it, receiving the vapour beam at an angle of about 20-25^{o} to the normal.

2.5(c). Estimation of the Rate of Deposition and the Thickness of Films:

The thickness of a film was estimated by assuming uniform spherical distribution of vapour atoms from a point source onto the plane substrate. Under this assumption, the thickness T of a spherical film of radius r is given as:

$$T = \frac{m_1 - m_2}{4\pi r^2 \rho} \qquad (2.12)$$

where m_1 and m_2 = masses of the source before and after evaporation,

ρ = density of the metal,

r = source-substrate distance.

The rate of deposition dT/dt is given as:

$$\frac{dT}{dt} = \frac{m_1 - m_2}{4\pi r^2 \rho t} \qquad (2.13)$$

where t = total time of deposition.

The more general equation for thickness of film is :

$$T = \left(\frac{m_1 - m_2}{4\pi r^2 \rho t} \right) \cos^3 \theta \qquad (2.14)$$

where θ = the angle of inclination of the vapour stream measured from the normal at the point considered.

The thickness of the metallic film calculated from eqn. (2.14) has been found to be satisfactory for the present conditions, for deposits on substrates at room temperature. The thickness calculated from the mass loss of the bead was in some cases verified by comparison with the mass gain of the substrate after deposition. In most of the cases the possible error has been found to be within 5%. The thicknesses of a few of the silver deposits were checked by a multiple-beam interference technique, using a Vickers projection microscope. The variation of these results from those calculated from equation (2.14) was found to be negligible. The film was first prepared in the usual way on a glass substrate. Then, a step was created along the length of the film by scratching it with a sharp and clean razor blade. Another evaporation was carried out on the top of this film to give a high reflecting power to the

scratched part of the specimen, but leaving the step-height unchanged. The specimen was then pressed against another very thin film prepared from the same metal on another glass substrate. Beautifully coloured Fizeau fringes were observed when examined under white light in the projection microscope. These fringes showed a distinct shift on the two sides of a step of the film, from which the number of fringes shifted could be counted and, knowing the wavelength of the particular colour of the fringe, the thickness of the step (which is also the thickness of the film) could be calculated. Monochromatic light (approximately) gave sharper fringes and greater accuracy. Figs. 3a and 3b show the fringe shifts across the steps of two silver specimens prepared at a residual air pressure of 2×10^{-4} torr.

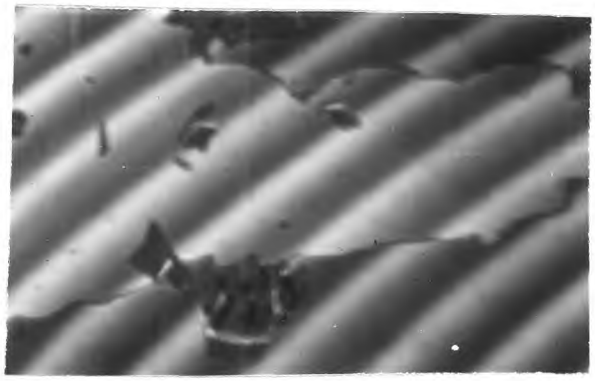

(a) At i = 0^{o}

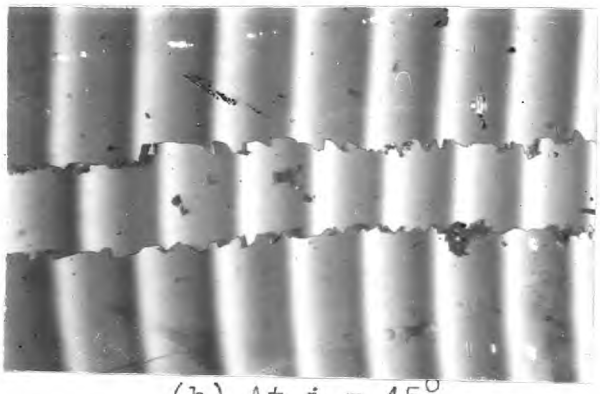

(b) At i = 45^{o}

Fig.3. Photographs of typical interference fringes for estimation of metal deposit thickness (filtered mercury arc light, green, λ = 5461A). The fringes were formed between the specimen surface (in back-reflection) and a silvered cover-slip pressed very closely against it. The specimen film had been scraped away along the central strip and the whole then silvered by deposition of silver in vacuum. The fringe-shifts were 3.2 fringes in (a) and 1.6 in (b) corresponding to 3.2 $\lambda/2$ and 1.6 $\lambda/2$ film thicknesses respectively, i.e. 8740A and 4370A.

SECTION 3.

RESULTS.

3.1. The Structure of Gold Films Condensed in Vacuum on to Polished Stainless Steel at Room Temperature at Approximately Constant Rate of Deposition (28 to 33 A/sec), in Relation to Film Thickness and Residual Air Pressure:

Spectroscopically pure gold was deposited on to polished stainless-steel substrates at room temperature in air at various residual pressures. The rate of deposition was maintained at 28-33 A/sec. The source to substrate distance was fixed at 1 cm.

The experimentally observed results are presented in graphical form in Fig.4. The results at different thicknesses of films and residual air pressures are presented below in greater detail.

A few deposits from commercially pure gold wire (99.8% pure) were also prepared at 5 $x10^{-3}$ torr. These showed only random orientation up to a thickness of about 9000 A. However, further work with this gold was discontinued, and the results discussed here are from the deposits of the spec-pure gold.

3.1(a). The Structure of the Gold Deposits Condensed at Normal Incidence of the Vapour Stream:

Gold condensed at pressures from 1 X10^{-8} torr to 5 x10^{-3} torr on to stainless steel substrates at room temperature showed initially randomly oriented crystals having normal f.c.c. structure (Fig.4). At a certain thickness, increasing with increasing residual air pressure, the deposits began to show (111) preferred orientation. The electron diffraction photographs show refraction effects indicating the development of the densely populated octahedral faces on the upper part of the growing crystals. The minimum thickness at which (111) orientation was observed was 240 A, in deposits prepared at 1 x10^{-8} torr. This critical thickness at which (111) orientation developed at the highest pressure (5 x10^{-3}) was ~700 A.

Above a particular thickness the (111) orientation was found to change to a mixture of (111) + {111} twinning. At a later stage a mixture of (111) + (211) orientation was found. In a few cases a mixture of (211) + (100) was observed. Beyond this particular thickness, stable (211) orientation was obtained at all the pressures under consideration.

While the change in orientation from random to (111) was quick, the change from (111) to (211) was

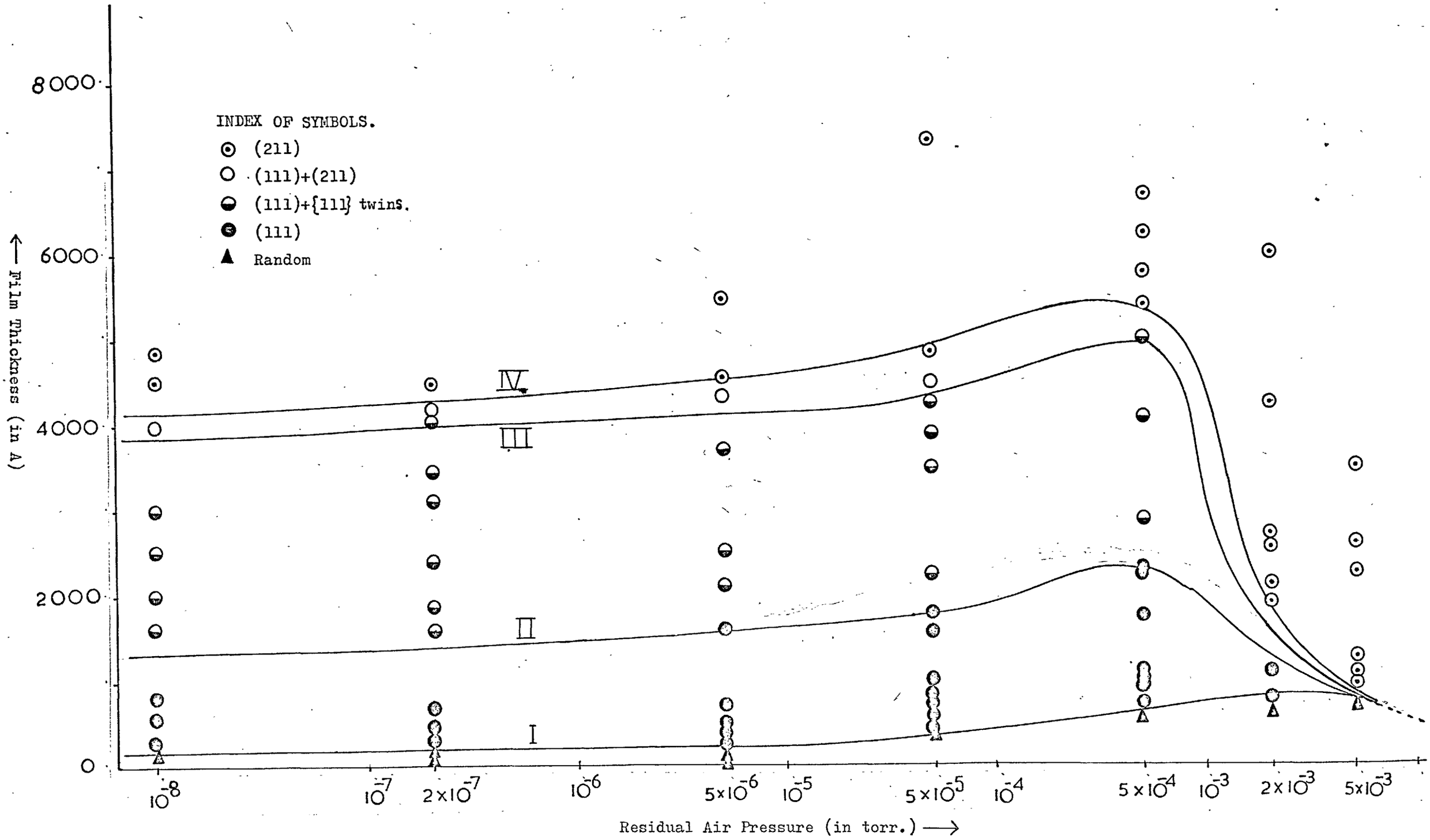

Fig.4. VARIATION OF SURFACE ORIENTATION OF GOLD FILMS CONDENSED ON STAINLESS-STEEL AT ROOM TEMPR., WITH FILM THICKNESS AND RESIDUAL AIR PRESSURE (RATE OF DEPOSITION 30 to 33A/SEC.).

$\angle i = 0^\circ$

relatively slow. At the pressure 5 x10^{-3} torr, the thickness at which (211) was first found to develop was 1250 A, which was the minimum thickness observed for this preferred orientation.

The electron diffraction evidence on which the above general observations are based is described below.

3.1a (i). <u>The Structure of the Gold Deposits at the Initial Random Orientation Stage</u>:

The electron diffraction patterns e.g. Figs.5 (a-f) showed random polycrystalline orientation in deposits of small thicknesses. The limiting thickness increases with increase of pressure of the residual air from about 150 A at 1 x10^{-8} torr to about 700 A at 5 x10^{-3} torr. Fig.5(a) from a 150 A thick specimen shows diffuse rings, mostly drawn downwards vertically due to the refraction effect at the smooth surface.

Figs. 5(b) and 5(c) are from specimens 185 A and 340 A thick, prepared at a pressure of 2 x10^{-7} torr and 5 x10^{-6} torr respectively. Here also, the rings are slightly diffuse and drawn downwards showing the formation of atomically smooth faces at this early stage.

Figs. 5(d-f) also show continuous ring patterns, but that the rings are sharper and do not show as much refractive drawing out as in Figs. 5(a-c). This indicates

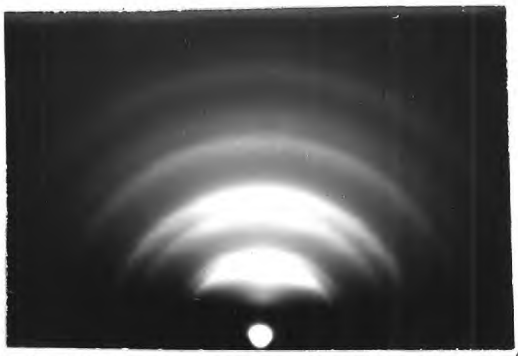

(a) Thickness = 150A at i=0°
Pressure = 1×10^{-8} torr
Angle i = 0°

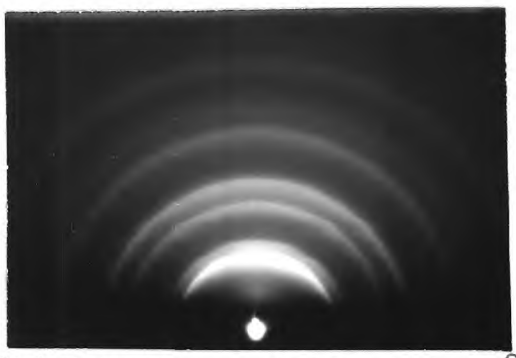

(b) Thickness =185A at i =0°
Pressure =2×10^{-7} torr
Angle i = 0°

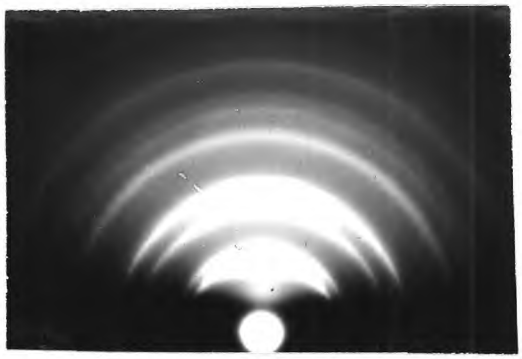

(c) Thickness = 340A at i=0°
Pressure = 5×10^{-6} torr
Angle i = 0°

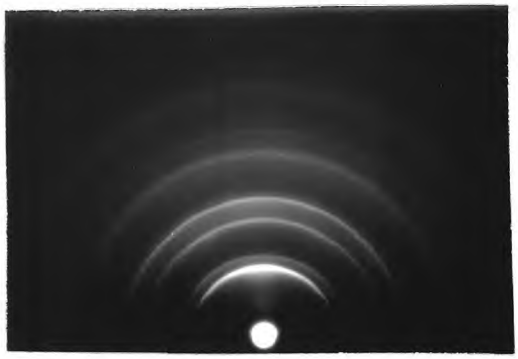

(d) Thickness =350A at i = 0°
Pressure =5×10^{-5} torr
Angle i = 0°

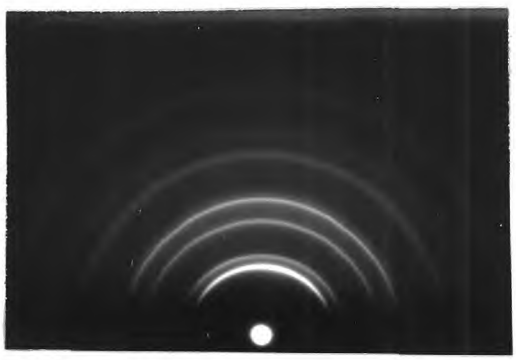

(e) Thickness = 500A at i = 0°
Pressure = 5×10^{-4} torr
Angle i = 0°

(f) Thickness = 700A at i=0°
Pressure = 5×10^{-3} torr
Angle i = 0°

Fig.5. Electron Diffraction Patterns from the Gold Deposits showing Random Crystal Orientation.

that there is not much strong facet formation on the surface of the deposits, thus the diffractions correspond mainly to transmission of the electron beam through the relatively steeply inclined projections on the deposits.

It is hence observed that at the early stage of the deposits, the strong facet formation is favoured more and more as the residual air pressure is gradually reduced.

The mean crystal diameter 't' of the deposits can be calculated as from Laue's equation

$$t = \frac{K \lambda L}{\beta_{\frac{1}{2}} \cos \theta} \qquad (3.1)$$

where $K = 0.9$, $\beta_{\frac{1}{2}}$ = "half width" of the rings,
θ = Bragg's angle at grazing incidence,
λ and L are the usual wavelength of the electron beam and the camera length respectively.

Using the proper values of the above quantities and measuring the half widths of the different rings, the mean crystal diameter at this stage of orientation has been found to lie between 250 A to 325 A.

Since the estimate of $\beta_{\frac{1}{2}}$ is small, the crystal diameter thus estimated may be regarded as a minimum value and the true mean crystal size may be up to several times larger than this.

3.1a(ii). The Structure of the Gold Deposits at the Stage of Thickness where (111) Orientation Developed:

From Fig.4 it is seen that the critical thickness above which the preferred orientation with an octahedral plane parallel to the substrate begins to develop increases roughly exponentially with the pressure of the residual air in the evaporation chamber as this rises from 1 $x10^{-8}$ torr to 5 $x10^{-3}$ torr.

Figs. 6 (a-f) show the electron diffraction patterns of these deposits. Fig.6(a) is from a deposit 250 A thick prepared at 1 $x10^{-8}$ torr. This is the earliest stage of development of (111) orientation. An appreciable development of an arc of detectable intensity is seen on the 111 ring centred on the plane of incidence of the electron beam.

A theoretical diffraction pattern from (111) oriented f.c.cubic crystals (with azimuthally random orientation) is shown in Fig.7(a). The shadow-edge corresponds to the intersection of the substrate surface with the plane of the photographic plate and normal to it lies the projection of the [111] axis of orientation, which is parallel to the substrate normal. The layer lines or the horizontal Laue-zones in Fig.7(a) define, by their intersection with the ring positions, the positions where the diffractions will occur.

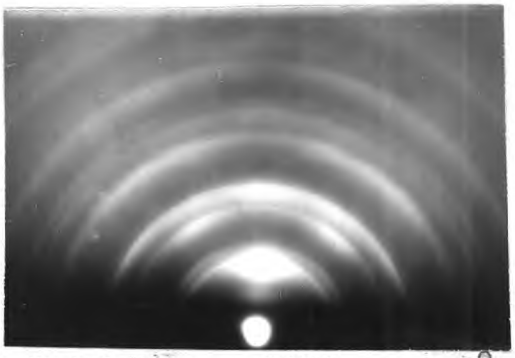

(a) Thickness = 240A at i=0°
Pressure = 1×10^{-8} torr
Angle i = 0°

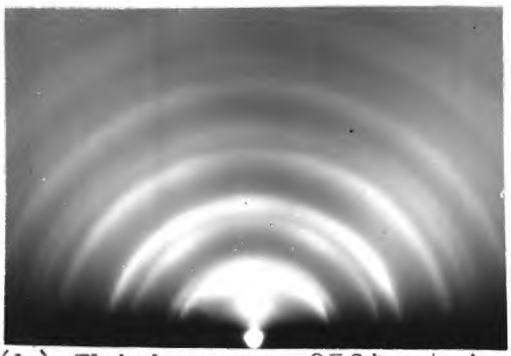

(b) Thickness = 250A at i =0°
Pressure = 2×10^{-7} torr
Angle i = 0°

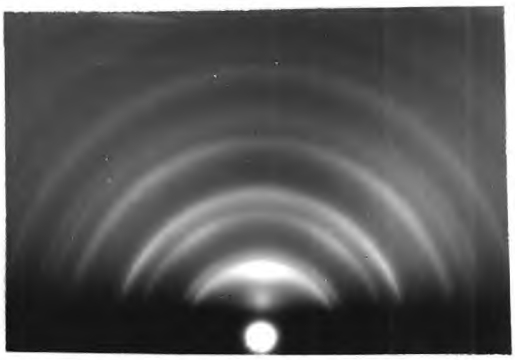

(c) Thickness = 28A at i=0°
Pressure = 5×10^{-6} torr
Angle i = 0°

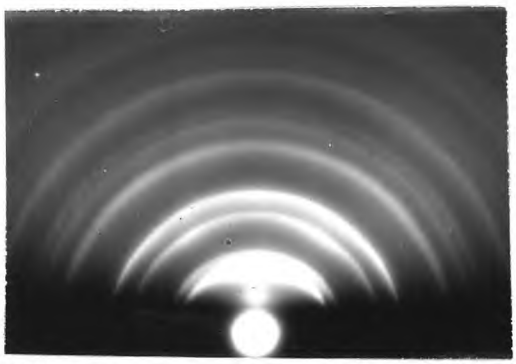

(d) Thickness = 450A at i=0°
Pressure = 5×10^{-5} torr
Angle i = 0°

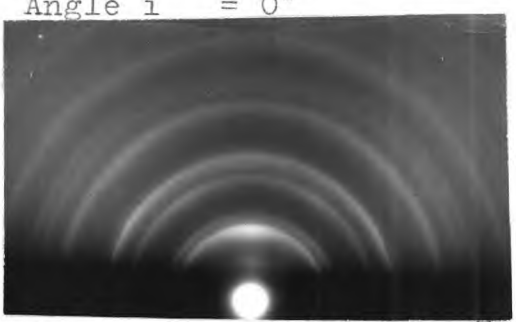

(e) Thickness = 710A at i=0°
Pressure = 5×10^{-4} torr
Angle i = 0°

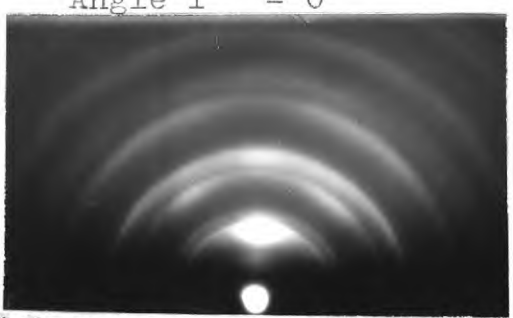

(f) Thickness = 750A at i=0°
Pressure = 2×10^{-3} torr
Angle i = 0°

Fig.6. Electron Diffraction Patterns of Gold Deposits showing (111) Orientation.

The comparison of Fig.6(a) with Fig.7(a) unambiguously established the (111) type of orientation of Fig.6(a). The arcing of the diffractions with a spread of about $\pm 10^{\circ}$ from the mean indicates a corresponding spread of orientation of the crystals. The drawing out of the arcs vertically downwards towards the shadow-edge indicates refraction of the electron beam by the atomically smooth crystal surfaces, which must therefore be of octahedral-face type normal to the vapour beam direction.

Diffraction patterns similar to the above were also obtained from specimens 250 A thick deposited at 2×10^{-7} torr, 450 A thick at 5×10^{-5} torr, 710 A thick at 5×10^{-4} torr and 750 A thick deposited at 2×10^{-3} torr. The general features of these patterns were the same excepting in the variation in intensities of the arc patterns and their spreads. The development of octahedral planes seems to be relatively quicker at the lower pressures. While the refraction effect is very prominent for Figs.6 (a,b,c), it is considerably less in Fig.6(d). This pattern shows relatively sharp rings but with long arcs. Fig.6(e) has a considerably long diffuse arc centred on the plane of incidence on the 200 and 220 rings giving additional confirmation of the (111) orientation of this specimen.

The (111) orientation, thus, developed very quickly from the random state, and once it sets in it goes on

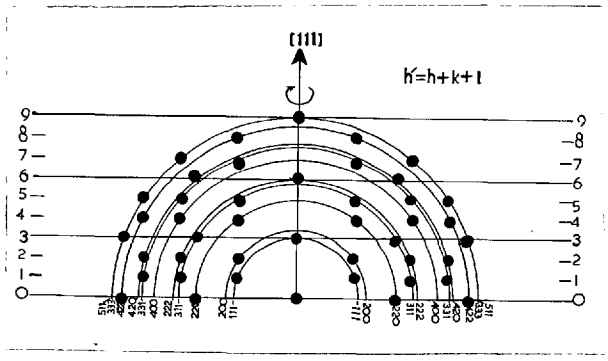

Fig.7(a). Theoretical (111) Electron Diffraction Pattern of Gold.

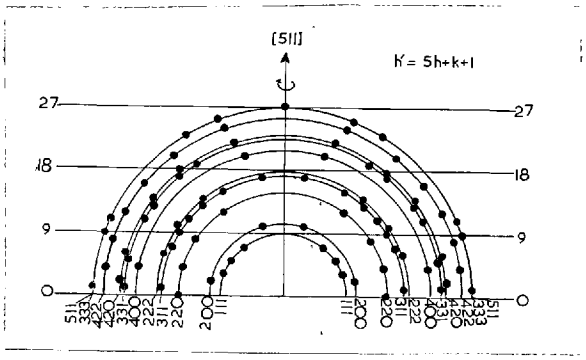

Fig.7(b). Theoretical (511) Electron Diffraction Pattern of Gold.

developing rapidly up to a certain thickness of the deposits.

Figs. 8(a-f) are from relatively thicker specimens. Fig.8(a) shows strong (111) orientation from a specimen 925 A thick prepared at 1 $x10^{-8}$ torr. The strong arcs indicate the preferential growth of crystals having {111} planes parallel to the substrate or nearly so. As in Fig.6(a), the arcs on the 111, 200, 220 rings are prominently drawn towards the shadow edge indicating high smoothness, on the atomic scale, of the growing deposit. The arc centred on the plane of incidence on the 111 ring has a spread of $\pm 5^{o}$, showing still higher perfection of the development of the octahedral orientation.

Fig.8(c) is from a specimen 1544 A thick prepared at 5 $x10^{-6}$ torr. The pattern is in general similar to Fig.8(a), but the spread of the arc from the plane of incidence, on the 111 ring, is $\pm 3^{o}$ - still shorter than the above. This indicates that near the upper limit of (111) orientation region, the orientation becomes more and more strong indicating more and more extensive {111} planes on the crystals in the upper regions of the growing deposit.

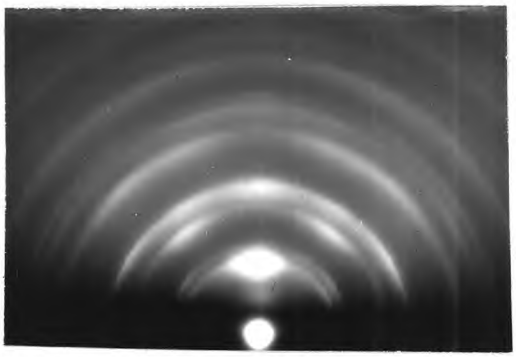

(a) Thickness = 925A at i=0°
Pressure = $1x10^{-8}$ torr
Angle i = 0°

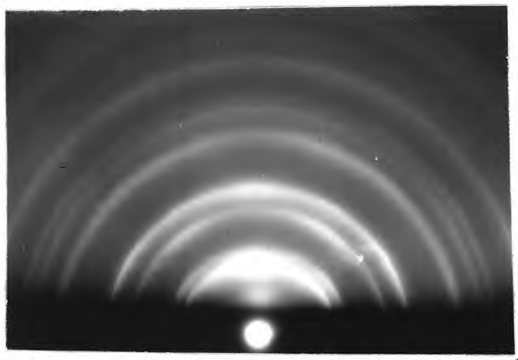

(b) Thickness = 760A at i=0°
Pressure = $2x10^{-7}$ torr
Angle i = 0°

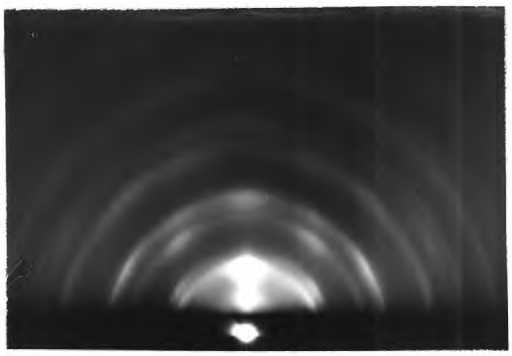

(c) Thickness =1544A at i=0°
Pressure = $5x10^{-6}$ torr
Angle i = 0°

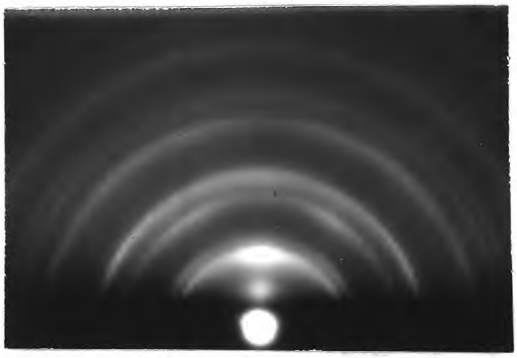

(d) Thickness = 810A ati=0°
Pressure = $5x10^{-5}$ torr
Angle i = 0°

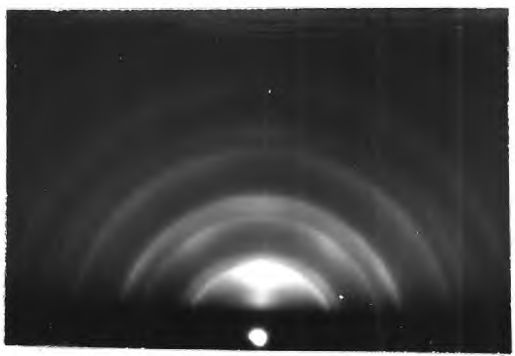

(e) Thickness =1000A at i=0°
Pressure = $5x10^{-4}$ torr
Angle i = 0°

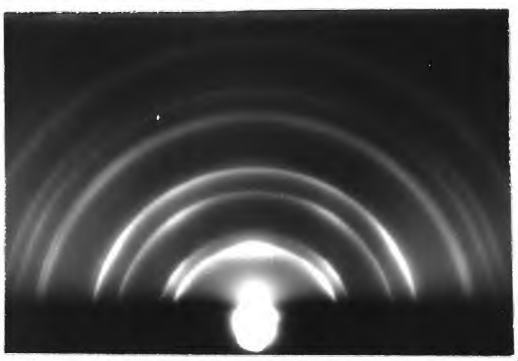

(f) Thickness =1700A at i=0°
Pressure = $2x10^{-3}$ torr
Angle i = 0°

Fig.8. Electron Diffraction Patterns from the Gold Deposits showing (111) Orientation.

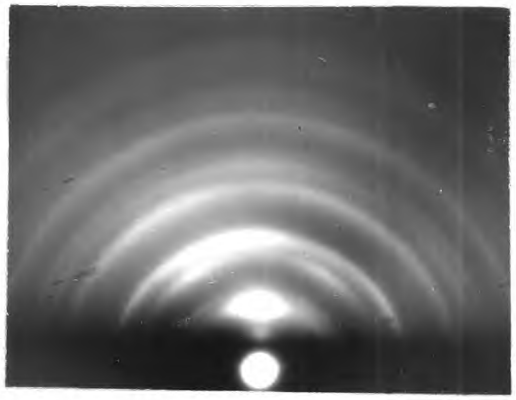

(a) Thickness =2100A at i=0°
Pressure = 5×10^{-6} torr
Angle i = 0°

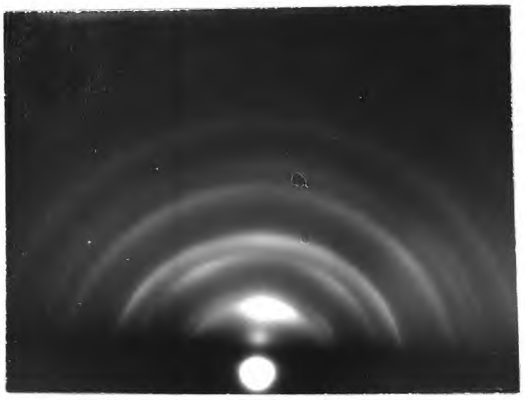

(b) Thickness =2100A at i=0°
Pressure = 5×10^{-6} torr
Angle i = 45° Vapour

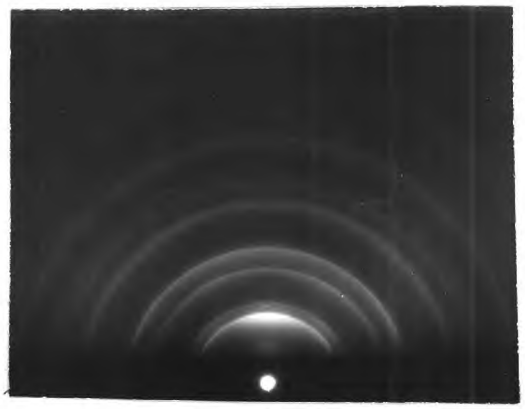

(c) Thickness =1570A at i=0°
Pressure = 5×10^{-6} torr
Angle i = 0°

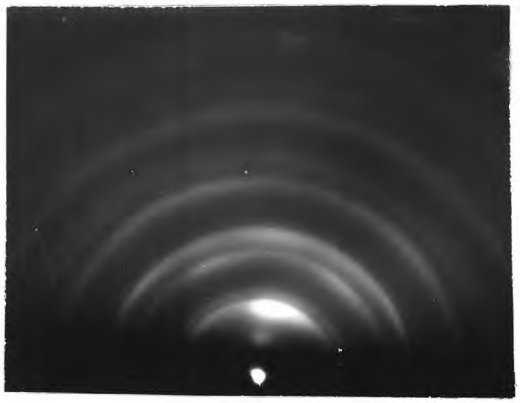

(d) Thickness =1570A at i=0°
Pressure = 5×10^{-6} torr
Angle i = 45° Vapour

Fig.9. Electron Diffraction Patterns from the Gold Deposits showing (111) Orientation.

3.1a(iii). The Structure of the Gold Deposits at the Stage of Thickness where (111) Orientation and {111} Twinning Developed:

From deposits at this stage (see Fig.4) the electron diffraction patterns show diffractions due to (111) orientation with additional short arcs due to the octahedral twins of these crystals, as in Figs.10(a-e).

In all five photographs the strong (111) orientation is seen along with the additional arcs from the twins, e.g. in Fig.10(a) from a specimen 2516 A thick at i = 0 prepared at 1 $x10^{-8}$ torr at 28 A/sec. In addition to the pattern from the (111) oriented crystals, there are diffractions from (511) oriented crystals. The two short arcs almost symmetrically situated near the plane of incidence, on the 200 ring, are due to the twins on the octahedral planes. The strengthening in intensity at the plane of incidence on the 331 ring may be due partly to the coalescence of the two arcs expected due to the (511) oriented crystals and partly to the spread of the (111) orientation from the mean which will bring the {331} planes parallel to the surface of the substrate.

Figs. 10(d) and (e) are patterns from the positions of normal and 45^{o} incidence of the vapour stream, in a specimen 1400 A thick at i = 0, prepared at 32 A/sec, at

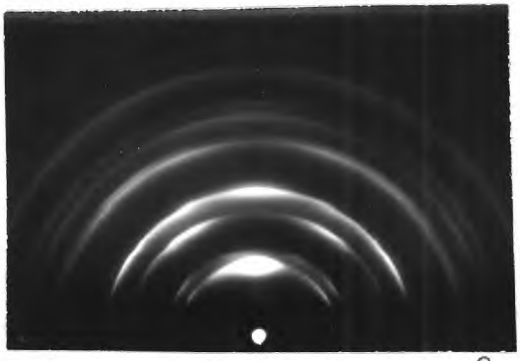

(a) Thickness = 2516A at i=0°
Pressure = $1x10^{-8}$ torr
Angle i = 0°

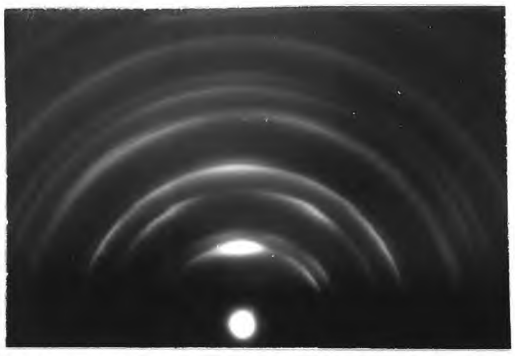

(b) Thickness =2694A at i=0°
Pressure = $1x10^{-8}$ torr
Angle i = 0°

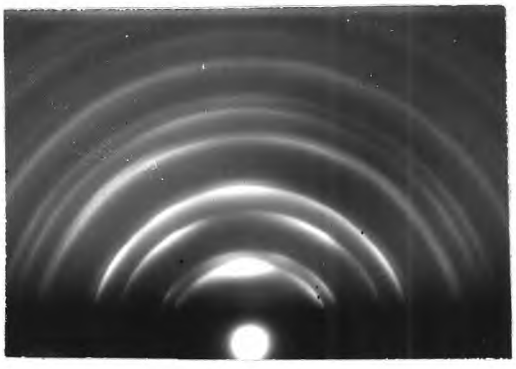

(c) Thickness = 4333 A
at i = 0°
Pressure = $1x10^{-8}$
torr
Angle i = 0°

Transpose photographs.

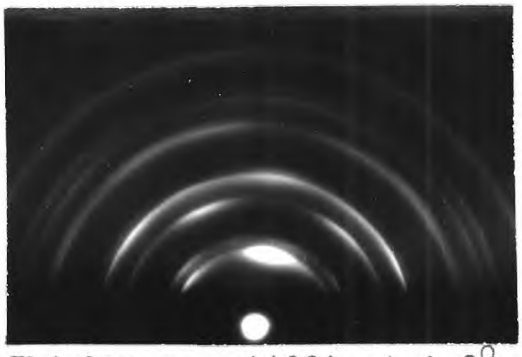

(d) Thickness = 1400A at i=0°
Pressure = $5x10^{-6}$ torr
Angle i = 0°

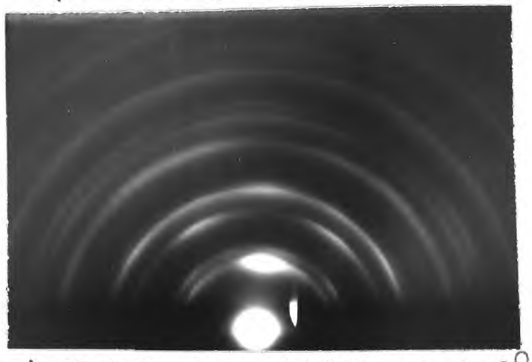

(e) Thickness =1400A at i=0°
Pressure = $5x10^{-6}$ torr
Angle i = 45°

Vapour

Fig.10. Electron Diffraction Patterns from the Gold Deposits showing (111) Orientation + {111} Twinning.

5 x10^{-6} torr. The [111] axis in Fig.10(d) is tilted away from the normal to the substrate by about 10° towards the vapour stream. The (111) arcs in both the patterns are drawn towards the shadow-edge, indicating strong development of {111} planes on the (111)-oriented crystals parallel to the surface of the substrate, but no smooth surface parallel to the substrate in the {111} twins.

The positions of the diffraction spots and the orientation axis when {111} twinning occurs can be shown as follows.

Fig.11(a) shows the side view of a cubic unit cell of a crystal oriented with a (111) plane parallel to the substrate and Fig.11(b) shows the rotation twin, derived from Fig.11(a) by rotation through 180° about a cube diagonal such as [11$\bar{1}$], other than the one normal to the substrate. In this lattice, which is the twin of that of Fig.11(a), the (115) plane is parallel to the substrate, and thus the [115] axis is normal to it.

When a cubic lattice is twinned by 180° about an axis [UVW], then a lattice vector [uvw] (relative to the initial lattice) after the twinning operation, takes up the new position having indices [u'v'w'] (relative to the initial lattice such that:

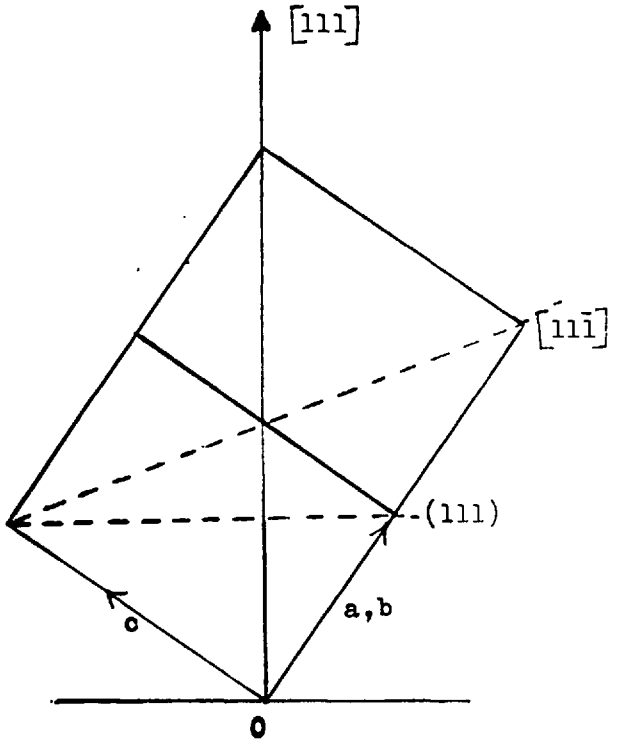

Fig.11(a). Side view of the cubic unit cell of the (111) oriented gold.

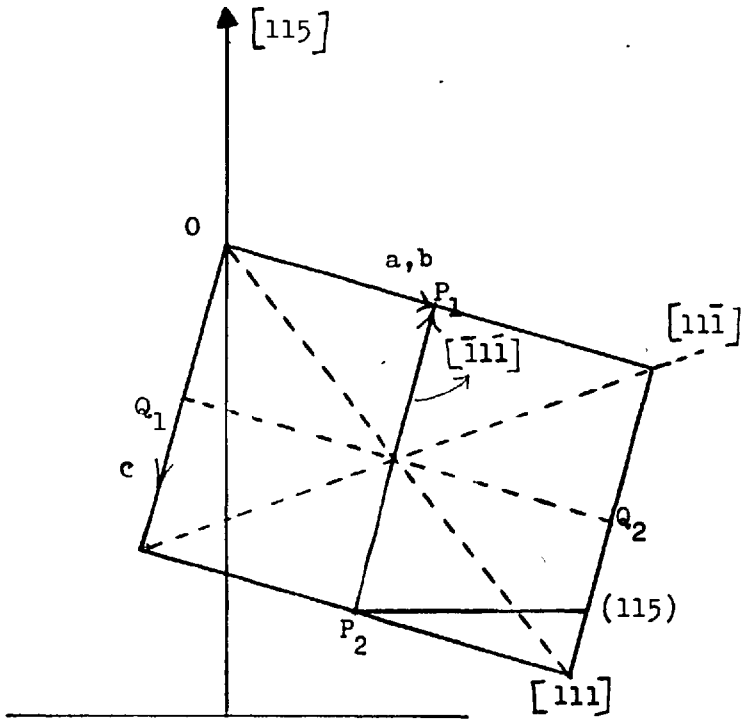

Fig.11(b). Side view of the cubic unit cell of the [11$\bar{1}$] primary twin of the (111) oriented gold.

$$\begin{aligned} u' &= -u + 2UF \\ v' &= -v + 2VF \\ w' &= -w + 2WF \end{aligned} \qquad (3.2)$$

where $F = (uU+vV+wW)/(U^2+V^2+W^2)$

This new vector [u'v'w'] has the indices [uvw] relative to the twin axes.

Another way of expressing it is that if a certain vector in the twin lattice has the indices [u'v'w'] relative to the initial lattice, then the same vector has the indices [uvw] relative to the twin axes.

In the present case of a rotational twin about $[11\bar{1}]$ we have from eqn. (3.2):

$$\begin{aligned} u' &= -u + \tfrac{2}{3}(u + v - w) \\ v' &= -v + \tfrac{2}{3}(u + v - w) \\ w' &= -w + \tfrac{2}{3}(u + v - w) \end{aligned} \qquad (3.3)$$

Since [u'v'w'] is now [111], then by solving equations in (3.3) we have $u = \bar{1}/3$, $v = \bar{1}/3$ and $w = \bar{5}/3$. Hence a (115) plane of the twin lattice is now parallel to the substrate (i.e. normal to the [115] axis) and also to the (111) plane of the initial lattice.

The azimuthal range of (111)-oriented crystals is completely random about the normal to the substrate and so also is the azimuthal range of orientation of the twins on {111}. The theoretical positions of the diffractions

due to these twins will correspond to the pattern from a one-degree (115) orientation relative to the substrate, as is illustrated in Fig.7(b).

3.1a(iv). The Structure of the Gold Deposits at the Stage of Thickness where a Mixed (111) + (211) Orientation Developed:

Referring to Fig.4 again, it is seen that above the upper limit of thickness of the deposits where (111) + {111} twinning developed, in a few of the cases of the deposits a mixture of (111) and (211) orientation were found. At this stage of these deposits, the new orientation with the (211) planes parallel to the substrate begins to develop. This, obviously, is a transitional stage from (111) to (211) type of orientation.

Figs.12(a-d) show some of these results. Fig. 12(a) and (b) are the diffraction patterns from the points of normal and 45° incidence of the vapour stream of a specimen 970 A thick at i = 0, prepared at 28 A/sec at 5×10^{-3} torr. The strengthening in intensity at the position of the plane of incidence on the 111 ring in effect may consist of three arcs coalescing into a long strong arc. The one at the middle, on the plane of incidence of the electron beam is due to (111) type of orientation, and the two on either side of it are due to the (211) type of

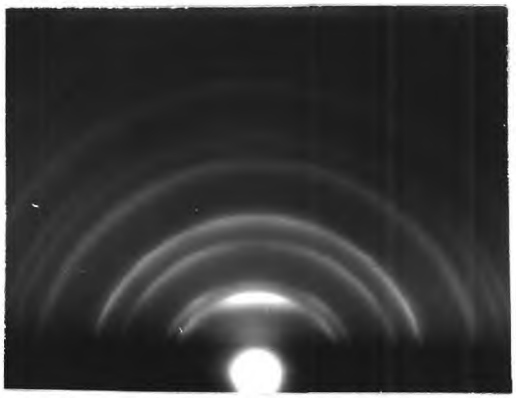

(a) Thickness = 970A at i=0°
Pressure = 5×10^{-3} torr
Angle i = 0°

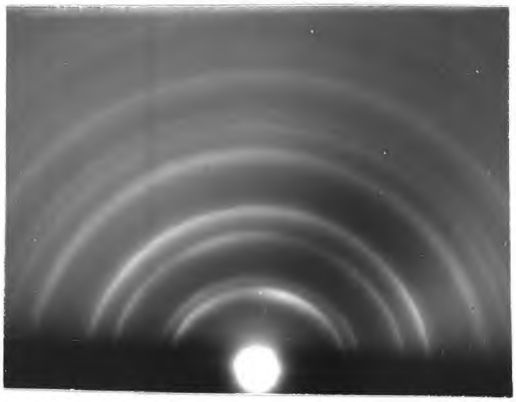

(b) Thickness = 970A at i=0°
Pressure = 5×10^{-3} torr
Angle i = 45°

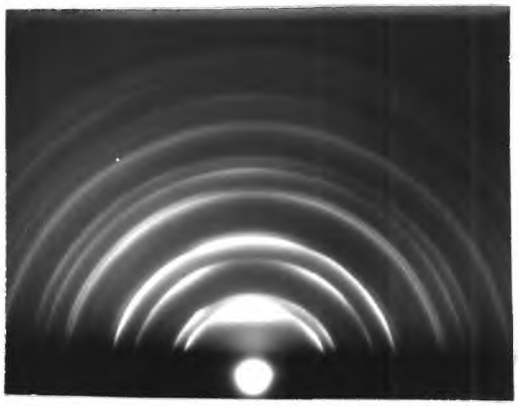

(c) Thickness =4010A at i=0°
Pressure = 2×10^{-7} torr
Angle i = 0°

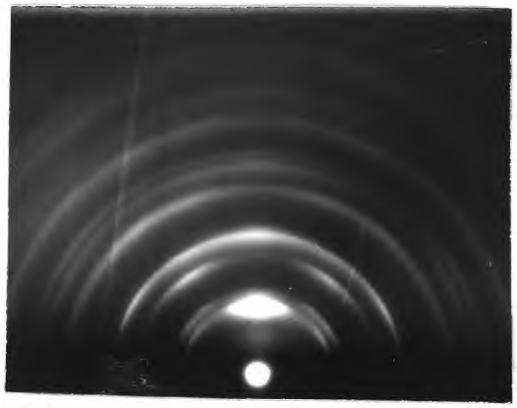

(d) Thickness =4200A at i=0°
Pressure = 2×10^{-7} torr
Angle i = 0°

Fig.12. Electron Diffraction Patterns of the Gold Deposits showing (111) + (211) Orientations.

orientation. A slight strengthening of intensity at the plane of incidence on the 422 ring (seen on the actual negative plate) along with the two lateral axes on the 200 ring confirms the presence of {211} planes parallel to the substrate along with the {111}. Fig.12(b) is from a thinner part of the specimen and the pattern mostly consists of diffraction arcs corresponding to (111) type of orientation. The orientation axis is tilted towards the vapour beam away from the normal by about 9°. In Figs. 12(c) and 12(d) the development of (211) orientation is more prominent than in Fig.12(a). In both these two cases the central arc (which consists of three arcs) on the 111 ring is drawn out towards the shadow edge, showing refraction by these smooth crystal faces.

3.1a(v). <u>The Structure of the Gold Deposits at the Stage of Thickness where (211) Orientation Developed</u>:

Beyond the transitional stage showing the mixture of (111) and (211) orientations there comes the stage of thickness of the deposits when the surface structure ceases to show the (111) orientation and the (211) orientation begins to preponderate. The change of orientation from (111) to (211) in gold deposits is not very rapid. Some of the results are illustrated in Figs. 13, 14 and 15.

Fig.13(a) is from a region of $i = 0^{\circ}$ of a

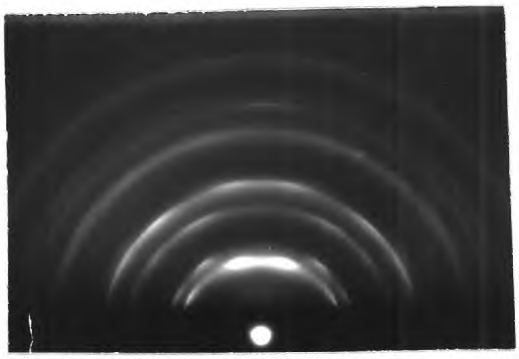

13a. Thickness =2520A at i=0°
Pressure = $2x10^{-3}$ torr
Angle i = 0°

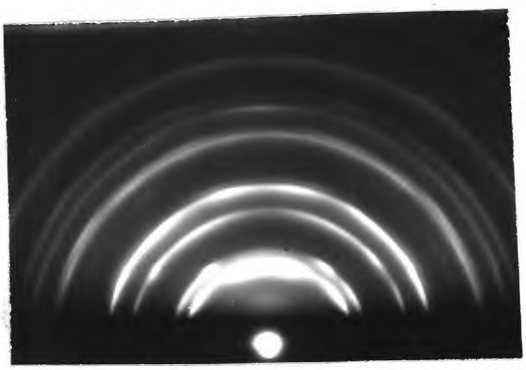

13b. Thickness =6250A at i=0°
Pressure = $5x10^{-4}$ torr
Angle i = 0°

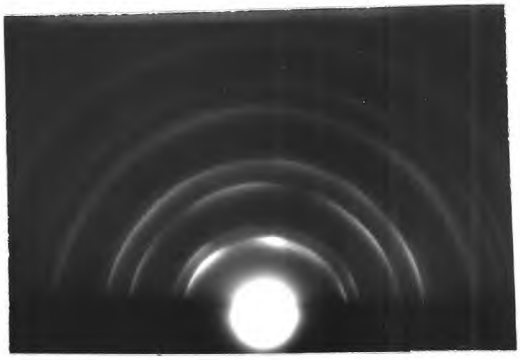

13c. Thickness =2520A at 1=0°
Pressure = $2x10^{-3}$ torr
Angle i = 45°

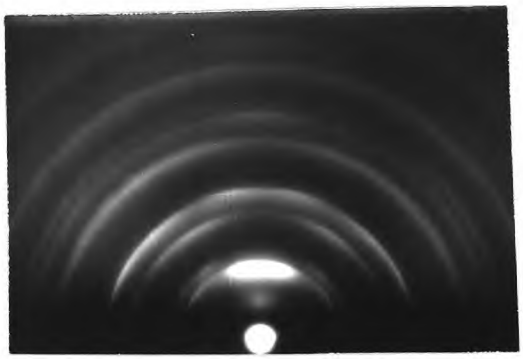

13d. Thickness =4562A at i=0°
Pressure = $5x10^{-5}$ torr
Angle i = 0°

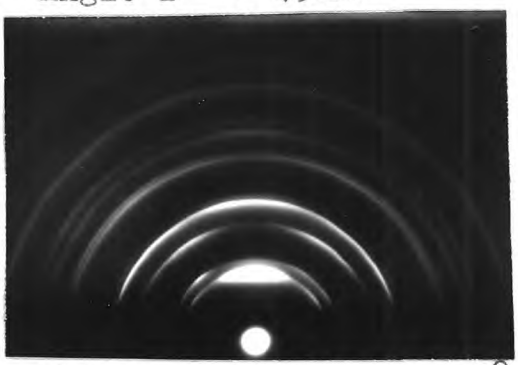

14a. Thickness =4156A at i=0°
Pressure = $2x10^{-7}$ torr
Angle i = 0°

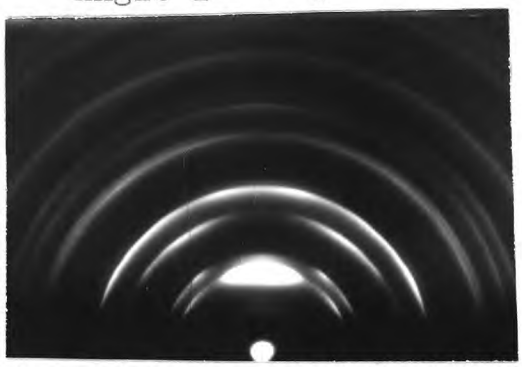

14b. Thickness =4333A at i=0°
Pressure = $1x10^{-8}$ torr
Angle i = 0°

Figs.13 and 14. Electron Diffraction Patterns of the Gold Deposits showing (211) Orientation.

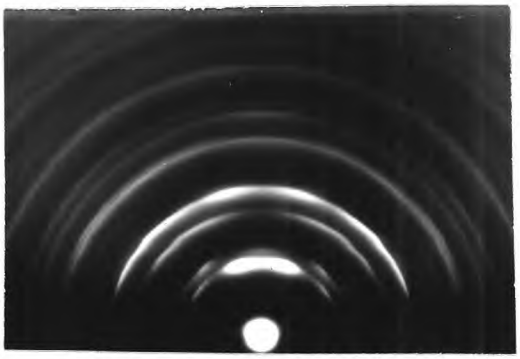

14c. Thickness =2108A at i=0°
Pressure = 2×10^{-3} torr
Angle i = 0°

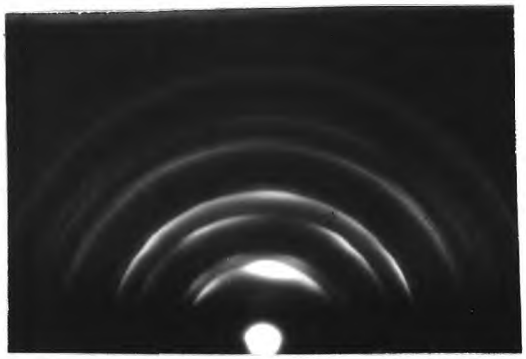

14d. Thickness =2108A ati=0°
Pressure = 2×10^{-3} torr
Angle i = 45° Vapour

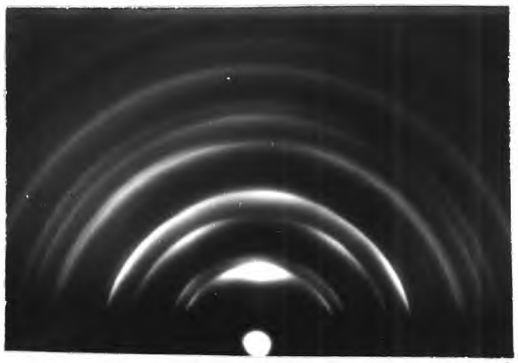

15a. Thickness =4850A at i=0°
Pressure = 1×10^{-8} torr
Angle i = 0°

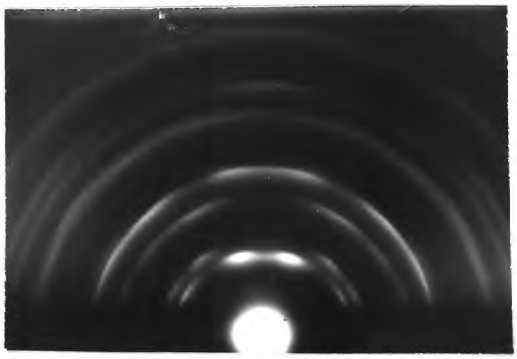

15b. Thickness =2600A at i=0°
Pressure = 5×10^{-5} torr
Angle i = 0°

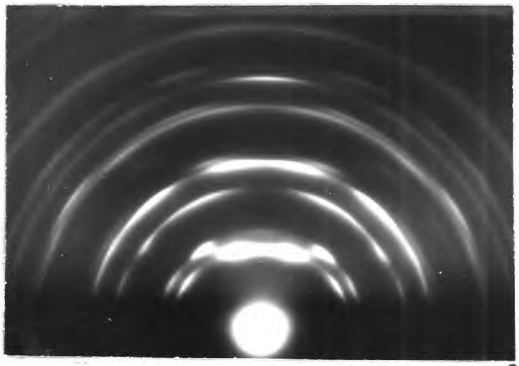

15c. Thickness =4760A at i=0°
Pressure = 2×10^{-3} torr
Angle i = 0°

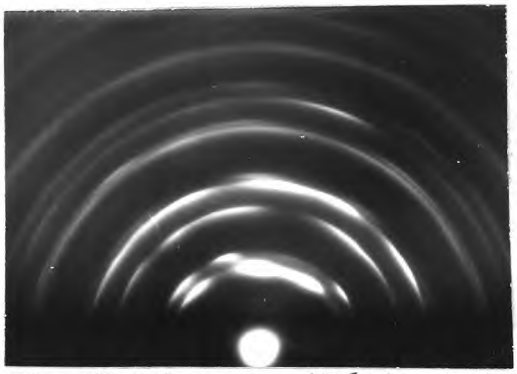

15d. Thickness =4760A at i=0°
Pressure = 2×10^{-3} torr
Angle i = 45° Vapour

Figs. 14 and 15. Electron Diffraction Patterns of the Gold Deposits showing (211) Orientation.

specimen 2520 A thick deposited at 30 A/sec in a residual air pressure of 2 $x10^{-3}$ torr. The two strong short arcs near the plane of incidence of the electron beam on the 111 ring are well separated with distinct fall in intensity in between them. These two lateral arcs, along with the two on either side of the plane of incidence on the 200 ring, lie on the same layer line parallel to the shadow edge. Further up in the 311 and 222 rings all the four lateral arcs (a pair each about the plane of incidence) also lie on the same layer line. The 422 arc on the 422 ring along the normal to the shadow edge from the central spot is also clearly visible. All these distinct features agree with the (211) theoretical pattern of gold, shown in Fig.16.

Fig.13(b) is from a specimen prepared at 5 $x10^{-4}$ torr of air at i = 0. The two lateral arcs on the (111) ring are just separated. The 211 arc on the 422 ring is prominent. The arcs about the plane of incidence of the electron beam on the 111 ring show some drawing out towards the shadow edge. This indicates the development of an atomically smooth surface with {211} types of planes growing parallel to the substrate surface or nearly so.

Fig.13(c) is from the same specimen but from a region where the vapour stream was incident at i = 45^{o}. The tilt of the [211] orientation axis away from the normal

to the substrate is 22° towards the vapour stream.

Fig.14(b) is from a specimen 4333 A thick at i = 0°, prepared at 32 A/sec, at 1 $x10^{-8}$ torr of air. The lateral arcs on the 111 ring, about the normal to the substrate, show a little coalescence. The 422 arc is extended along the ring and the spread is $\pm 12^{\circ}$. The pattern corresponds clearly to a (211) type of orientation. The angle subtended by the two neighbouring lateral arcs on the 200 ring at the central spot is about 79°, corresponding to 80° in the theoretical pattern. There is a slight strengthening in intensity at the plane of incidence region of the 200 ring. This may indicate the development of some cube face orientation along with the main (211). But the long 422 arc on the 422 ring suggests that there is considerable rocking of the [211] orientation axis about its mean position (and henceof the {422} planes) about the plane of incidence of the electron beam. This rocking operation will occasionally bring along some of the (100) planes parallel to the substrate surface, which may give rise to Bragg reflections at the plane of incidence of the electron beam, on the 200 ring. The absence of any intensity at the region of the plane of incidence on the 400 ring further ruled out any strong (100) orientation.

Fig.15(c) is another very interesting diffraction

pattern corresponding to i = 0^{o} of a specimen prepared at 2 x10^{-3} torr. The fall in intensity between the two lateral arcs on the 111 ring is distinct. The spread of the 422 arc is comparatively small ($\pm$ 8^{o}), which suggests less rocking of the [211] axis about the mean and consequently the chance of any cube face becoming parallel to the substrate is less, due to which there is considerably uniform fall in intensity at the region of the plane of incidence of the 200 ring.

It is observed from these results that one-degree (211) orientation sets in earlier at higher pressures than in lower pressures and the development of the {211} planes parallel to the substrate surface is quicker in the high pressure region. The (211) orientation is quite strong at the high pressure region, as indicated by the shortness of the diffraction arcs and absence of continuous ring intensity between the arcs (cf. Figs. 13(a), 14(c) and 15(c)).

3.1(b). <u>The Structure of the Gold Deposits Condensed at Oblique Incidence of the Vapour Stream</u>:

As discussed in section 2, the substrate was so arranged below the vapour source that one of its ends received the vapour at an angle of incidence i = 45^{o} with respect to the normal to the substrate. In all the electron diffraction examinations the beam was normal to the plane of

incidence of the vapour stream at the region of interest on the substrate.

It was realised that the diffraction patterns obtained from oblique vapour incidence regions should not be examined as individual specimens. To avoid erroneous interpretation, regions of normal and oblique incidences were explored from the same specimens.

The orientation axis showed a definite amount of tilt towards the vapour stream direction. Fig.17(b) is from the region of 45° incidence of a specimen 2225 A thick at i = 0, prepared at 5 $x10^{-3}$ torr at 31 A/sec. The actual thickness and rate of deposition at i = 45° are roughly one third of these values at i = 0°. The mean orientation axis shows a tilt $\sim 25^{\circ}$ away from the normal towards the vapour stream for i = 45°. There is a little lack of symmetry in the intensity distribution of the arcs. This indicates that even at such obliquity of the orientation axis the orientations of the crystal are not strongly azimuthally limited. The pattern shows a strong (211) type of orientation of the crystals at normal incidence of the vapour stream. This orientation has not changed with the obliquity of the vapour stream direction. The appreciable transmission of the electron beam by the deposit crystal surfaces in the region investigated indicates that these

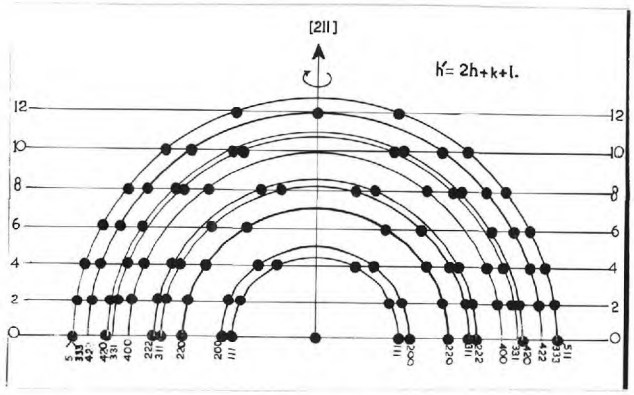

Fig.16. Theoretical (211) Electron Diffraction Pattern of Gold

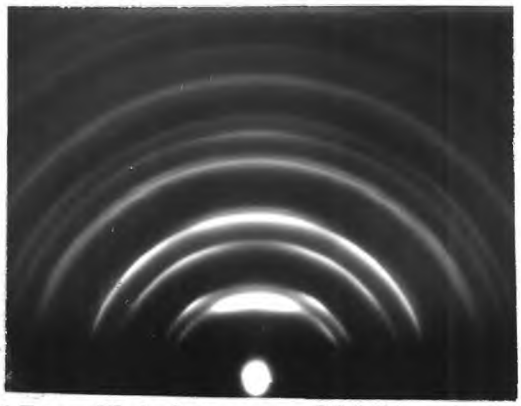

17a. Thickness =2225A at i=0°
Pressure = 5×10^{-3} torr
Angle i = 0°

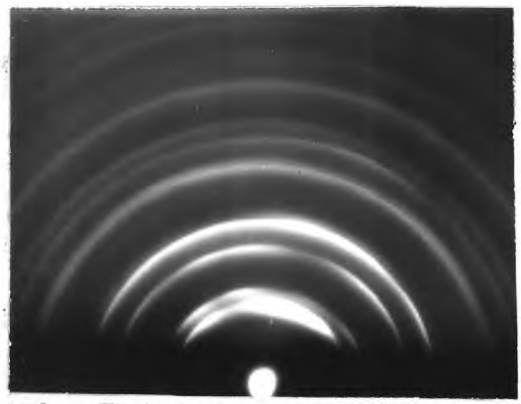

17b. Thickness and Pressure as in 17(a)
Angle i = 45° Vapour

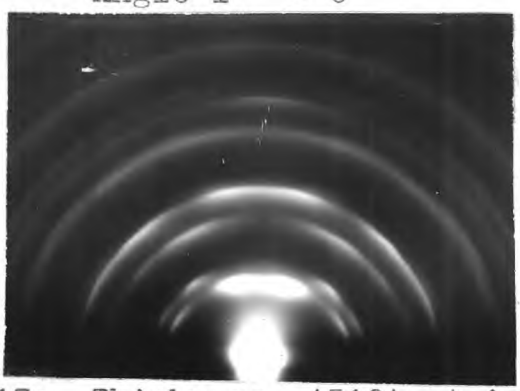

17c. Thickness =4510A at i=0°
Pressure = 5×10^{-3} torr
Angle i = 0°

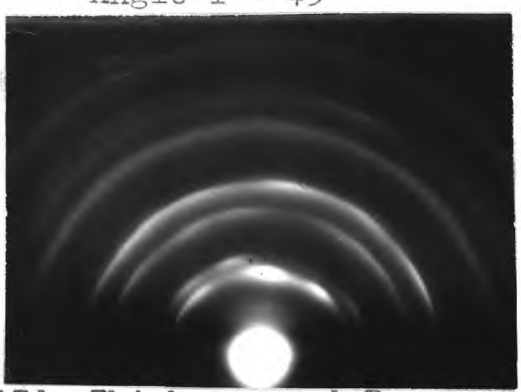

17d. Thickness and Pressure as in 17(c)
Angle i = 45° Vapour

Fig.17. Electron Diffraction Patterns of Gold Deposits showing (211) Orientation.

surfaces are relatively smooth up to that region of 45° incidence. The two lateral arcs on the 111 ring about the mean orientation axis and the central arc on the 422 ring (on the actual negative plate) can still be observed.

Fig.13(c) is from the region of $i = 45^{\circ}$ from a specimen 6250 Å thick at $i = 0$ prepared at a pressure of 5×10^{-4} torr. Fig.13(c), like Fig.13(b), agrees well with the theoretical pattern (Fig.16) for (211) orientation. The 422 arc in the central region of the 422 ring, the two lateral arcs about the plane of incidence of the electron beam are recognisable. In comparison with Fig.13(b), these arcs in Fig.13(c) are much longer, indicating a considerable amount of rocking of the tilted [211] axis about the mean position, at this region of the specimen.

Fig.17(d) is from the $i = 45^{\circ}$ region of a specimen 4510 Å thick at $i = 0^{\circ}$ prepared at 5×10^{-3} torr. The strong (211) type of orientation of the crystals is obvious. The tilt of the orientation axis is 22°. The intensity distribution is very nearly symmetrical in the pairs of axes symmetrically disposed about the [211] axis direction. This again indicates that at the region of oblique incidence there is no azimuthal preference of the crystals about the direction of the oblique orientation axis.

Figs.18(a-c) show the (δ,t) (i.e. tilt, thickness

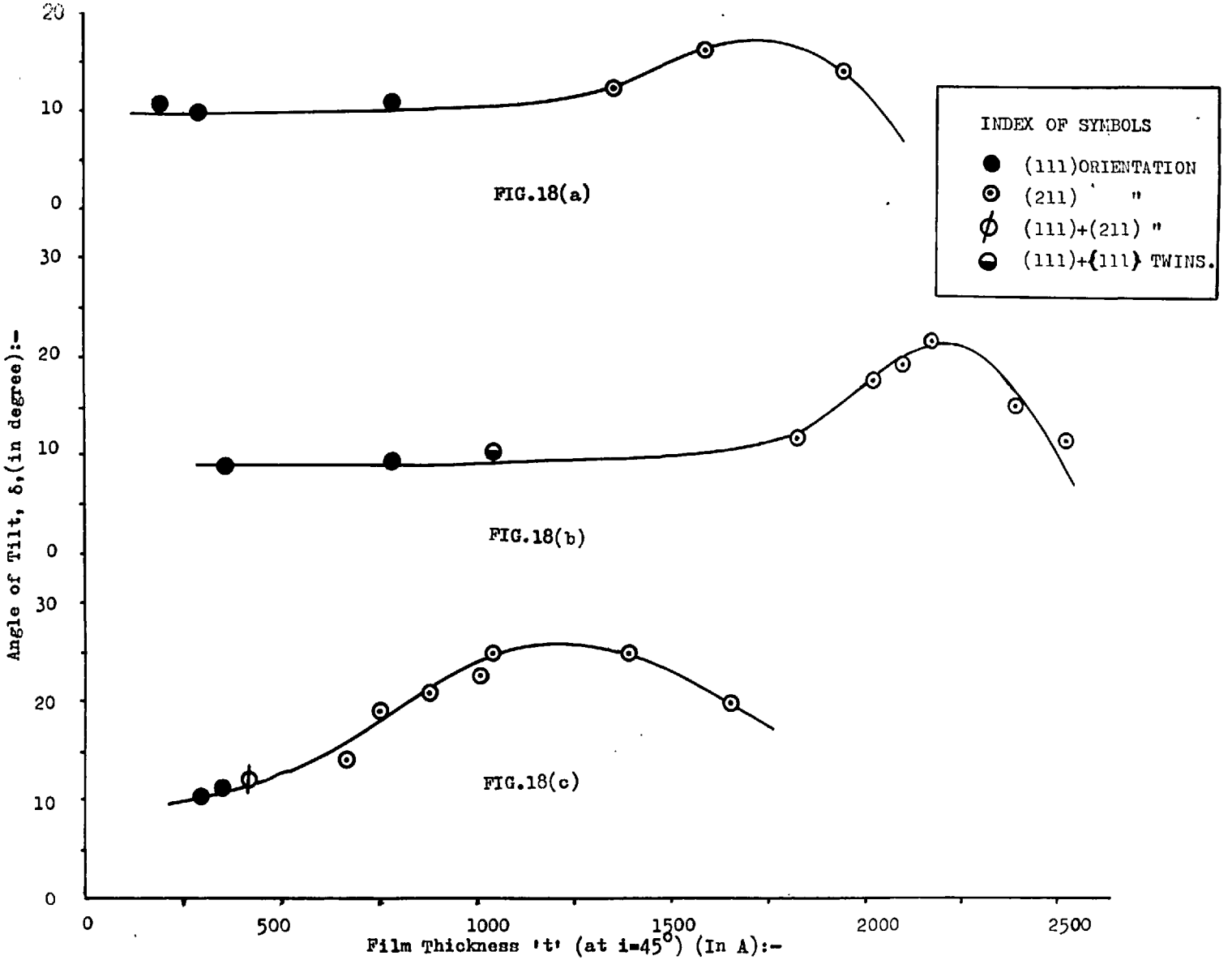

FIG.18(a) THICKNESS(AT i=45°)-TILT (t,δ) PLOT OF THE GOLD DEPOSITS CONDENSED ON STAINLESS-STEEL AT ROOM TEMPERATURE, AT P = 5×10^{-5} TORR.

18(b) " " " " " " AT P = 5×10^{-4} TORR.

18(c) " " " " " " AT P = 2×10^{-3} TORR.

of deposits at $i=45^{0}$) plots corresponding to the pressures 2×10^{-3}, 5×10^{-4} and 5×10^{-5} torr, for $i = 45^{0}$. In each of the plots there is a general tendency of increase in tilt with thickness of the specimen up to a certain value beyond which the tilt angle falls down. The tilt of a [111] axis of orientation is less than that of the [211] axis in all the cases. While at 2×10^{-3} torr the tilt increases rapidly with thickness, the increase is slower at lower pressures, viz. at 5×10^{-4} torr and 5×10^{-5} torr. The maximum tilts observed were~25^{0} (corresponding to t = 1050 A) at $p = 2 \times 10^{-3}$ torr;~22^{0} (corresponding to t = 2225 A) at $p = 5 \times 10^{-4}$ torr and~17^{0} (corresponding to t = 1750 A) at $p = 5 \times 10^{-5}$ torr. It is thus observed that as the pressure of the residual air is lowered, the amount of the maximum tilt of the orientation axis decreases.

3.1(c). <u>The Effect of Residual Air Pressure on the Structure of the Gold Deposits Condensed at Normal Incidence</u>.

The systematic results on all gold deposits are shown in Fig.4, and it is seen that the lowest region, below the line marked I, shows random orientation of the crystals for increasing thicknesses with increase of pressure. The upper limit of this stage of thickness of the deposits changes very slowly within the pressure range 1×10^{-8} torr to 5×10^{-6} torr. Above 5×10^{-6} torr the rise in this limiting thickness is appreciable.

The region between the lines I and II gives the stage of thickness where (111) type of orientation develops. Here also, the upper limit of the thickness increases very slowly with increasing pressure up to 5 $x10^{-6}$ torr, and above that the change is quicker. The line II shows a peak value for a thickness of about 2500 A at about 5 $x10^{-4}$ torr. Above that pressure the graph falls down quickly.

The region between the lines II and III indicates the stage of thickness where (111) orientation with {111} twins develops in the crystals. The line III shows a hump at about 5 $x10^{-4}$ torr, and above this it falls rapidly.

There appears to be a small region between lines III and IV, which shows a mixture of (111) and (211) orientations. The region between the lines II and IV indicates the transitional stage of the (111) orientation to (211). The region beyond the line IV is the region of stable (211) orientation.

Thus, it is clear from Fig.4 that although the sequence of occurrence of the different orientations in gold deposits is the same at all the pressures investigated, yet, the initial thicknesses at which these different orientations occur are different at different pressures.

3.2. The Structure of the Silver Deposits Condensed in Vacuum onto Polished Stainless-steel at Room Temperature, at a Rate of 30 to 35 A/sec, in Relation to Thickness and Residual Air Pressure:

Thin films of silver were condensed onto polished stainless-steel at room temperature, at a nearly constant rate of deposition of 30 to 35 A/sec. The specimens were prepared at 1 $x10^{-6}$ and 2 $x10^{-7}$ torr of air, using the U.H.V. system. Dutta (1968) investigated the structure of silver films prepared at residual air pressures from 7 $x10^{-3}$ torr down to 7 $x10^{-6}$ torr at a rate of 30 to 35 A/sec. Keeping the same rate of deposition, the present experiments provide further results down to lower air pressure.

The results at normal incidence of the vapour stream are presented in Fig.19. For silver deposits, also, the crystals are randomly oriented at the early stages of growth. They begin to develop octahedral faces and a preferred orientation with an octahedral plane parallel to the substrate, as the thickness of the deposits increases. At a still higher thickness the (111) orientation is accompanied by {111} twinning, which at a later stage of growth changes completely to one-degree (211) type of orientation.

Further interpretations of the results are presented in the subsequent sections.

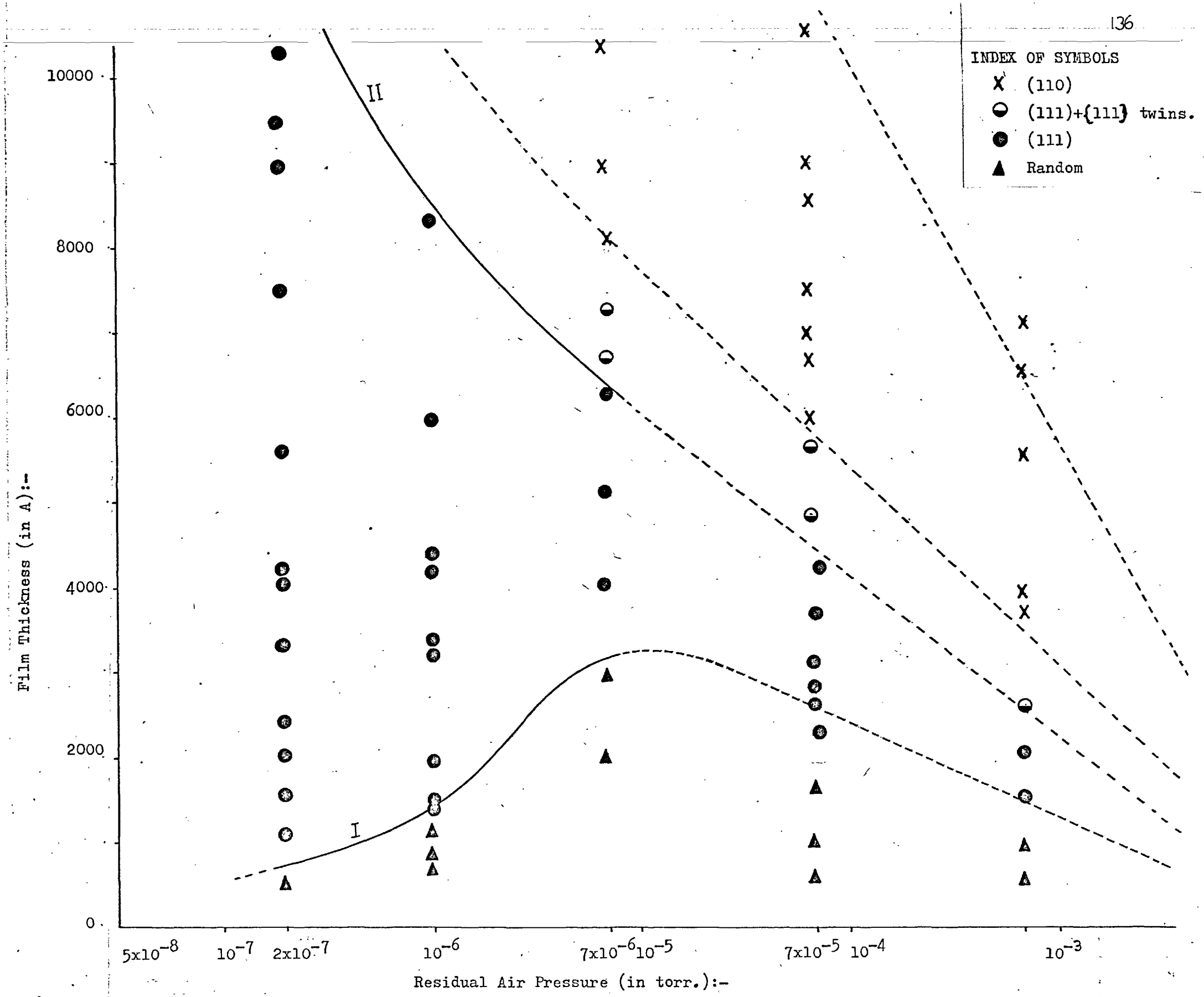

Fig.19. VARIATION OF SURFACE ORIENTATION OF SILVER FILMS CONDENSED ON STAINLESS-STEEL AT ROOM TEMPR., WITH FILM THICKNESS AND RESIDUAL AIR PRESSURE (RATE OF DEPO.30to35A/SEC.). $\angle i = 0°$

3.2(a). The Structure of the Silver Deposits at the Earliest Stage of Thickness where Random Orientation Developed:

In the present range of pressures used (2×10^{-7} and 1×10^{-6} torr), the silver deposits up to a thickness of $\sim$ 1000 A showed the polycrystalline random structure. The upper limit of their critical thickness was observed to decrease with decrease of pressure, unlike the observations of Dutta (1968) made at higher pressures.

Figs.20(a-d) are typical, showing continuous rings. The rings do not show appreciable drawing out at their inner edge due to refraction of the electron beam. This indicates that there is no strong facet formation on the surface of the deposit at this stage of thickness. The surface may be assumed to consist of relatively steeply projecting crystal surfaces which allow transmission of the electron beam with negligible refraction.

Fig.20(c) is from a specimen $\sim$700 A thick prepared at 1×10^{-6} torr, at 32 A/sec. The rings are sharp and distinct and without much refraction. Using eqn. (3.1) the mean crystal diameter of the specimen can be estimated. Considering the 200 ring, the $\beta_{\frac{1}{2}}$ value is found to be 0.32 mm. Allowances must be made for the broadening of the rings due to the finite width of the primary beam as

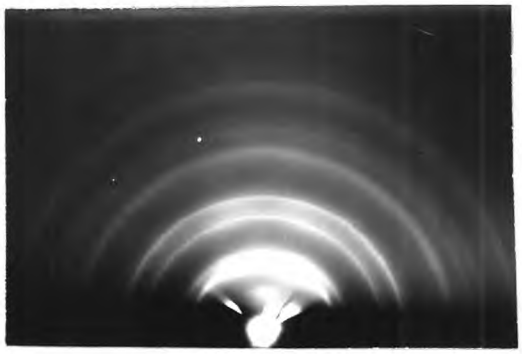

(a) Thickness = 533A at i=0°
Pressure = 2×10^{-7} torr
Angle i = 0°

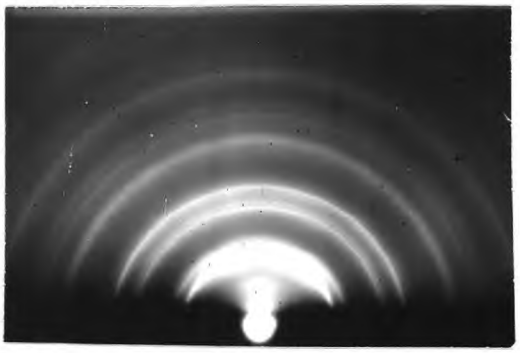

(b) Thickness and Pressure as in (a)
Angle i = 45° Vapour

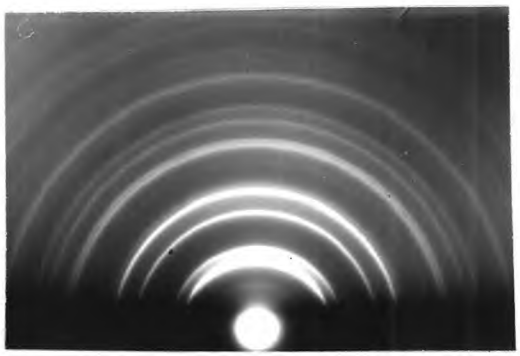

(c) Thickness = 700A at i=0°
Pressure = 1×10^{-6} torr
Angle i = 0°

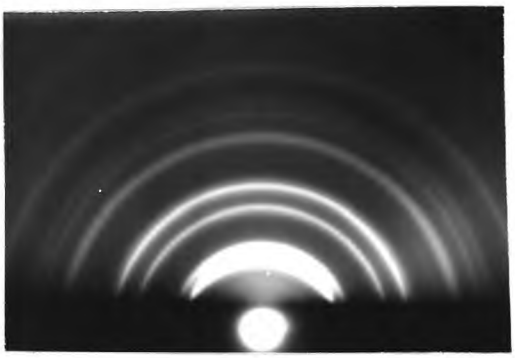

(d) Thickness =1100A at i=0°
Pressure = 1×10^{-6} torr
Angle i = 0°

Fig.20. Electron Diffraction Patterns from the Silver Deposits showing Random Crystal Orientation.

estimated from the central spot of the pattern (~0.10 mm), and also due to the breadth of the specimen traversed by the electron beam at low angle of incidence which corresponds effectively to the camera length.

In the present case L = 50 cm and the breadth of the specimen is ~0.5 cm. Hence, the broadening of the ring radius due to this cause is about 1% of the radius of any ring. For the 200 ring (radius 1.1 cm) it is 0.11 mm. Thus, the half-width $\beta_{\frac{1}{2}}$ attributable to the diffraction broadening is approximately estimated as $\beta_{\frac{1}{2}}$ = (0.32 - 0.10 -0.11) mm = 0.11 mm. Taking λ = 0.0509 A corresponding to an accelerating voltage 55 KV, $\theta \sim 0^{\circ}$, the mean crystal diameter is calculated as 210 A.

Considering the pattern in Fig.20(d), the value of $\beta_{\frac{1}{2}}$ is 0.185 mm, λ = 0.053 A, and the mean crystal diameter is ~130 A.

3.2(b). <u>The Structure of the Silver Deposits at the Stage of Thickness where (111) Orientation Developed</u>:

At a certain stage of thickness depending upon the pressure (see Fig.19), there is preferred growth of crystals having an octahedral plane parallel to the substrate or nearly so. The thickness at which (111) orientation initially develops gradually decreases with decrease of pressure. The thicknesses at which (111) orientation is

first observed at 1 x10^{-6} torr and 2 x10^{-7} torr are 1350 A and 990 A respectively. The locus I in Fig.19 marks the film thickness at which (111) orientation begins to develop. The locus II defines the upper limit of the region of thickness characetrised by (111) orientation, and in further deposition another orientation, (211), begins to grow (Dutta 1968).

Figs.21(a-d) and Figs.22(a-d) are typical photographs. Fig.21(a) is at normal incidence of vapour stream, 4072 A thick and prepared at 2 x10^{-7} torr of air, at 35 A/sec. The pattern shows a clear and strong (111) orientation of the crystals. The arcs are relatively short and sharp and are drawn out towards the inner side of the rings, especially the inner rings. This indicates that there is a strong development of the {111} faces which are parallel to the substrate or nearly so. The angular spread of the central arc on the 111 ring is about $\pm$ 11^{o}.

Fig.21(b) is from the region where i = 30^{o} in the same specimen. Comparing this pattern with the theoretical one for (111) orientation of a f.c.c. metal (Fig.7a), it can be recognised as showing a (111) type of orientation. There is no appreciable tilt of the orientation axis for this obliquity of the vapour stream. The lack of asymmetry in the intensity distribution of the pattern

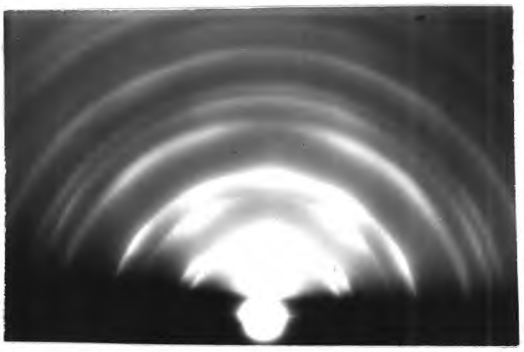

(a) Thickness =4072A at i=0°
Pressure = 2×10^{-7} torr
Angle i = 0°

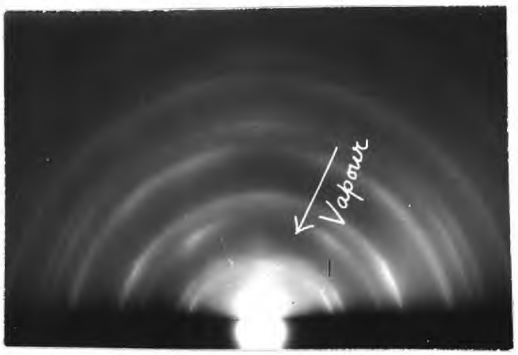

(b) Thickness and Pressure as in (a)
Angle i = 30°

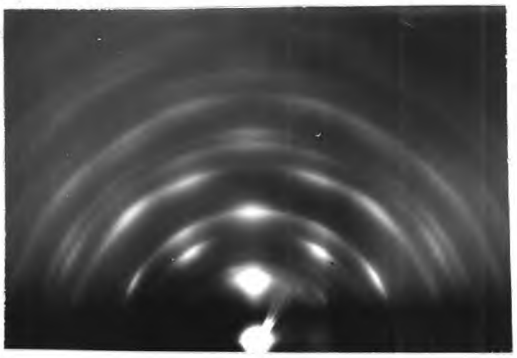

(c) Thickness =4366A at i=0°
Pressure = 1×10^{-6} torr
Angle i = 0°

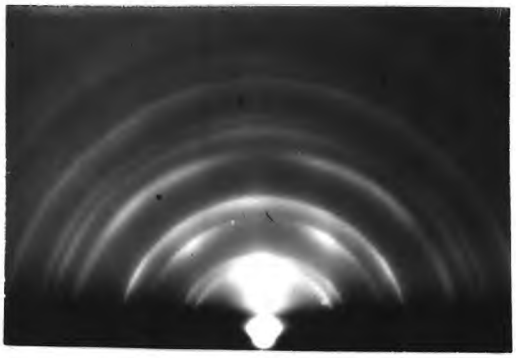

(d) Thickness =2418A at i=0°
Pressure = 2×10^{-7} torr
Angle i = 0°

Fig.21. Electron Diffraction Patterns from the Silver Deposits showing (111) Orientation.

indicates that there is no appreciable azimuthal limitation of the crystals about the direction of the vapour stream, at this region of the specimen. The spread of the central arc on the 111 ring is $\pm 20^{\circ}$ - showing similar spread of the $\{111\}$ faces about the mean axis of orientation.

Fig.22(a) is from the region of normal incidence of the vapour stream of a specimen 1550 A thick prepared at 1×10^{-6} torr at 35 A/sec. This also shows a clear (111) type of orientation pattern. The central 111 arc is short and sharp with an angular spread of $\sim \pm 10^{\circ}$. The pattern shows a considerable amount of refraction towards the shadow edge, indicating development of atomically smooth octahedral faces parallel to the substrate or nearly so.

Similarly Fig.22(c) is from the $i = 0^{\circ}$ region of a specimen 3196 A thick prepared at 1×10^{-6} torr of air at 28 A/sec. The angular spread of the central 111 arc is about $\pm 8^{\circ}$ only, showing very little spread of the crystal orientation from the mean (111) orientation. There is again strong refraction of the electron beam by the evidently smooth (111) faces.

It was observed that the (111) orientation once started begins to develop rapidly. The orientation becomes stronger as the thickness increases irrespective of the pressure of the residual air.

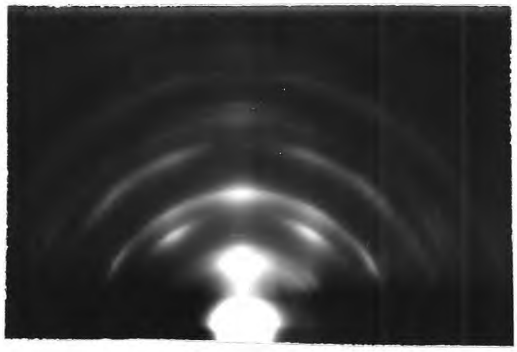

(a) Thickness =1350A at i=0°
Pressure = $1x10^{-6}$ torr
Angle i = 0°

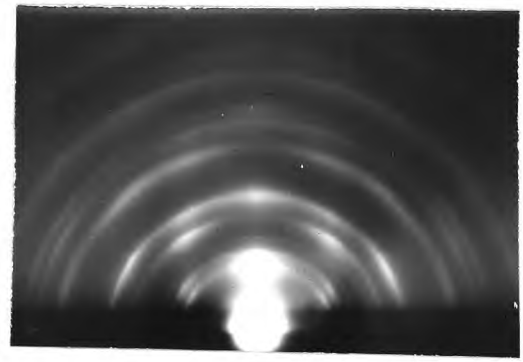

(b) Thickness =6000A at i=0°
Pressure = $1x10^{-6}$ torr
Angle i = 0°

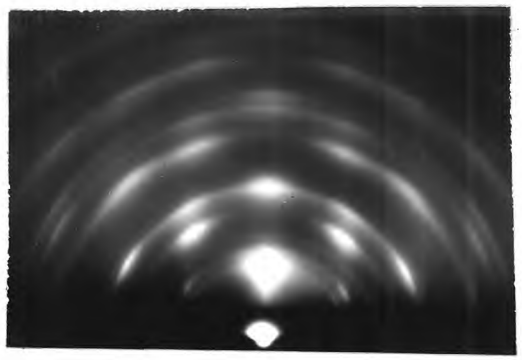

(c) Thickness =3196A at i=0°
Pressure = $1x10^{-6}$ torr
Angle i = 0°

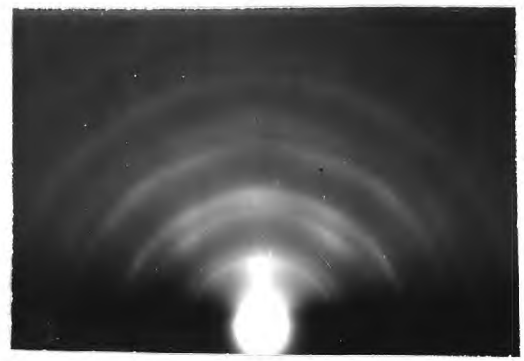

(d) Thickness =1947A at i=0°
Pressure = $2x10^{-7}$ torr
Angle i = 0°

Fig.22. Electron Diffraction Patterns from the Silver Deposits showing (111) Orientation.

Figs.23 and 24(a and b) are electron micrographs of the i = 0, i = 23^{o} and i = 45^{o} regions respectively of a silver specimen 1547 A thick prepared at 30 A/sec, at 2 x10^{-7} torr of air. The specimens were examined by self-shadowed Pt/C replica technique in a J.E.O.L. JEM 7 electron microscope. The electron voltage was 80 KV, the shadowing angle 15^{o} and magnification 50,000 X.

All the three photographs show the roughness of the surface to some extent. The film surface is continuous, the crystals meeting one another along more or less irregular polyhedral boundaries. No distinct variation in crystal size is obvious from the three photographs taken from the three regions of the same specimen, the mean crystal diameter being about 200-250 A. No very clear plane crystal faces can be recognised.

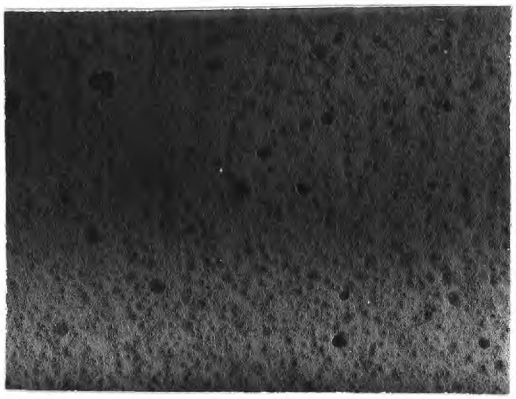

Fig.23. Electron Micrograph from the i=0° region of the Surface of a 1547A thick Silver Deposit.

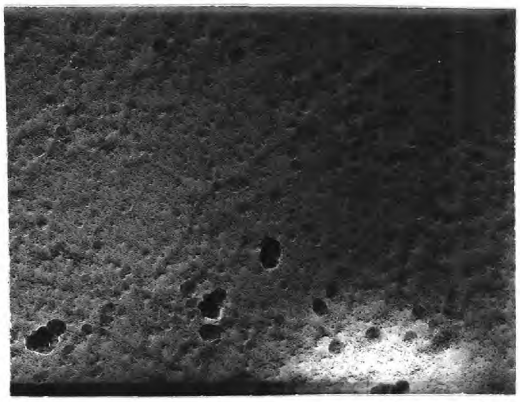

Fig.24a. Electron Micrograph from the i = 23° region of the same specimen as in Fig.23.

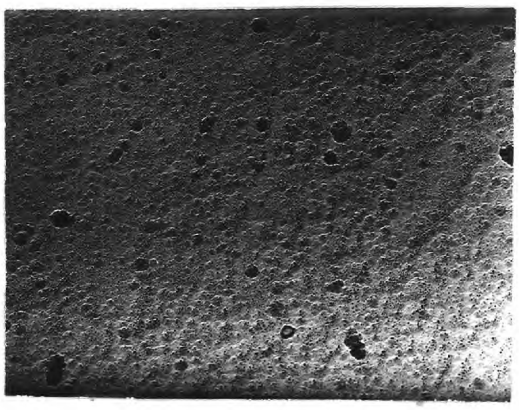

Fig.24b. Electron Micrograph from the i = 45° region of the same specimen as in Fig.23.

Magnification for all the Micrographs = 50,000 X.

Pressure = 2×10^{-7} torr

3.3. The Structure of the Copper Deposits Condensed in Vacuum onto Polished Stainless-steel at Room Temperature at 17 to 22 A/sec in Relation to Thickness and Residual Air Pressure:

Spectroscopically pure copper was evaporated and condensed onto polished stainless steel and glass substrates at room temperature under various residual air pressures. The method for preparing the films was as for gold and silver described earlier in 3.1 and 3.2. Since the heating current could not be increased beyond a certain limit and since it was desired to keep the distance between the bead and the substrate the same (= 3 cm; as in the case of silver), the rate of deposition could not be raised beyond 22 A/sec. As mentioned in 2.5(b), the copper bead had to be preheated for about 8 minutes before each evaporation. The pressure rose considerably (by a factor of ~5) during this operation, and sufficient time was allowed for the evaporating system to attain the required pressure every time before the actual evaporation process.

The results obtained are presented in Fig.25 for normal incidence of the vapour stream. Detailed discussions of the results are presented in the subsequent sub-sections.

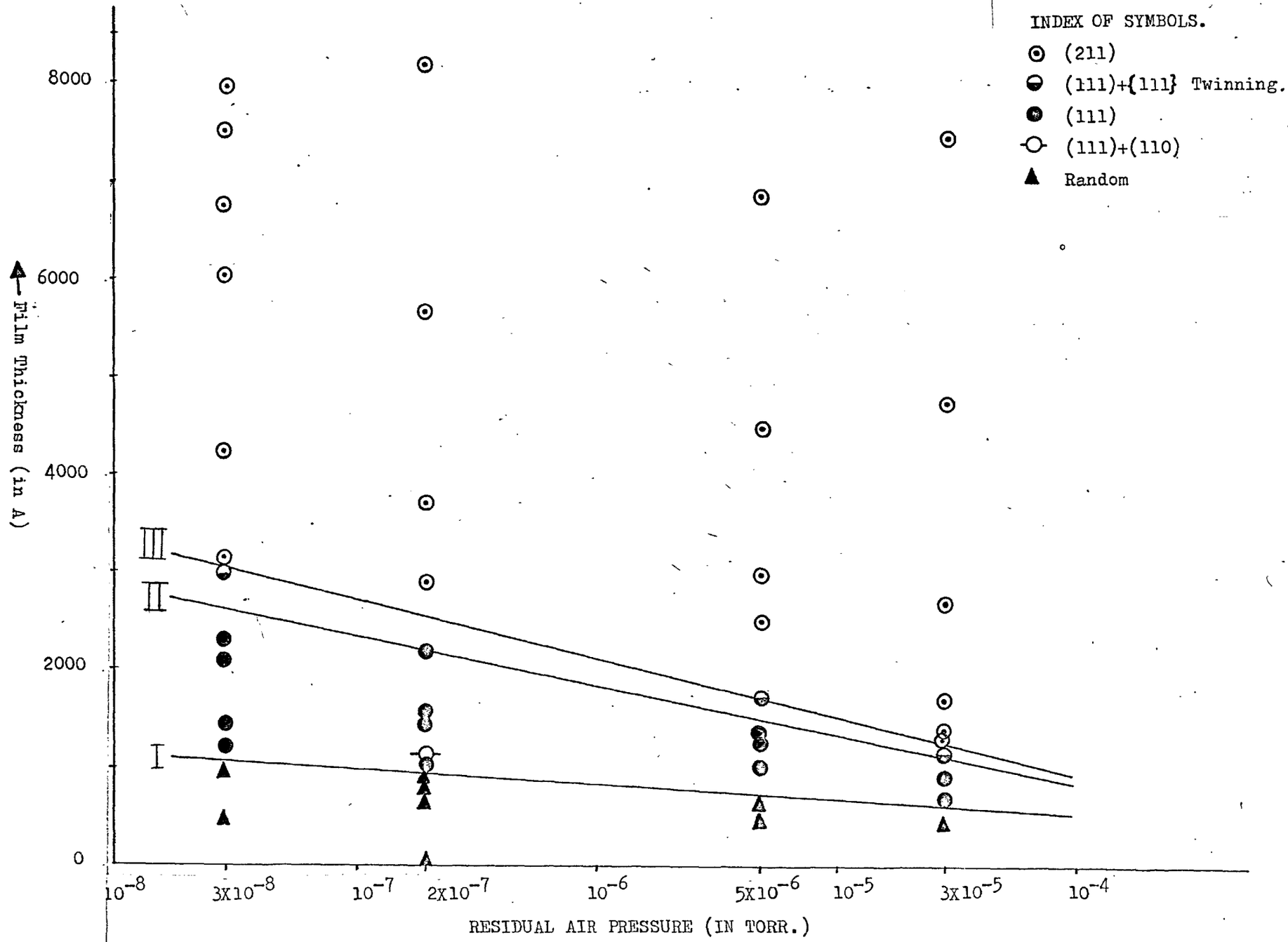

FIG.25. VARIATION OF SURFACE ORIENTATION OF COPPER FILMS CONDENSED ON STAINLESS-STEEL AT ROOM TEMPR., WITH FILM THICKNESS AND RESIDUAL AIR PRESSURE (RATE OF DEPOSITION APPROXIMATELY 20A/SEC.)

$\angle i = 0^\circ$

3.3(a). The Structure of the Copper Deposits Condensed at Normal Incidence of the Vapour Stream:

As in the previous two cases of gold and silver, copper deposits condensed on glass and polished stainless steel at room temperature showed randomly oriented crystals at the early stage of growth with normal f.c.c. structure. The range of pressures of the residual air in which the films were prepared was 3×10^{-5} to 3×10^{-8} torr. Fig.25 shows that at certain ranges of thickness, decreasing with increasing pressure, different kinds of preferred orientation developed in the deposits.

At a certain thickness (locus I in Fig.25) increasing with decreasing pressure of residual air, the octahedral faces begin to grow parallel to the substrate, the crystals having a preferred (111) type of orientation. The minimum thickness at which (111) type of orientation was observed in the copper deposits is 650 A, in films prepared at 3×10^{-5} torr. At the lowest pressure, 3×10^{-8} torr, the first signs of (111) orientation were observed at a thickness of about 1200 A.

At a certain upper limit of thickness of the deposits, at locus II in Fig.25, the (211) type of orientation sets in. At 3×10^{-5} torr, the (211) orientation was first observed at 1240 A thickness which

which was the minimum thickness observed for this type of orientation. This critical thickness increased almost linearly with decrease of the logarithm of the pressure and at the lowest pressure in this investigation (3×10^{-8} torr) this minimum thickness was found to be about 3000 A.

In only one case, a mixture of (110) and (111) orientations was obtained for a specimen 1200 A thick prepared at 2×10^{-7} torr of air, and still in another case a mixture of (111) orientation + {111} twinning was obtained for a specimen 1725 A thick prepared at 5×10^{-6} torr.

The changes in orientation from the random to (111) type and from (111) to stable (211) type were rapid in comparison with those of gold.

Thus, the region below the locus I is the region of random orientation of the crystals, that between I and II is the region of (111) type of orientation and the region beyond the locus II is the region where stable (211) type of orientation developed.

The electron diffraction evidence of the development of the above mentioned orientations are described below step by step.

3.3:a(i). <u>The Structure of the Copper Deposits at the Initial Random Orientation Stage</u>:

This stage of thickness increased from about 490 A at 3 $x10^{-3}$ torr of air to about 1010 A at 3 $x10^{-8}$ torr as the pressure of the air decreased.

Figs.26(a-d) show typical electron diffraction patterns consisting of continuous rings of copper with some cuprous oxide rings. Fig.26(a) is from a specimen 910 A thick prepared at 3 $x10^{-8}$ torr at 20 A/sec. The continuous sharp rings show that this has not been any preferred growth of any type of crystal plane parallel to the surface of the substrate. Some faint Cu_2O rings are visible along with the main pattern. There is little or no drawing out of the rings towards the inner edges of the rings, which indicates that there is no strong development of facets on the crystals. The pattern is hence due to the transmission of the electron beam through the projecting tips of the crystals at the deposit surface.

Figs.26(c and d) are from specimens 500 A and 470 A thick prepared at 5 $x10^{-6}$ and 3 $x10^{-5}$ torr respectively, at 21 A/sec. The presence of Cu_2O is prominent in the specimens as is indicated by the strong Cu_2O rings in both the patterns. The main copper pattern can be recognised without much confusion. The rings are continuous and fine

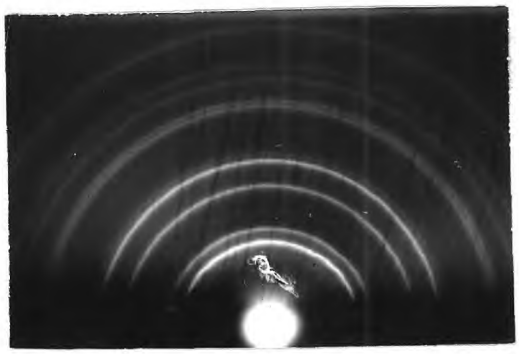

(a) Thickness = 910A at i=0°
Pressure = $3x10^{-8}$ torr
Angle i = 0°

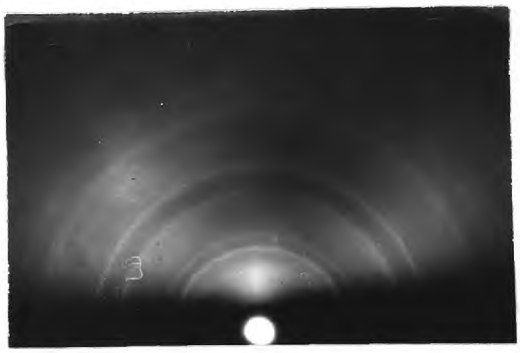

(b) Thickness = 800A at i=0°
Pressure = $2x10^{-7}$ torr
Angle i = 0°

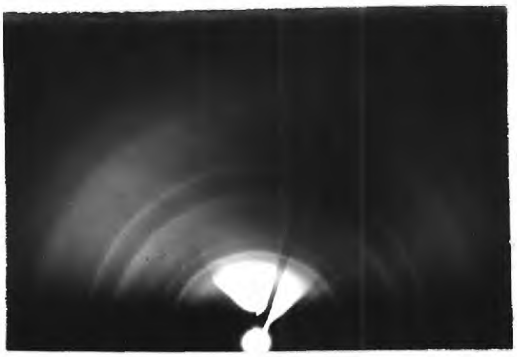

(c) Thickness = 500A at i=0°
Pressure = $5x10^{-6}$ torr
Angle i = 0°

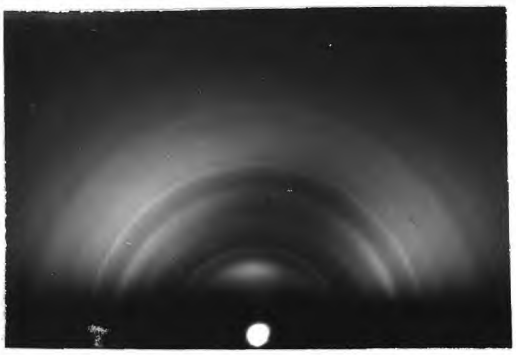

(d) Thickness = 470A at i=0°
Pressure = $3x10^{-5}$ torr
Angle i = 0°

Fig.26. Electron Diffraction Patterns from the Copper Deposits showing Random Crystal Orientation.

and do not show much refraction of the electron beam. In all the four specimens it is observed that at the early stage of growth of the crystals there first develops a rough surface, on the atomic scale. The situation is independent of any variation in the pressure of residual air in the evaporating system.

The mean crystal diameter of the deposits can be estimated from Laue's equation (3.1). Considering the 111 ring of Fig.26(a), the ring radius is 1.15 cm, the measured half-width of the ring is 0.35 mm and the width of the primary electron beam as estimated from the central spot is 0.15 mm. Taking λ = 0.05 A for an accelerating voltage of 55 KV and camera length L = 48 cm, we have the broadening effect of any ring due to the width of the specimen (6 mm) as 0.125% of the ring radius. Hence the actual $\beta_{\frac{1}{2}}$ value for the 111 ring is (0.35 - 0.15 - 0.14) mm = 0.06 mm. Using this value of $\beta_{\frac{1}{2}}$ in equation (3.1) the mean diameter of the crystal is about 360 A.

Fig.26(c) is from a specimen 500 A thick prepared at 5 x10^{-6} torr of air. The $\beta_{\frac{1}{2}}$ value in this case for the 111 ring is estimated as (0.34 - 0.1 - 0.165) mm = 0.075 mm. Thus, corresponding to λ = 0.05 A and L = 48 cm, the mean crystal diameter of this specimen is about 288 A.

As in the previous cases of gold and silver, since

$\beta_{\frac{1}{2}}$ is very small, the estimated crystal diameters can best be regarded as minimum values and the true mean crystal size may be much larger than these calculated values.

3.3a(ii). The Structure of the Copper Deposits at the Stage of Thickness at which (111) Orientation Developed:

Beyond a certain thickness of the copper films the crystals begin to show (111) type of orientation. Fig.25 shows that the critical thickness of the deposits at which (111) type of orientation begins to develop increased nearly rectilinearly with decrease of the logarithm of the pressure, within the range of 3×10^{-5} to 3×10^{-8} torr of air.

Figs.27(a-d) and 28(a-d) illustrate typical diffraction patterns.

Fig.27(a) is from the $i = 0^{\circ}$ region of a specimen 2300 A thick, prepared at 3×10^{-8} torr and deposited at 20 A/sec. The central arc on the 111 ring together with the two lateral ones are recognisable. (in the actual negative plate). The pattern undoubtedly indicates a (111) type of orientation. The central arc on the 111 ring has a spread of roughly about $\pm 11^{\circ}$, indicating a corresponding spread of the (111) orientation. The Cu_2O pattern is also strongly present. The relative ring positions of the Cu and the Cu_2O are shown in Fig.27(b), for easy reference.

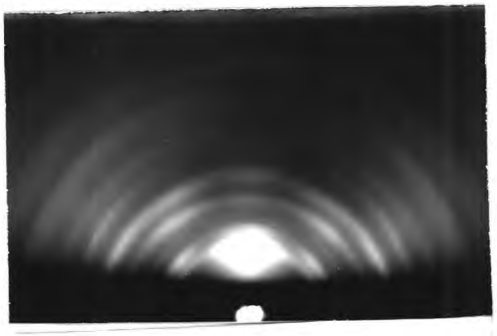

(a) Thickness =2300A at i=0°
Pressure = 3×10^{-8} torr
Angle i = 0°

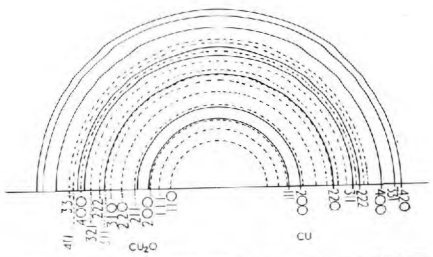

(b) Relative Ring Positions of Copper (solid rings) and Cu_2O (broken rings).

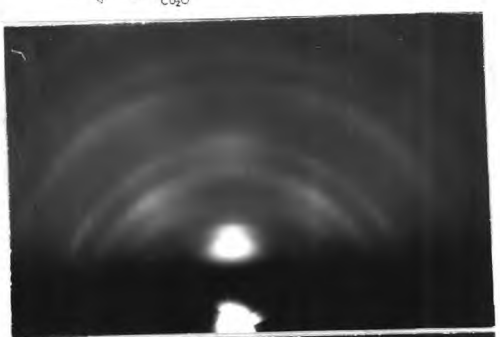

(c) Thickness =1550A at i=0°
Pressure = 2×10^{-7} torr
Angle i = 0°

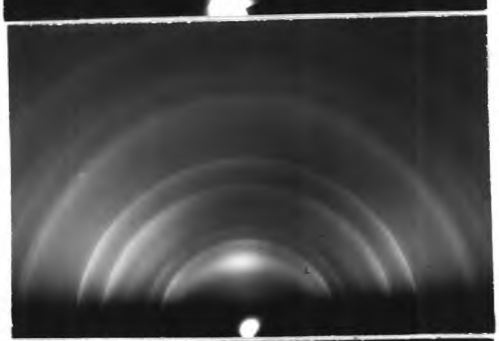

(d) Thickness =1300A at i=0°
Pressure = 5×10^{-6} torr
Angle i = 0°

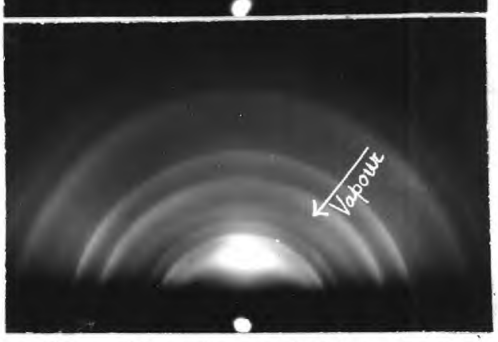

(e) Thickness and Pressure as in (d)
Angle i = 45°

Fig.27. Electron Diffraction Patterns from the Copper Deposits showing (111) Orientation.

Fig.27(c) is from the i = 0° region of a specimen 1550 A thick prepared at 2 x10^{-7} torr of air at 18 A/sec. The pattern shows strong (111) orientation of the copper, along with the strong (111) orientation of Cu_2O. The spread of arcing and hence of the orientation from the mean, is $\pm$ 10°. Here also, the strong refraction of the electron beam indicates development of (111) faces, which are nearly parallel to the electron beam.

Figs.28(c) and 28(d) are from the i = 0° and i = 45° regions respectively of a specimen 2200 A thick prepared at 2 x10^{-7} torr of air. Both the patterns show (111) type of orientation. The Cu pattern arcs are relatively sharper than those of the Cu_2O. The spread of arcing is $\pm$ 12°. The patterns in Fig.28(d) show the same features as those of Fig.28(c). There is no detectable tilt of the orientation axis even though the direction of the vapour stream is 45° at the point where the beam grazed the specimen. The corresponding Cu_2O pattern also does not show any tilt of its orientation axis.

The maximum thickness beyond which (111) type of orientation ceased to develop was about 2500 A at 3 x10^{-8} torr.

One specimen 1150 A thick prepared at 2 x10^{-7} torr showed a mixture of (111) and (110) orientations (Figs.29(a) and (b)). While all conditions during its preparation were

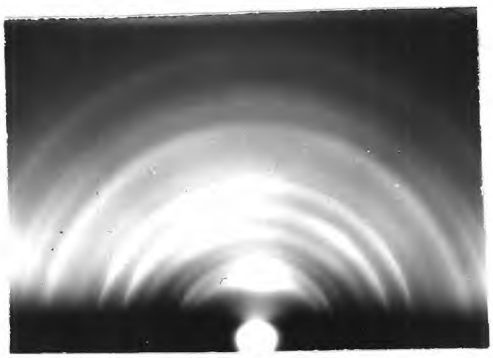

(a) Thickness = 2100A at i=0°
Pressure = 3×10^{-8} torr
Angle i = 0°

(b) Thickness =1450A at i=0°
Pressure = 3×10^{-8} torr
Angle i = 0°

(c) Thickness = 2200A at i=0°
Pressure = 2×10^{-7} torr
Angle i = 0°

(d) Thickness and Pressure as in (c)
Angle i = 45°

Fig.28. Electron Diffraction Patterns from the Copper Deposits showing (111) Orientation.

identical with those in that region, the thickness estimation may perhaps have been in error. The reason for this anomalous result is not clear.

3.3a(iii). The Structure of the Copper Deposits at the Stage of Thickness where (111) Orientation + {111} Twinning Developed:

Beyond the locus II in Fig.25 is the stage at which this kind of mixed orientations develops. This region is confined between the loci II and III. In only three deposits such development of {111} twinning along with (111) orientation was observed.

The diffraction photographs showed preferential growth of the crystals having {111} planes nearly parallel to the substrate together with the (115) orientation which develops due to twinning on the {111} planes (cf. 3.1a(iii)).

Figs.30(a,b,c) illustrate some of these results. Fig.30(a) and 30(b) are from the $i = 0^{\circ}$ and $i = 45^{\circ}$ regions respectively of a specimen 1800 A thick prepared at 5×10^{-6} torr of air. In Fig.30(a), in addition to the main (111) type of diffraction pattern, some arcs corresponding to (511) type of orientation are visible. The two lateral arcs on the 111 ring on radii at $\pm 35^{\circ}$ from the plane of incidence are due to the (511) type of orientation of the crystals. The two arcs on the 200 ring on either side of the plane of

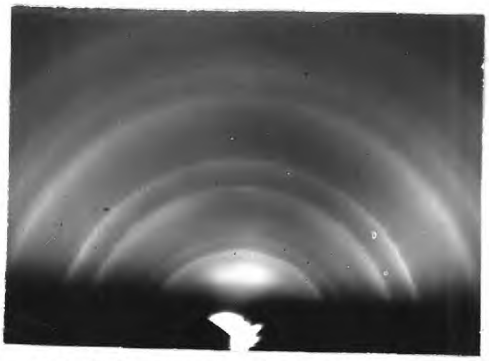

29a. Thickness =1150A at i=0°
Pressure = 2×10^{-7} torr
Angle i = 0°

29b. Thickness and Pressure as in 29(a)
Angle i = 45°

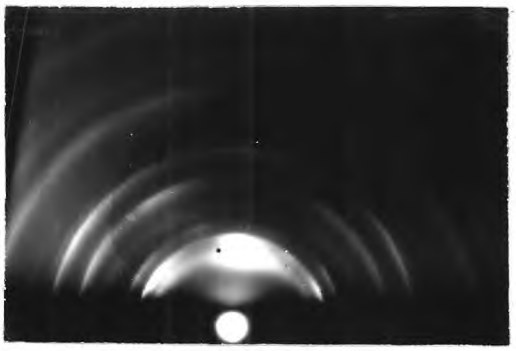

30a. Thickness =1800A at i=0°
Pressure = 5×10^{-6} torr
Angle i = 0°

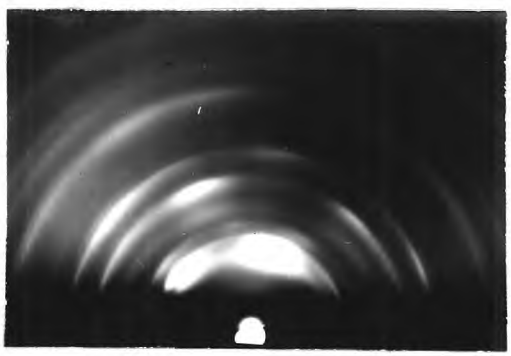

30b. Thickness and Pressure as in 30(a)
Angle i = 45°

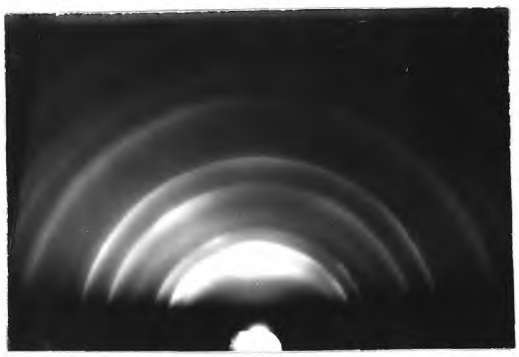

30c. Thickness =3010A at i=0°
Pressure = 3×10^{-8} torr
Angle i = 0°

Figs.29 and 30. Diffraction Patterns from the Copper Deposits showing (111)+(110) Orientations (29a & b) and (111) Orientations + {111} Twinning (30 a, b & c).

incidence of the vapour stream are also very distinct (at about the 11 o'clock and 1 o'clock positions). Some strengthening in intensity is also visible in the central region of the 511 ring (in the actual negative). The directions of the [111] orientation axis and the [511] orientation axis seem to coincide, both being normal to the substrate. The slight strengthening in intensity at the central region of the 331 copper ring may be due to the coalescence of the two arcs expected in that region due to (511) type of orientation.

The pattern in Fig.30(b) shows the same features as in Fig.30(a), but here both the main [111] and [511] axes are inclined towards the vapour stream by slightly different angles. Though the two neighbouring arcs on either side of the central arc are on the 111 ring are not visible distinctly, yet the two other neighbouring arcs on the 200 ring are clearly visible. There is very little asymmetry in the intensity distributions of the identical arcs on either side of the orientation axis. This may mean that there is no azimuthal limitation for the grazing crystals about the orientation axis.

3.3a(iv) <u>The Structure of the Copper Deposits at the Stage of Thickness where (211) Orientation Developed</u>:

Unlike the case of gold, copper deposits did not

appear to show any mixture of (111) and (211) types of orientation in the transitional stage. The change in orientation from (111) to (211) is relatively rapid in this case. Beyond the stage indicated by the locus III in Fig.25 the octahedral orientation mixed with its twinning ceases to develop and the (211) type of orientation sets in. Here also, the thickness of the deposits for first development of (211) orientation increased almost linearly with decrease of the logarithm of the pressure of the residual air in the system. The minimum thickness observed was ~1300 A, the deposit being at a pressure of 3×10^{-5} torr of air.

Figs. 31, 32 and 33 illustrate typical diffraction patterns obtained.

Figs.31(a) and 31(b) are the diffraction patterns from the i = 0 and i = 45° regions respectively of a specimen 1700 A thick prepared at 3×10^{-5} torr at 20 A/sec. Considering Fig.31(a), the two short lateral arcs on the 111 ring on either side of the plane of incidence of the electron beam are well separated by the zero-intensity region on the central part. These two arcs along with the two similar lateral arcs on the 200 ring lie on the same layer line (4^{th} layer line) which is parallel to the shadow edge. The arcs lying on the 2^{nd} layer line on these two rings are also visible. The two lateral arcs further up

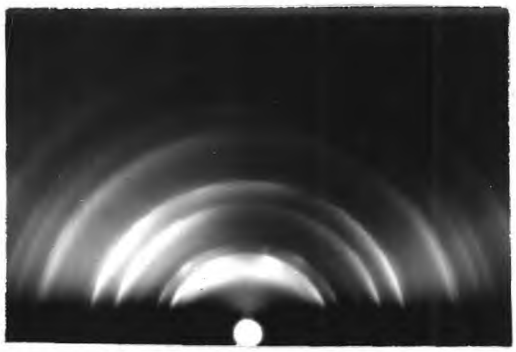

(a) Thickness =1700A at i=0°
Pressure = 3×10^{-5} torr
Angle i = 0°

(b) Thickness and Pressure as in (a)
Angle i = 45°

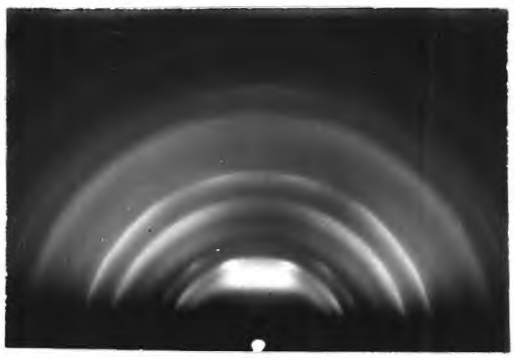

(c) Thickness =1250A at i=0°
Pressure = 5×10^{-6} torr
Angle i = 0°

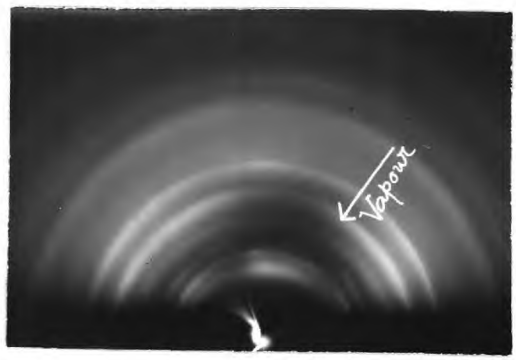

(d) Thickness and Pressure as in (c)
Angle = 45°

Fig.31. Electron Diffraction Patterns from the Copper Deposits showing (211) Orientation.

in the 311 ring near and on either side of the plane of incidence are also seen to be separated by nearly zero intensity in between. The 422 arc on the central region of the 422 ring is visible with a spread of about $\pm 11^{o}$. All these distinct features show this agrees clearly with a (211) type of orientation. The {211} planes have developed parallel to the surface of the substrate within an azimuthal spread of $\pm 11^{o}$ (approx.) about the vapour stream direction. The short and sharp arcs on the 111 and 200 rings do not show any refraction effect of the electron beam. This means that there is no strong development of facets on the growing crystals.

The pattern in Fig.31(b) shows the same (211) type of orientation but with the orientation axis tilted towards the vapour stream.

Fig.31(c) is from the i = 0 region of a specimen 1250 A thick prepared at 5 $x10^{-6}$ torr. This also shows a clear (211) orientation pattern with the 422 arc on the central region of the 422 ring distinctly visible along with the other features. The Cu_2O pattern also shows a (211) type of orientation.

Fig.32(a) shows the diffraction pattern from the i = 0 region of a specimen 8500 A thick prepared at 2 $x10^{-7}$ torr. The two lateral arcs on the 111 ring near the plane

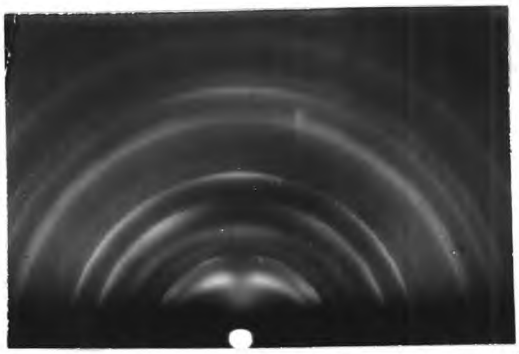

32a. Thickness =8500A at i=0°
Pressure = 2×10^{-7} torr
Angle i = 0°

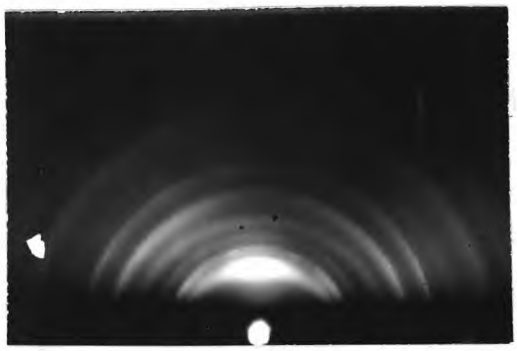

32b. Thickness=2700A at i=0°
Pressure = 3×10^{-5} torr
Angle i = 0°

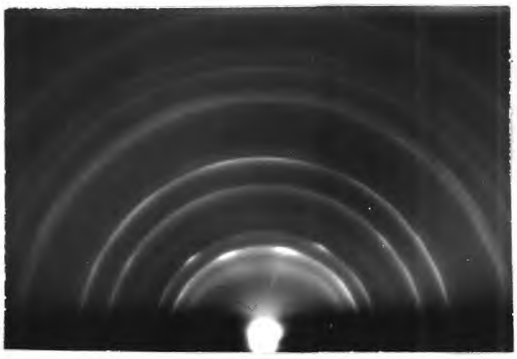

33a. Thickness =6900A at i=0°
Pressure = 5×10^{-6} torr
Angle i = 0°

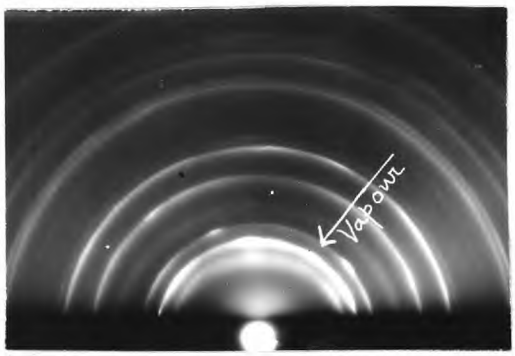

33b. Thickness and Pressure as in 33a.
Angle i = 45°

Figs.32 and 33. Electron Diffraction Patterns from the Copper Deposits showing (211) Orientation.

of incidence are distinctly separated. The Cu_2O pattern which is strong here also shows (211) type of orientation. The strengthening in intensity at the central region of the 331 ring may be either due to the coalescence of the two neighbouring lateral arcs expected in that region due to (211) type of orientation, or may be due to some of the {331} planes coming into the Bragg's reflection position due to considerable rocking of the {211} planes of the crystals.

All the photographs show very little refraction effect. The conclusion is that there is no strong {211} facet formation parallel to the substrate and the surface of the growing crystals is relatively rough on the atomic scale. The strong Cu_2O pattern is due to the highly reacting habit of copper with oxygen either in the preparation chamber or during transit to the camera.

3.3(b). <u>The Structure of the Copper Deposits Condensed at Oblique Incidence of the Vapour Stream</u>:

The electron diffraction examination of the regions of the inclined incidence of the vapour stream on the substrate was carried out for several specimens. In most of the cases there was no change in orientation except in a few described below, where the orientation changes from (211) to (111), or from (111) + {111} twinning. In all the examinations the electron beam was normal to the plane of incidence of the vapour stream.

The orientation axes indicated by the diffraction patterns showed varying amounts of tilt although the obliquity of the vapour stream was constant. While at higher pressures the tilt was appreciable, at the ultra-high vacuum region it was almost unnoticeable.

Fig.27(e) is such a diffraction pattern from the $i = 45^{\circ}$ region of aspecimen 1300 Å thick at $i = 0^{\circ}$, prepared at 5×10^{-6} torr of air. The [111] axis of orientation does not show any tilt towards the vapour beam direction. The pattern clearly corresponds to one of oblique (111) orientation. The 111 arc on the 111 ring is visible (more clearly in the actual negative plate). The tilt of the [111] axis is very small, $\sim 8^{\circ}$.

Fig.31(b) is from the $i = 45^{\circ}$ region of a specimen 1750 Å thick at $i = 0$, prepared at 3×10^{-5} torr. It shows partly a strong (211) orientation together with the (111) orientation. The two arcs on the 111 ring near the plane of symmetry on both sides of it, and the 422 arc on the line of symmetry of the pattern, are visible together with the intensification of intensity of the central region of the 111 ring. The tilt of the [211] axis is $\sim 16^{\circ}$ but the [111] axis shows almost no tilt.

Fig.28(d) is from the $i = 45^{\circ}$ region of a specimen 2200 Å thick at $i = 0$ prepared at 2×10^{-7} torr of air. The

Cu_2O pattern is strong and the Cu pattern is weak. Yet, the (111) orientation of both the patterns can be recognised. The [111] axis shows no tilt towards the vapour stream.

Figs.34(a and b) show the plot of tilt vs. thickness, i.e. (δ, t) for the specimens prepared at 5 $x10^{-6}$ and 3 $x10^{-5}$ torr respectively, for i = 45^{o} of the vapour stream and for constant rate of deposition. Fig.34(a) shows that the tilt of the orientation axis at the initial stage of thickness up to about 560 A (at i = 45^{o}) shows very little change. As the thickness increases the tilt also rises gradually up to a certain maximum after which it falls down again.

Fig.34(b) shows the (δ, t) plot for results obtained from deposits prepared at 3 $x10^{-5}$ torr. The general nature of the graph is identical with that of Fig. 34(a). The maximum tilt is around 26^{o} corresponding to a thickness $\sim$1500 A (at i = 45^{o}).

The electron diffraction patterns obtained from the i = 45^{o} regions of the specimens prepared in the ultra-high vacuum range, did not, however, show any tilt of the orientation axes. Two diffraction patterns of such specimens have already been presented in Figs.28(d) and 29(b). This behaviour seems to be very unusual and perhaps requires further checking.

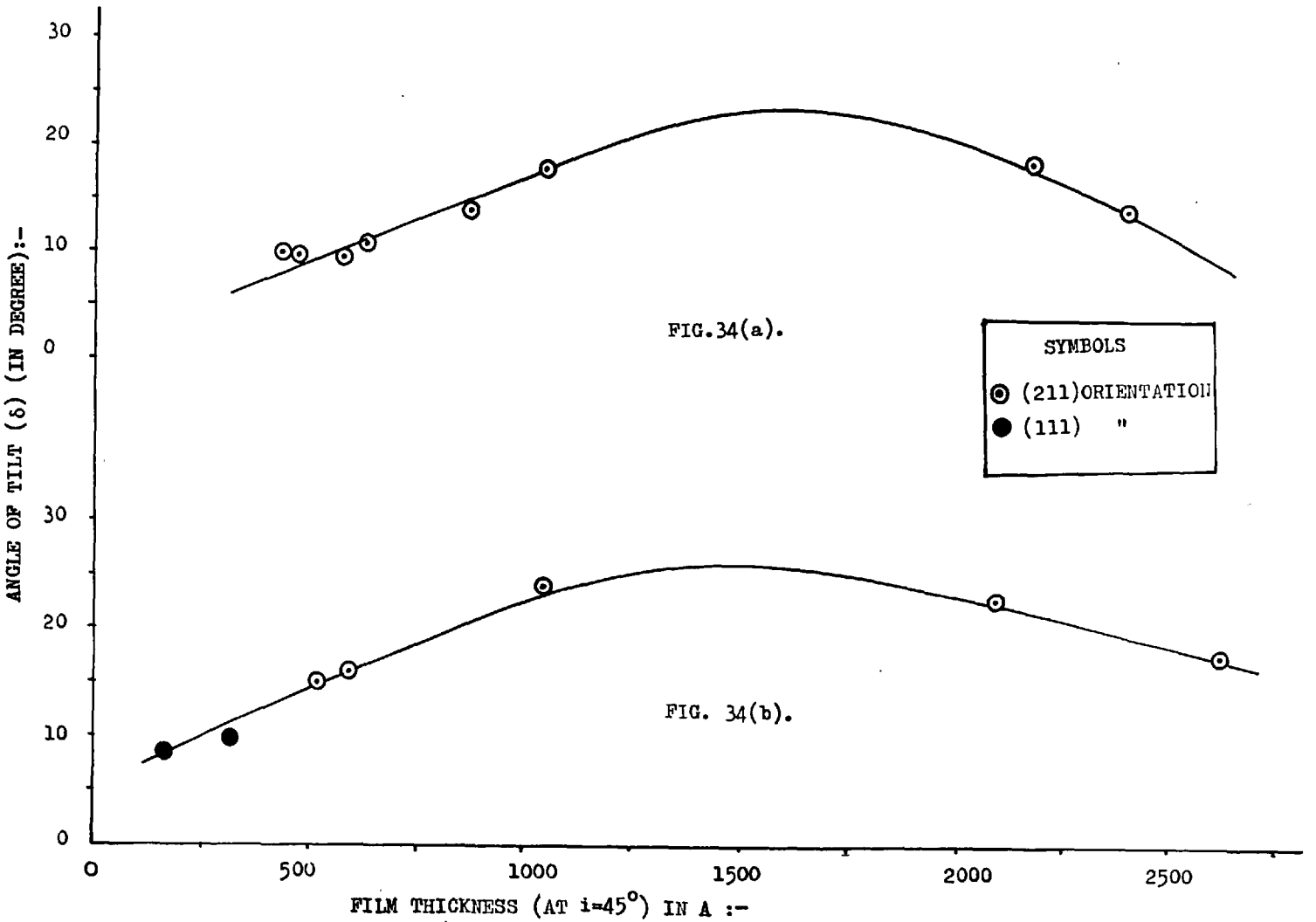

FIG.34(a).

FIG. 34(b).

FIG. 34(a). THICKNESS (AT i=45°) - TILT (t,δ) PLOT OF THE COPPER DEPOSITS CONDENSED ON STAINLESS-STEEL AT ROOM TEMPERATURE AT 5×10^{-6} TORR

34(b). " " " " " " " AT P= 3×10^{-5} TORR.

3.3(c). The Effect of Residual Air Pressure on the Structure of the Copper Deposits Condensed at Normal Incidence of the Vapour Stream:

The loci in Fig.25 show the effect of the pressure of the residual air on the structure of thin films of copper.

The sequence of the development of preferred orientations with increasing deposit thickness, in all the pressures investigated, is the same. In the initial stage the orientation is random, which gradually gives place to (111), (111) + {111} twinning and finally to (211).

The loci, I, II and III indicate the boundaries of these four stages. All the three loci rise rectilinearly with decreasing log (pressure), and have different slopes. This indicates that the minimum thickness to develop a particular orientation increases with decreasing pressure. For example, the minimum thicknesses at which (211) orientation was observed at 3×10^{-5} and 3×10^{-8} torr were 1250 A and 3150 A respectively. The loci, if extrapolated, would tend to meet at a pressure of about 10^{-3} torr.

It is hence concluded that the pressure of the residual air in the preparation chamber influences the orientation of the growing crystal deposits systematically, in addition to the effects caused by the other deposition parameters.

3.4. The Structure of Zinc and Cadmium Deposits Condensed on Glass and Stainless-steel Substrates at Room Temperature and Constant Initial Pressure, in Relation to Thickness and Rate of Deposition.

Spectroscopically pure zinc and cadmium were deposited on polished stainless-steel and in a few cases on glass substrates. The rate of deposition was varied for different specimens prepared at different constant pressures of air.

The tendency for splotchiness of the deposits of these metals (Evans, 1950) was avoided in the present work by taking still further precautions to ensure substrate cleanliness. The polished stainless-steel substrates, after being thoroughly washed by propyl alcohol, were heated in a pyrex test tube to about 150°C for a minute or two to vaporise any last traces of grease (for details see 2.4(d)). After cooling these substrates down to room temperature (in the test tube, with a wad of paper tissue, excluding free entry of room air), they were transferred to the deposition apparatus and evacuated, and films were prepared there.

For obtaining correct estimation of thickness of the films, reflexion of the vapour atoms of these metals from the walls of the enclosure was minimised by similarly degreasing the surrounding surfaces as far as practicable

(cf. 2.5(a)). Checks of the mean film thickness by direct weighing then confirmed that estimates based on mass loss from the bead, and the bead-substrate distance were correct within about 10-20%.

These hexagonal metals were highly reactive with the residual air in the system. These metals gettered the gas surrounding the bead and thereby lowered the pressure during the deposition process. In the case of the f.c.c. metals this phenomenon was not observed. So, for long deposition processes of Zn and Cd, the pressure was gradually diminishing with time due to the removal of the oxygen molecules by the metal bead and deposits. The pressures mentioned here, hence, are only the initial pressures.

Evans (1950) observed that Zn could not be deposited at low rates due to high mobility of the metal. In the present work while the trouble was appreciated, yet by introducing the improved method of substrate cleanliness, Zn and Cd could be deposited at rates as low as 25 A/sec.

The diffraction rings were sharp and spotty, indicating the growth of large crystals in the deposits, at least 500 A in diameter, or probably much more.

Further, most of the patterns showed some additional arcs due to the presence of ZnO, which was probably mainly formed during the transfer of the specimen.

The orientation of this hexagonal ZnO appeared to be similar to those of the Zn in the same specimen, corresponding to epitaxial relationship.

3.4(a). <u>The Structure of Zinc Deposits Condensed at Normal Incidence of the Vapour Stream at 5 x10^{-3} torr of Air on to Stainless-steel and Glass at Room Temperature</u>:

Spec-pure Zn was deposited mostly on stainless-steel substrates at rates of 25 to 990 A/sec to give films from 150 to 11,000 Å thick at 5 x10^{-3} torr of air.

The results are plotted in Fig.35. The plot shows four regions of different orientations observed in the zinc deposits condensed at this pressure.

In region I a mixture of (001), (100) and (101) orientations is developed. This region extends from about 610 Å to 3000 Å corresponding to rates from about 810 Å/sec to 930 Å/sec.

In region II one-degree (101) orientation occurs. This region extends roughly from about 150 Å to 2500 Å at 25 Å/sec or, to 4250 Å at 990 Å/sec.

Region III is a transitional stage from (101) to (112) orientation. This narrow region shows a mixture of (101) and (112) types of orientation. It extends from an estimated thickness of $\sim$1000 Å to $\sim$4500 Å corresponding to rates of deposition from $\sim$125 Å/sec to $\sim$650 Å/sec.

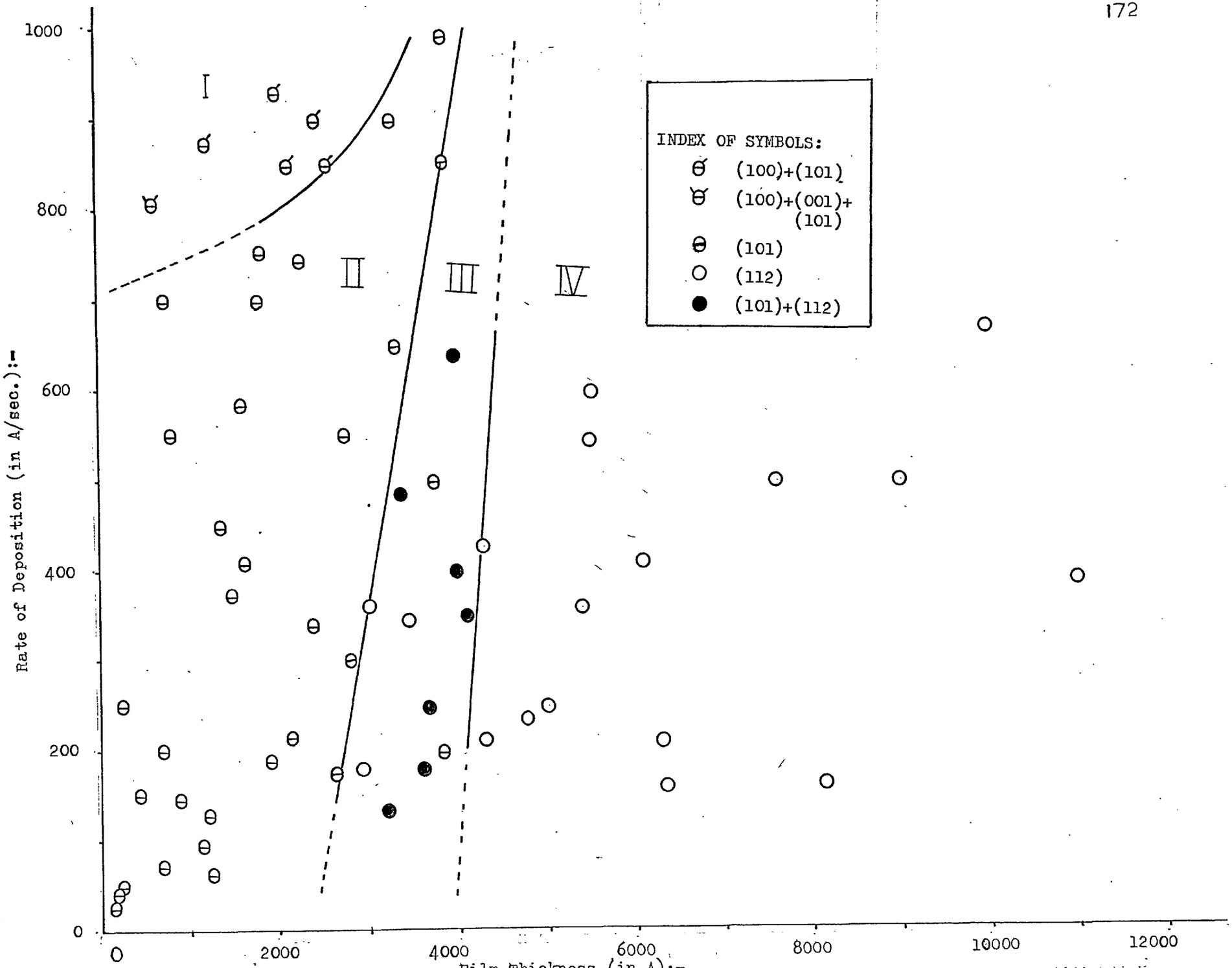

FIG.35. VARIATION OF SURFACE ORIENTATION OF ZINC FILMS CONDENSED ON STAINLESS-STEEL AT ROOM TEMP., WITH RATE OF DEPOSITION & FILM THICKNESS, AT RESIDUAL AIR PRESSURE 5×10^{-3} TORR.

$\angle i = 0^{\circ}$

The electron diffraction evidence of these separate regions is discussed below.

3.4a(i). <u>The Structure of Zinc Deposits at the Stage where (100) + (101) and (100) + (001) + (101) Orientation Developed</u>:

Referring to Fig.35 it is seen that it is the region I where these orientations are found to develop. This is a region of high rates of deposition with a minimum observed value about 810 A/sec.

Figs.36(a-d) show the diffraction patterns and some of these deposits.

Fig.36(a) gives the diffraction pattern from the $i = 0^{o}$ region of a specimen 680 A thick prepared at 5×10^{-3} torr of air, and 810 A/sec. Referring to the theoretical (100), (001) and (101) patterns, Fig.37(a,b,c), it is seen that this pattern consists of a mixture of these three orientations. The lone central arc on the plane of incidence, on the 002 ring, is visible, showing the development of {001} planes parallel to the surface of the substrate. There is a strong arc at the plane of incidence on the 100 ring with two lateral arcs near the shadow edge of the pattern. The second order diffraction at the plane of incidence on the 200 ring is also visible. The two lateral arcs on the 100 ring along with the two lateral arcs

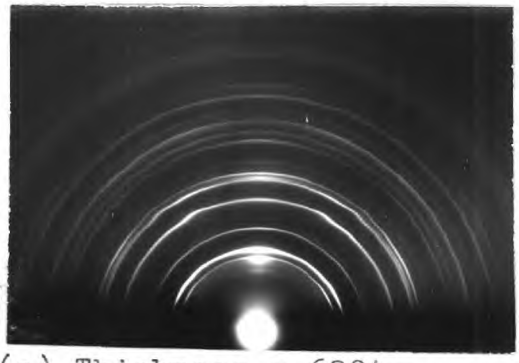

(a) Thickness = 680A
at 810A/sec at i=0°
Pressure = 5×10^{-3} torr
Angle i = 0°

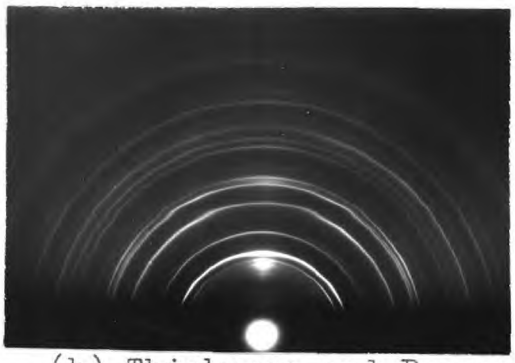

(b) Thickness and Pressure as in (a)

Angle i = 45° ← Vapour

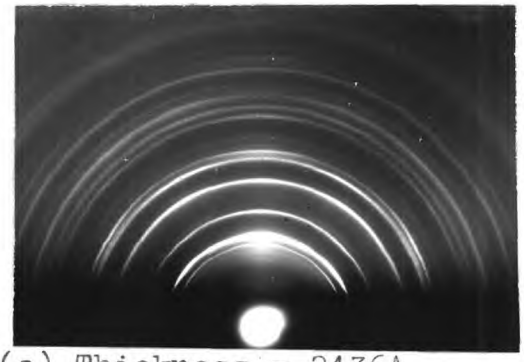

(c) Thickness = 2436A
at 900 A/sec at i=0°
Pressure = 5×10^{-3} torr
Angle i = 0°

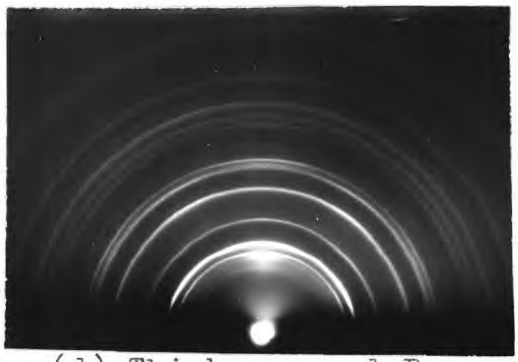

(d) Thickness and Pressure as in (c)

Angle i = 45° ← Vapour

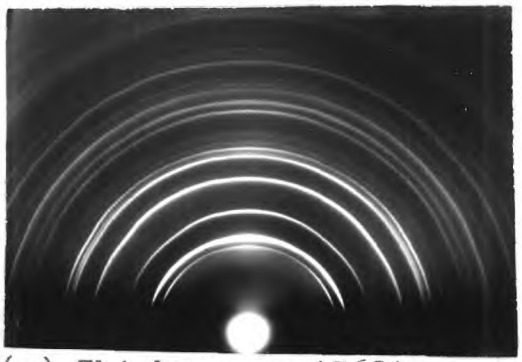

(e) Thickness = 1362A
at 875A/sec at i=0°
Pressure = 5×10^{-3} torr
Angle i = 0°

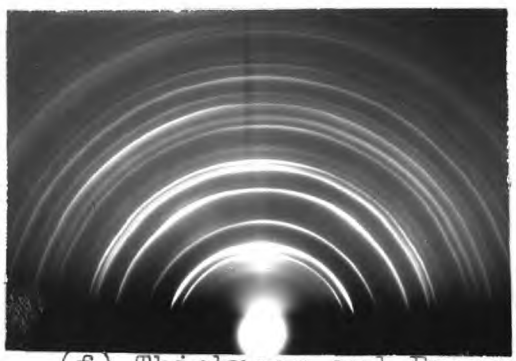

(f) Thickness and Pressure as in (e)

Angle i = 45° ← Vapour

Fig.36. Diffraction Patterns from the Zinc Deposits showing (100)+(001)+(101) Orientations (a,b,d,f) and (100) + (101) Orientations (e,c).

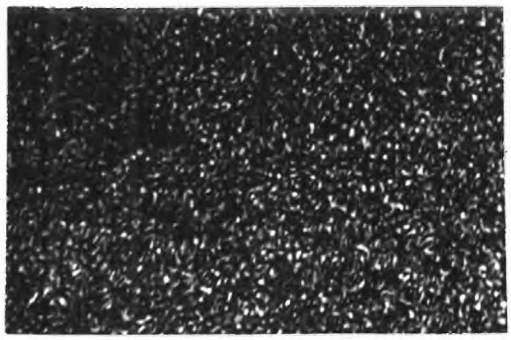

Fig.36(g) Optical Micrograph from the i=0° region of the Surface of a Zinc Deposit, 2141A thick, prepared at 850A/sec at P = 5×10^{-3} torr. Magnification 1220 X.

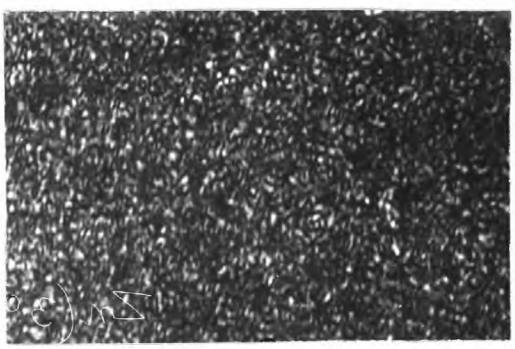

Fig.36(h). Optical Micrograph from the i=45° region of the same specimen as in Fig.36(g). Magnification 1220 X.

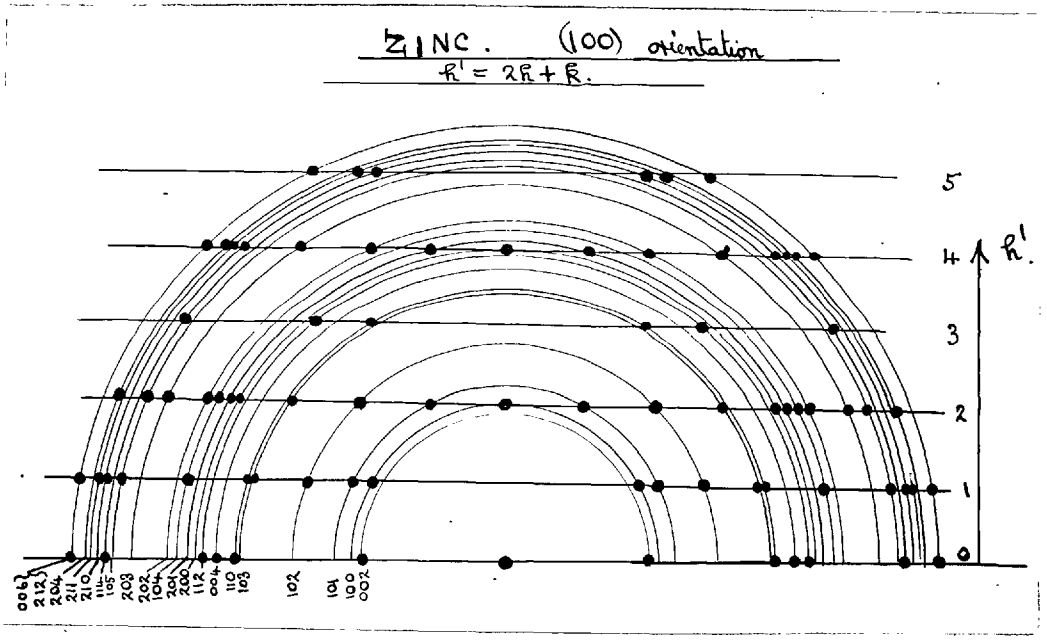

Fig.37(a). Theoretical (100) Electron Diffraction Pattern of Zinc.

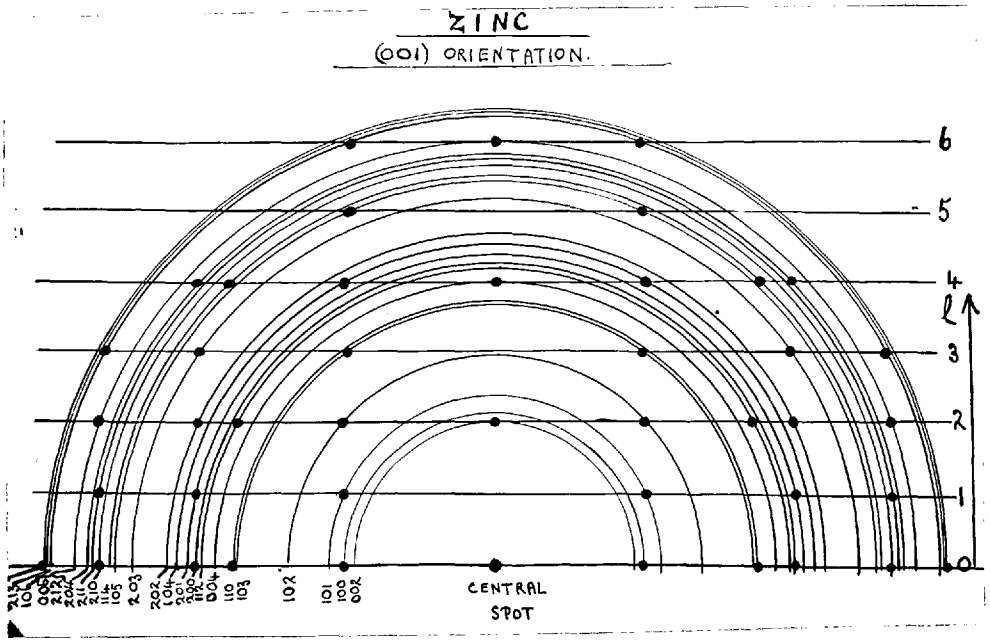

Fig.37(b). Theoretical (001) Electron Diffraction Pattern of Zinc.

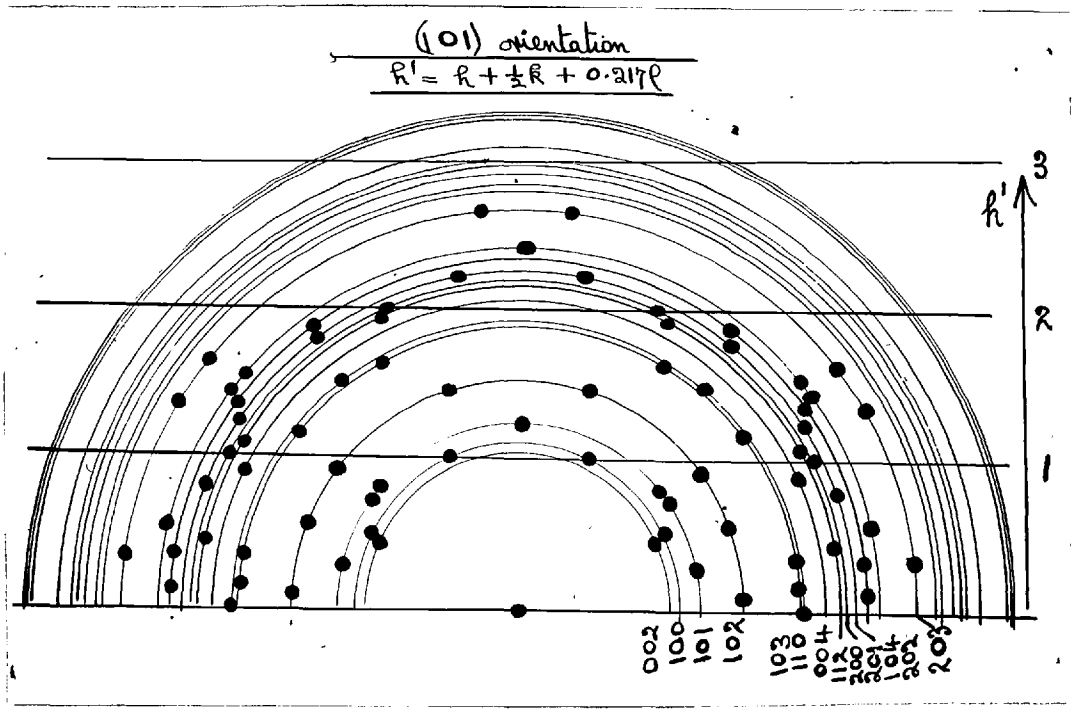

Fig.37(c). Theoretical (101) Electron Diffraction Pattern of Zinc.

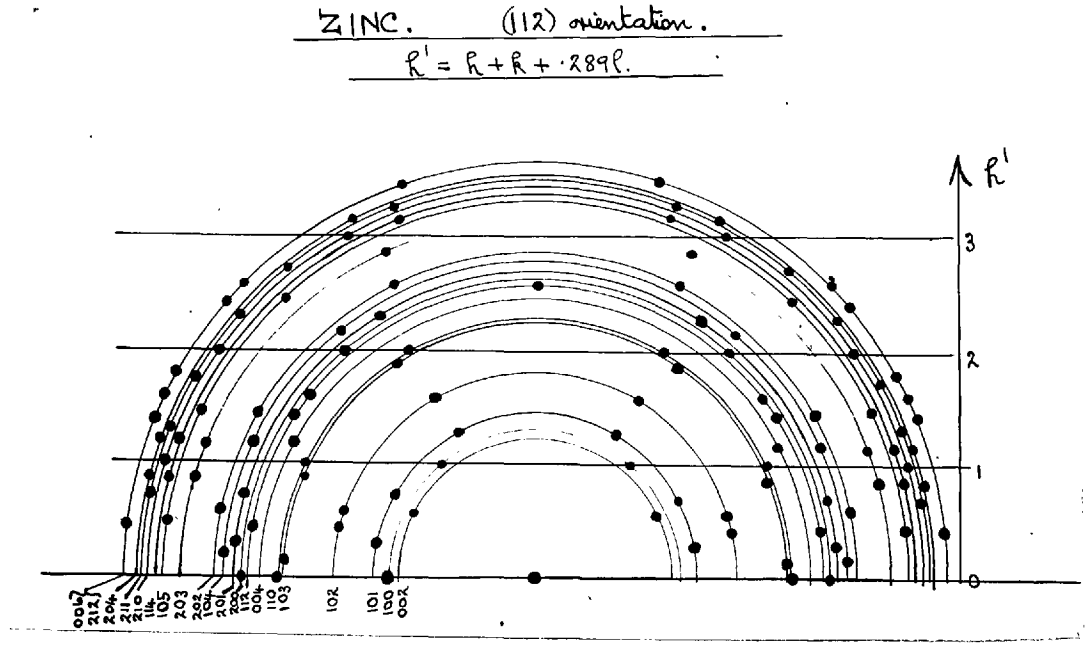

Fig.37(d). Theoretical (112) Electron Diffraction Pattern of Zinc.

on the 101 ring above the shadow edge lie on the first layer line. All these features, and the arc positions on other rings also, show the presence of zinc crystals oriented with a {100} plane parallel to the substrate or nearly so. On top of these two component patterns there is present the strong (101) pattern. The strong central arc on the (101) ring and a long lateral arc which is due to the coalescence of three arcs, on each side of it are clearly visible. The slight strengthening in intensity at the central region of the 102 ring is due to the coalescence of the two neighbouring arcs expected about the central region on that ring.

Fig.36(c) is from the $i = 0^{\circ}$ region of a specimen 2436 A thick prepared at the same pressure but at 900 A/sec. This pattern shows weak (100) and (101) orientations. The spread of arcing of the central arc on the 100 ring is about $\pm 16^{\circ}$, showing corresponding spread of the crystal orientation. The spread of the central arc on the 101 ring is also about $\pm 15^{\circ}$. The slight strengthening in intensity at the plane of incidence on the 201 ring is due to the coalescence of two neighbouring arcs expected at that region due to (101) type of orientation of the crystals.

Fig.36(e) gives the diffraction patterns from the $i = 0^{\circ}$ region of a specimen 1362 A thick prepared at 875 A/sec.

This also shows a mixture of (100) and (101) types of orientations. The spread of arcing in both the cases is about $\pm 15^{\circ}$.

In all these cases the diffraction patterns are more or less similar. The arcings show very little refraction of the electron beam, indicating development of relatively rough surface on the growing crystals. These diffraction patterns almost correspond to the transmission type, the beam passing through the projecting crystal tips.

Except in the case of Fig.36(a), the other illustrations did not show (001) type of orientation at $i = 0^{\circ}$; but all the specimens showed (001) type together with (100) and (101) at oblique incidence of the vapour stream.

Figs.36(g and h) illustrate the back-reflection optical microphotographs of the $i = 0^{\circ}$ and $i = 45^{\circ}$ regions respectively of a 2141 A zinc specimen prepared at 850 A/sec. The electron diffraction patterns of this specimen showed (100) + (101) at $i = 0^{\circ}$ and (100) + (001) + (101) at $i = 45^{\circ}$. The deposit is largely continuous and is rough-surfaced. The photographs are taken at a magnification of 1220 times.

Deposits of similar thickness prepared on glass substrates had a similar appearance as Fig.36(g and h) in

back-reflection microscopy. But in transmitted light they are fully opaque and therefore continuous films. Much thinner deposits (- a few hundred A) did show small isolated zinc crystals.

3.4a(ii). The Structure of Zinc Deposits at the Stage where (101) Orientation Developed:

In Fig.35 it is seen that it is in region II where (101) orientation developed. This region roughly extends from about 150 A at 25 A/sec to about 2500 A at a lower rate of deposition (~175 A/sec) and to about 4000 A at a high rate of deposition (~990 A/sec). However, the region of thicknesses between 250 A and 700 A at rates lower than about 75 A/sec was unexplored.

Some of the diffraction patterns of the results incorporated in this region of Fig.35 are illustrated in Figs.38(a-f) and 39(a-f).

Fig.38(a) gives the diffraction pattern from the $i = 0^{c}$ region of a specimen 198 A thick prepared at a rate of deposition of 40 A/sec. This is a relatively thin specimen prepared at this low rate of deposition. The central arc on the 101 ring has a long spread of about $\pm 25^{\circ}$. The fall in intensity at the region of the plane of incidence on the (100) ring is clear. The long arcing at this early stage of development of crystal growth may either be

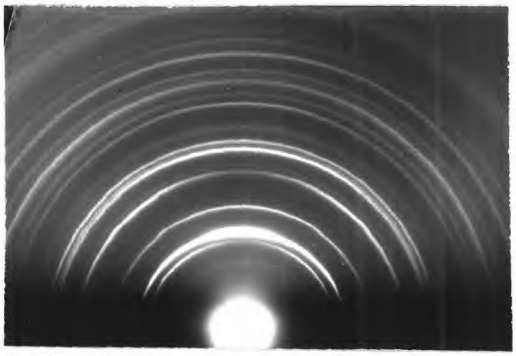

(a) Thickness = 198A
at 40A/sec at i=0°
Pressure = 5×10^{-3} torr
Angle i = 0°

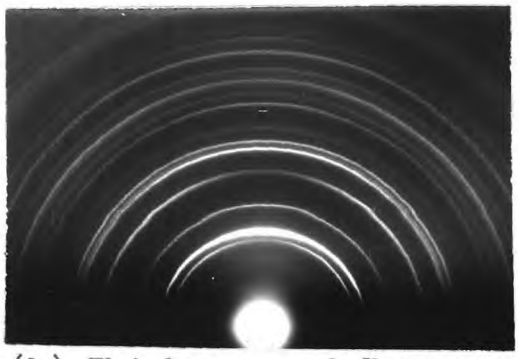

(b) Thickness and Pressure
as in (a)
Angle = 45° Vapour

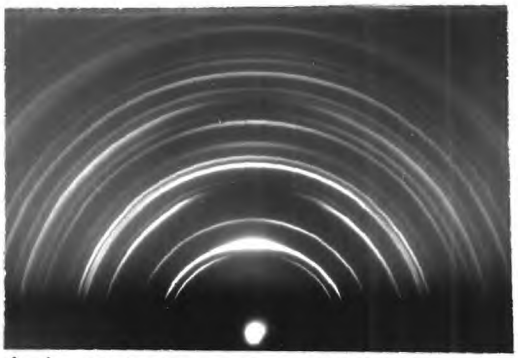

(c) Thickness = 452A
at 150A/sec at i=0°
Pressure = 5×10^{-3} torr
Angle i = 0°

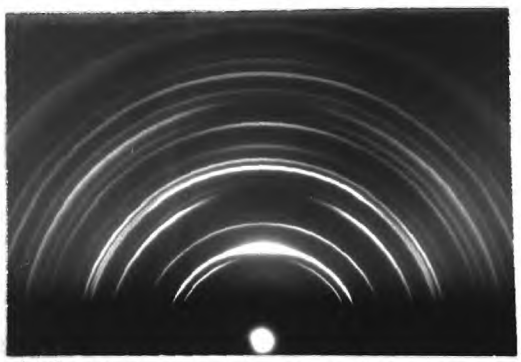

(d) Thickness and Pressure
as in (c)
Angle i = 45° Vapour

(e) Thickness = 718A
at 71A/sec at i=0°
Pressure = 5×10^{-3} torr
Angle i = 0°

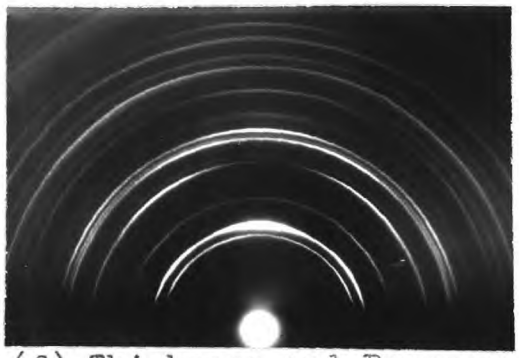

(f) Thickness and Pressure
as in (e)
Angle i = 45° Vapour

Fig.38. Electron Diffraction Patterns from the Zinc Deposits showing (101) Orientations.

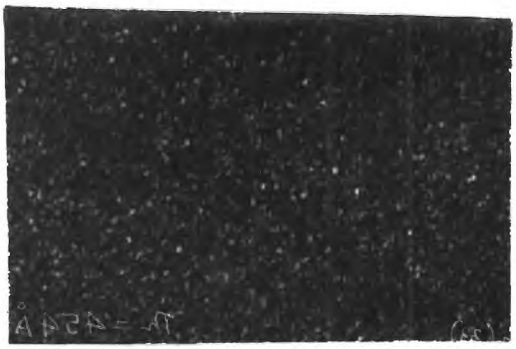

(g) Thickness = 454A at 150 A/sec.
Pressure = 5×10^{-3} torr
From the region at $i=0^{\circ}$

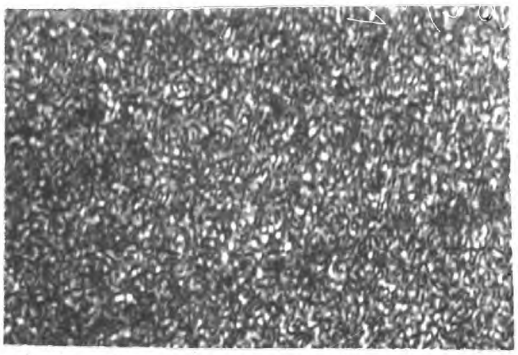

(h) Thickness and Pressure as in (g)
From the region at $i=45^{\circ}$

(i) Thickness =1017A at 127 A/sec.
Pressure = 5×10^{-3} torr
From the region of $i=0^{\circ}$

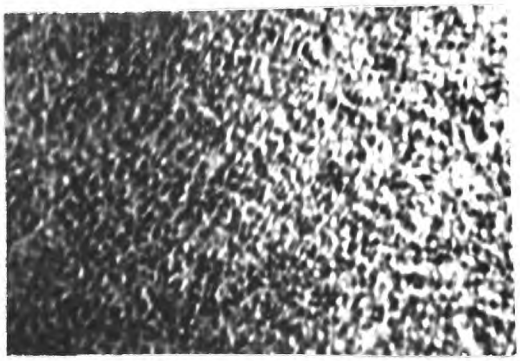

(j) Thickness and Pressure as in (i)
From the region of $i=45^{\circ}$

Fig.38(g-j). Optical Micrographs from the Surfaces of the Zinc Deposits (Magnification 1220 X)

due to prominently undulating surface of the substrate or to almost random orientation of the ccystals. The long arc on the 101 ring shows a little drawing out towards the inner edge of the ring. This indicates the beginning of the facet formation parallel to the substrate.

Fig.38(c) is from the i = 0^{o} region of a specimen 452 A thick prepared at 150 A/sec. This shows strong (101) orientation. The central 101 arc on the 101 ring is separated from the two lateral arcs on the same ring with slight fall in intensity at the tail regions of the arcs. Although there is a coalescence of the two lateral arcs on either side of the plane of incidence on the 112 ring, yet a slight fall in intensity in between them can be observed. The slight vertical drawing out of the 101 arc shows refraction of the electron beam due to the appreciable development of {101} planes parallel to the substrate.

Fig.38(e) shows a clear (101) pattern from the i = 0^{o} region of a specimen 718 A thick prepared at 71 A/sec. Although the spread of arcing of the 101 arc is about $\pm$ 13^{o}, yet it is distinct and well separated from the coalesced lateral arcs on it. The gaps at the region of the plane of incidence on the 100 ring, and on the 112 ring are visible. The refraction effect is appreciable.

Figs.39(a,c and e) are also from the i = 0^{o}

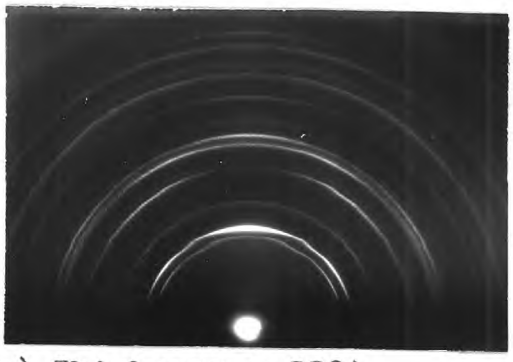

(a) Thickness = 880A
at 147A/sec at i=0°
Pressure = 5×10^{-3} torr
Angle i = 0°

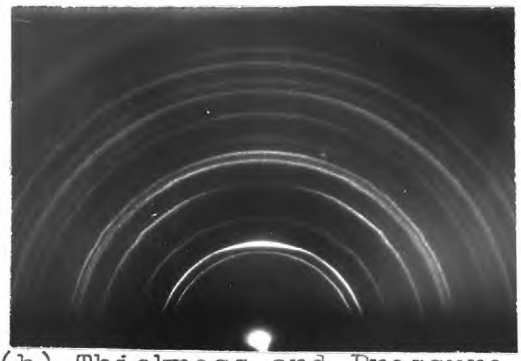

(b) Thickness and Pressure as in (a)
Angle i = 45° Vapour

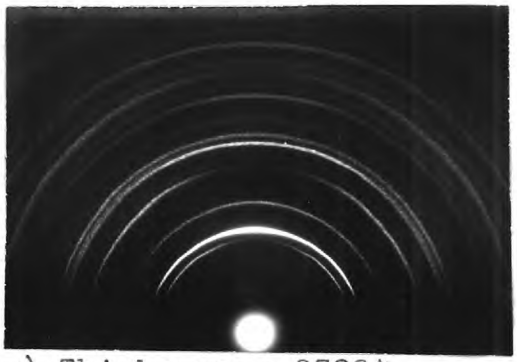

(c) Thickness = 2388A
at 341A/sec at i=0°
Pressure = 5×10^{-3} torr
Angle i = 0°

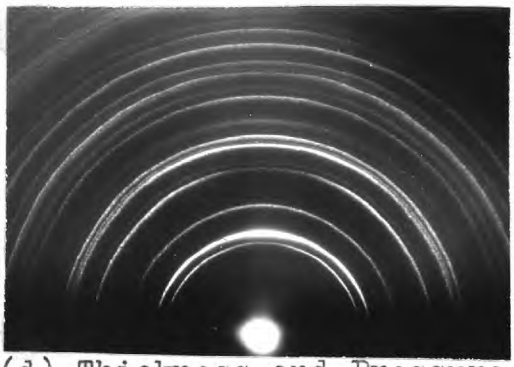

(d) Thickness and Pressure as in (c)
Angle i = 45° Vapour

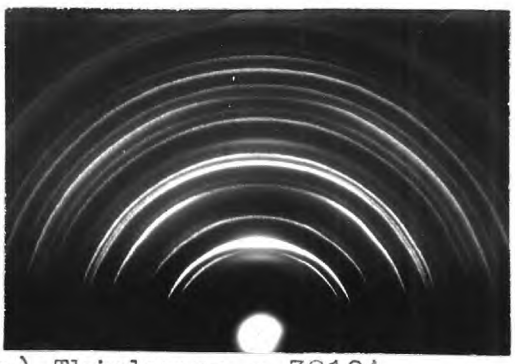

(e) Thickness = 3819A
at 860A/sec at i=0°
Pressure = 5×10^{-3} torr
Angle i = 0°

(f) Thickness and Pressure as in (e)
Angle i = 45° Vapour

Fig.39. Electron Diffraction Patterns from the Zinc Deposits showing (101) Orientation.

regions of thicker deposits. Fig.39(e) is from a specimen 3819 Å thick prepared at 860 A/sec. These specifications of deposition parameters indicate that it is very near to region III, where there is the development of (112) type along with (101). Here, (101) is very prominent. The strengthening in intensity at the region of the plane of incidence on the 112 ring is, hence, attributable to the beginning of the development of (112) type of orientation.

Figs.38(g-j) are the back-reflection optical micrographs of the different regions of two specimens whose diffraction patterns gave (101) type of orientation. The thicknesses and rates of deposition are indicated in the caption. Magnification is 1220 times. That the specimen surfaces are rough and largely continuous can be seen from the photographs.

3.4a(iii). <u>The Structure of Zinc Deposits where (101) + (112) Orientations Developed</u>:

Region III in Fig.35 is of slightly thicker deposits where (101), (112) or a mixture of both these orientations were found to develop. This perhaps is the transitional stage between (101) and (112) orientations. This region roughly extends from 2600 Å to 4000 Å at lower rate of deposition (150 A/sec) to about 3500 Å to 4500 Å corresponding to high rate of deposition (650 A/sec).

Diffraction patterns from two specimens from this region are illustrated in Figs.40(a-d). Fig.40(a) is from the $i = 0^{\circ}$ region of a 3206 A thick specimen prepared at a rate of 130 A/sec. That the pattern is a mixture of (101) and weak (112) can be ascertained by examining the important features of these two individual theoretical patterns (Figs. 37(c) and (d)). The strong and comparatively long 101 arc on the 101 ring along with the coalesced lateral arcs, one on each side of the plane of incidence are recognisable. Looking at the 112 ring, it is seen that the two lateral arcs on either side of the plane of incidence are connected by a slight strengthening in intensity in between the two (in the actual negative plate). Almost continuous intensity on the plane of incidence region of the 103 ring may be due to either of the two orientations.

Fig.40(c) is from the $i = 0^{\circ}$ region of a specimen about 4000 A thick, prepared at~400 A/sec. This is also a mixture of (101) and (112) types of orientation, The long arc on the plane of incidence region of the 112 ring is partly due to coalescence of the two lateral arcs expected due to (101) orientation and partly due to the weak (112) orientation of some of the crystals. A small proportion of the crystals on the growing deposit have developed with their $\{112\}$ planes parallel to the substrates along with $\{101\}$.

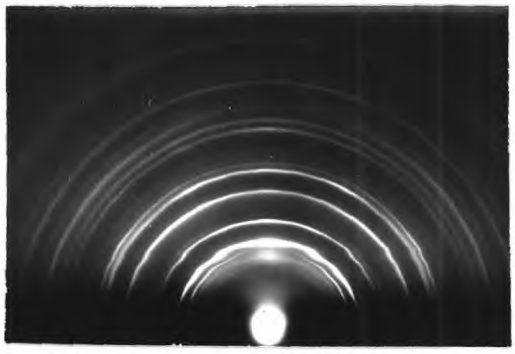

40a. Thickness = 3206A
at 130A/sec at i=0°
Pressure = 5×10^{-3} torr
Angle i = 0°

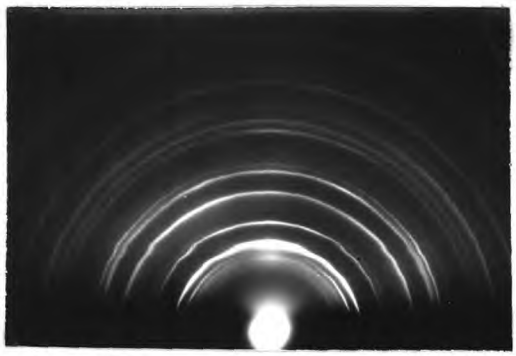

40b. Thickness and Pressure
asin (a)
Angle i = 45° ← Vapour

40c. Thickness = 4000A
at 400 A/sec at i=0°
Pressure = 5×10^{-3} torr
Angle i = 0°

40d. Thickness and Pressure
as in (c)
Angle i = 45° ← Vapour

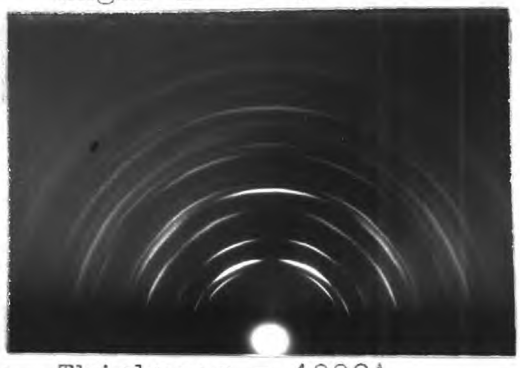

41a. Thickness = 4990A
at 250A/sec at i=0°
Pressure = 5×10^{-3} torr

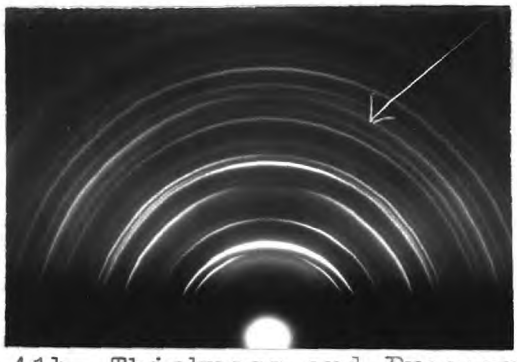

41b. Thickness and Pressure
as in 41a.
Angle i = 45°

Figs.40 and 41. Electron Diffraction Patterns from the Zinc Deposits showing (101)+(112) Orientation (Figs.40(a)-(d)) and (112) Orientation (Fig.41(a) and (b)).

The strengthening in intensity on the central region of the 201 ring is due to the coalescence of the two neighbouring lateral arcs arising due to (101) type of orientation.

3.4a(iv). The Structure of Zinc Deposits at the Stage where (112) Orientation Developed:

Region IV, of still thicker deposits, in Fig.35, shows where one-degree (112) orientation developed in the deposits. This region roughly extends beyond a thickness of about 4150 A. The rates of deposition varied between 150 A/sec and 670 A/sec. Within this range of the rates of deposition and beyond the above limiting thickness, the deposits showed stable (112) type of orientation.

Some of the diffraction patterns obtained from specimens corresponding to this region are presented in Figs.41(a-f).

Fig.41(a) is from a 4990 A thick specimen prepared at 250 A/sec. The strong 112 arc on the plane of incidence of the 112 ring is visible. The four arcs, two on each side of the plane of incidence, on the 101 ring are clearly recognisable with reductions in intensity in between them. The two lateral arcs about the 112 arc on the 112 ring are also well distinguishable. All these features show this is a strong (112) type of orientation, with [112] axis normal to the surface of the substrate. The spread of arcing is about

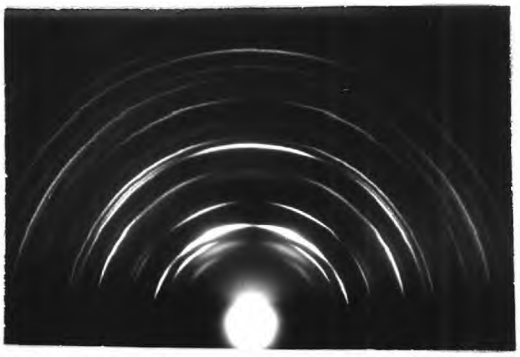

(c) Thickness = 5470A
at 550A/sec at i=0°
Pressure = 5×10^{-3} torr
Angle i = 0°

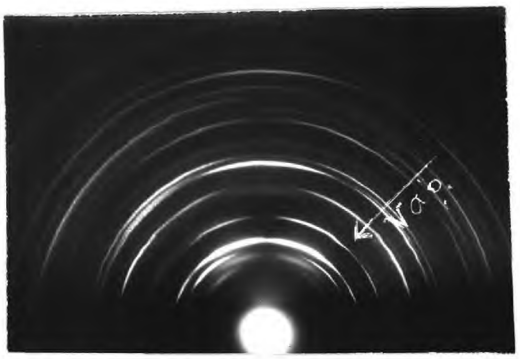

(d) Thickness and Pressure as in (c)
Angle = 45°

(e) Thickness = 10,000A
at 670A/sec at i=0°
Pressure = 5×10^{-3} torr
Angle i = 0°

(f) Thickness and Pressure as in (e)
Angle i = 45°

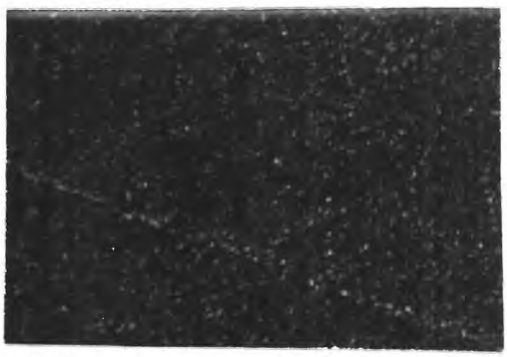

(g) Optical Micrograph of the specimen as in (e)

(h) Optical Micrograph of the specimen as in (f)

Magnification 1220X

Fig.41(c-f). Electron Diffraction Patterns from the Zinc Deposits showing (112) Orientation.

$\pm$ 20°. The pattern does not show appreciable refraction, showing development of relatively rough surface in the growing deposit.

Fig.41(c) shows a strong (112) orientation pattern from a 5470 A thick specimen prepared at 550 A/sec. The strong arc at the plane of incidence on the 112 ring has a spread of about $\pm$ 20°. The two lateral arcs on the 101 ring are well separated by a fall in intensity between them. The two lateral arcs on the 1st layer line of the 100 ring are also seen to be well distinguishable. The slight rise in intensity at the plane of incidence of the 212 ring is due to the coalescence of two neighbouring lateral arcs. The arcs on the low order rings show refraction of the electron beam, showing strong development of {112} faces on the growing deposit. The line drawn from the middle of the 112 arc to the central spot is normal to the shadow edge of the specimen, showing that the {112} planes are developed normal to the vapour stream and all azimuthal orientations occur about it. The two rings with strong arcings below the 100 ring are due to some ZnO.

Fig.41(e) is another strong (112) pattern from the i = 0° region of a~10,000 A thick deposit prepared at~670 A/sec. All the features of a (112) pattern are present in it. The spread of arcing is about $\pm$ 21° about the mean

orientation axis, indicating similar spread of the orientation. The refraction effect is appreciable and hence the strong facet formation is conclusive. The {112} facets have developed perpendicular to the vapour stream direction.

Figs.41(b,d and f) correspond to the $i = 45^{\circ}$ region of the specimens mentioned above. These results are discussed in a later section.

Figs.41(g and h) are the optical microphotographs of the $i = 0^{\circ}$ and $i = 45^{\circ}$ regions of the specimen whose diffraction patterns are illustrated in Figs.41(e and f) respectively.

3.4(b). <u>The Structure of Zinc Deposits Condensed at the Normal Incidence of the Vapour Stream at a Pressure of 2 $x10^{-4}$ torr of Air on to Stainless Steel Substrates at Room Temperature</u>:

The results from the deposits prepared at 5 $x10^{-3}$ torr suggested that at lower air pressures there might be more tendency to develop more (100) and (001) orientations in thin zinc deposits.

The deposits prepared at 2 $x10^{-4}$ torr did indeed show mostly a mixture of (101) and (100) orientations at the thinner stage, up to about 750 A (region I in Fig.42). However, at slightly larger thicknesses (~750 - 1750 A), a new kind of orientation approximately intermediate between (101) and (112) was observed (region II in Fig.42).

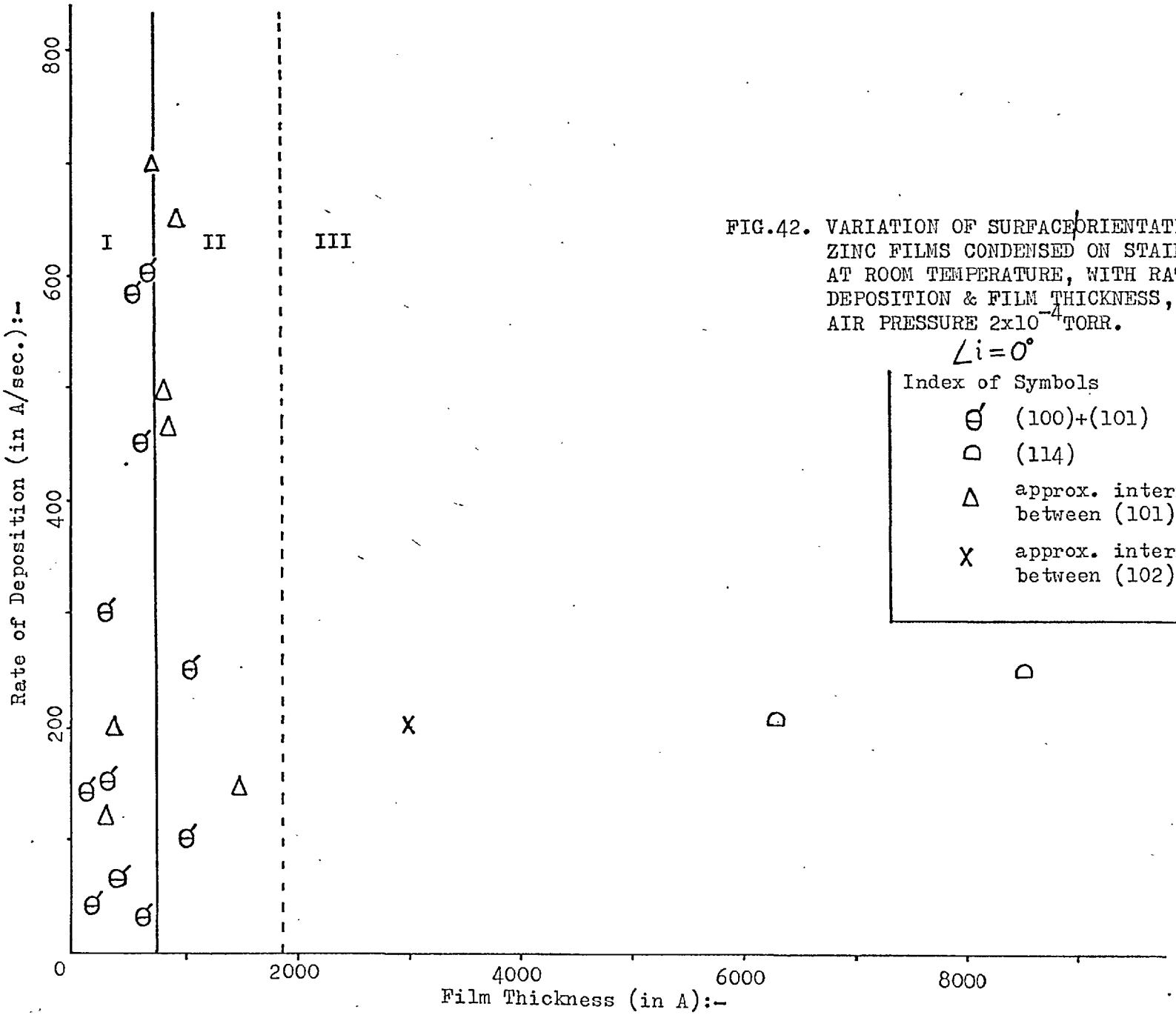

FIG.42. VARIATION OF SURFACE ORIENTATION OF THE ZINC FILMS CONDENSED ON STAINLESS-STEEL AT ROOM TEMPERATURE, WITH RATE OF DEPOSITION & FILM THICKNESS, AT RESIDUAL AIR PRESSURE 2×10^{-4} TORR.

$\angle i = 0°$

Index of Symbols

- (100)+(101)
- (114)
- approx. intermediate between (101) & (112)
- approx. intermediate between (102) & (103)

Typical diffraction patterns from deposits in region I are shown in Fig.43. Fig.43(a) is from the i = 0^{o} region of a 190 A thick specimen prepared at 38 A/sec. This shows a mixture of mainly (101) and to a very small extent in part, (100) orientation. The lateral arcs on the 112 ring about the plane of incidence are well separated showing no possibility of (112) orientation. The medium strong 100 arc on the 100 ring is recognisable. The second order 200 arc on the 200 ring is faint, but the two lateral arcs on the 100 ring are very strong. These features indicate the development of weak (100) orientation along with the main (101) orientation. Obviously, (101) orientation has been favoured more than the (100). The very little refraction of the arcings shows development of at least some proportion of almost atomically smooth surface on the growing deposits.

Fig.43(c) is from the i = 0^{o} region of a 300 A thick specimen prepared at 150 A/sec. This is also a mixed strong (101) and weak (100) orientation pattern. The spread of arcing is about $\pm$ 20^{o} about the mean. Since the {201} planes are inclined to the {101} at an angle less than this, the rocking of the $[101]^{*}$ axis may bring some of the {201} planes to Bragg-reflection position, thereby causing the 201 arc to be strengthened in intensity, in addition to

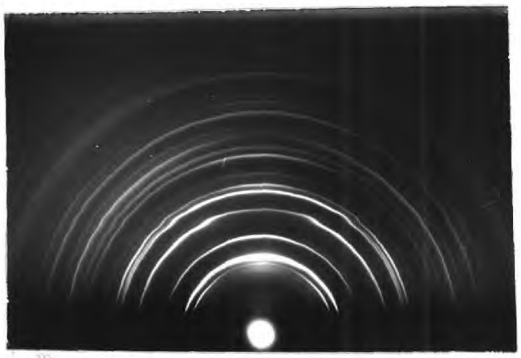

(a) Thickness = 190A
at 38A/sec at i=0°
Pressure = 2×10^{-4} torr
Angle i = 0°

(b) Thickness and Pressure as in (a)
Angle i = 45°

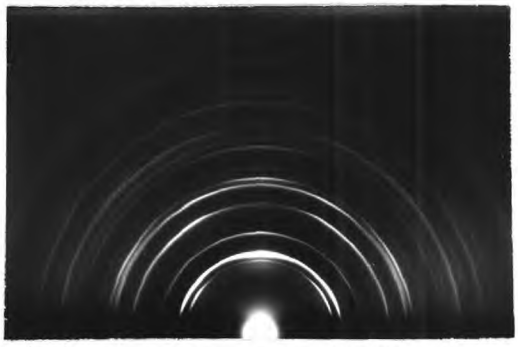

(c) Thickness = 300A
at 150 A/sec at i=0°
Pressure = 2×10^{-4} torr
Angle i = 0°

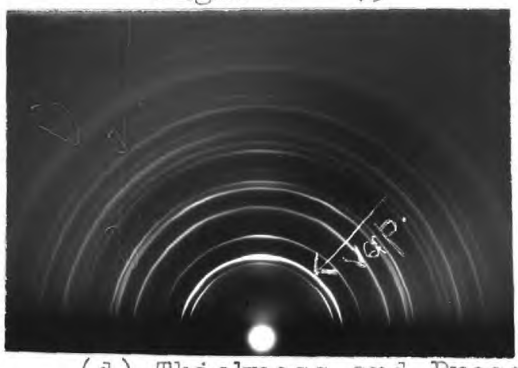

(d) Thickness and Pressure as in (c)
Angle i = 45°

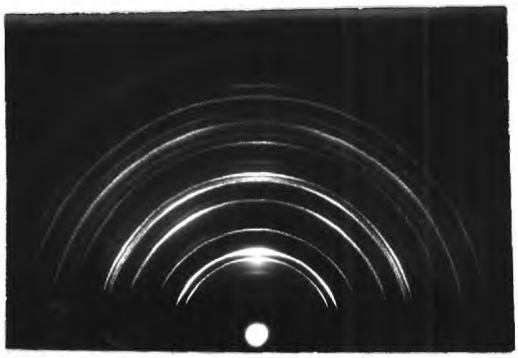

(e) Thickness =1029A
at 100 A/sec at i=0°
Pressure = 2×10^{-4} torr
Angle i = 0°

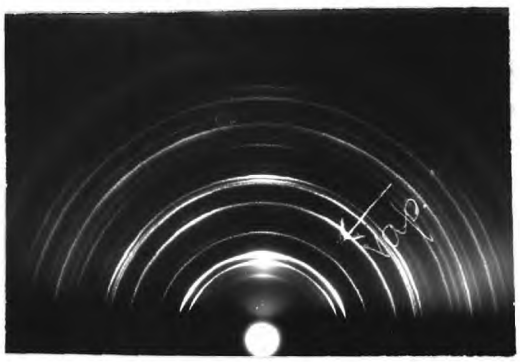

(f) Thickness and Pressure as in (e)
Angle i = 45°

Fig.43. Electron Diffraction Patterns from the Zinc Deposits showing (101)+(100) Orientations.

the coalescence of the two lateral arcs as is seen in the diffraction pattern. The faint 100 arc on the 100 ring is well recognisable along with the two long lateral arcs near the shadow edge.

The other patterns from region I deposits at higher rates (to~800 A/sec) were closely similar to Figs. 43(a) and (c).

In or around the region II of Fig.42, seven deposits showed a mean orientation which had diverged away from a (101) orientation by about 10° towards (112). Figs. 44(a-d) are from some of these specimens, whose orientations were intermediate between (101) and (112).

Taking Fig.44(a) it is seen that the two short arcs near the plane of incidence on the 101 ring are separated by a weakening in between them. The [101]* (the * denoting reciprocal-lattice indices) orientation axis is tilted away from the specimen normal by about $\pm 10^{\circ}$. Similarly the [112]* axis is deviated away by about $\pm 15^{\circ}$. Thus, it is neither a perfect (101) nor a (112) orientation. However, this orientation axis appears to be intermediate between these two directions, practically in their plane, because the angle between them is about 26°, i.e. the sum of the above two angles.

Almost similar patterns are shown in Figs. 44(b)

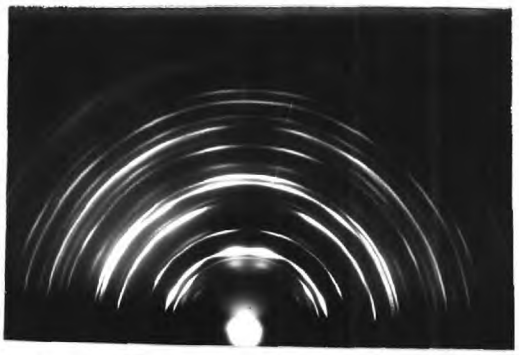

(a) Thickness = 840A
at 650 A/sec
Pressure = 2×10^{-4} torr
Angle i = 0°

(b) Thickness = 625A
at 450 A/sec
Pressure = 2×10^{-4} torr
Angle i = 0°

(c) Thickness and Pressure
as in (b)
Pressure = 2×10^{-4} torr
Angle i = 45°

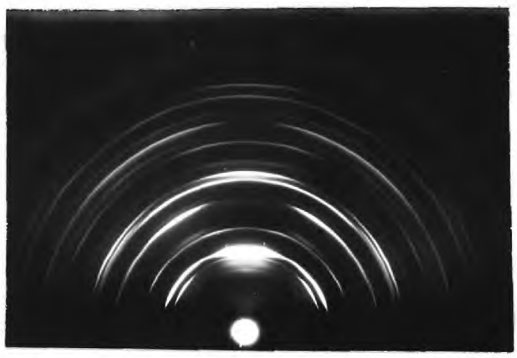

(d) Thickness = 300 A
at 125 A/sec
Pressure = 2×10^{-4} torr
Angle i = 0°

Fig.44. Electron Diffraction Patterns from Zinc Deposits showing Orientation approximately between (101) and (112).

and (d) from two other deposits from the region II.

Only three experiments were carried out on thicker deposits in region III of Fig.42. Fig.45(a) is from the $i = 0^{\circ}$ region of a specimen 3020 A thick prepared at 175 A/sec. The 103 arc on the 103 ring is long and the 102 arc on the 102 ring is short. The lateral arcs on the 101 ring are well separated. The pattern approximately conforms to the theoretical pattern for (103) orientation. Fig.45(b) corresponding to the $i = 45^{\circ}$ region shows asymmetry in intensity and arc positions. This might be regarded as indicating a practically (102) orientation azimuthally limited due to the development of {001} faces. The crystals which have grown preferentially have azimuthal orientations such that the (001) face is most nearly normal to the vapour stream. The 001 arc is produced by the crystals in this most preferred azimuth and lies on a radius perpendicular to that of the 002 arc. The presence of the 110 arc shows that a range of azimuths up to at least $\pm 30^{\circ}$ is present. The 10ℓ row of diffractions is indicated by a straight line in the figure. The 00ℓ row below this line and 11ℓ and 20ℓ rows above it are also clearly visible.

The presence of extensive (001) faces on the crystals during their growth at this later stage of deposition is probably associated with the oxygen partial

pressure having become much reduced by the gettering action of the condensed zinc in the apparatus.

An alternative explanation of Fig.45(b) is possible, however. Since this pattern contains not only the 00ℓ, 10ℓ and 20ℓ rows of arcs, but also the 11ℓ row which is also parallel to them, with the 110 arc centred on the same radius as the 100 and 200, it can be considered to indicate practically a (001) orientation with its axis [001] along the vapour stream direction ((001) face perpendicular to this), and having an azimuthal distribution round this [001] axis of more than $\pm 30^{\circ}$, from the main azimuth of the above described (102) orientation. This therefore corresponds to a continuous azimuthal range round the [001] axis, in view of the hexagonal symmetry round this axis. This interpretation seems to be best, because (1) the 102 arc in the plane of incidence is not strong enough to be contributed to by the main bulk of the crystals; (2) the 11ℓ row line is substantially parallel to the 00ℓ, 10ℓ and 20ℓ, and (3) 100, 200 and 110 arcs are all centred on the same radius. The range of crystal orientations in the specimen surface region corresponding to the two interpretations is nearly the same, however, when the spread of $\pm 15^{\circ}$ of the orientation axis is taken into account.

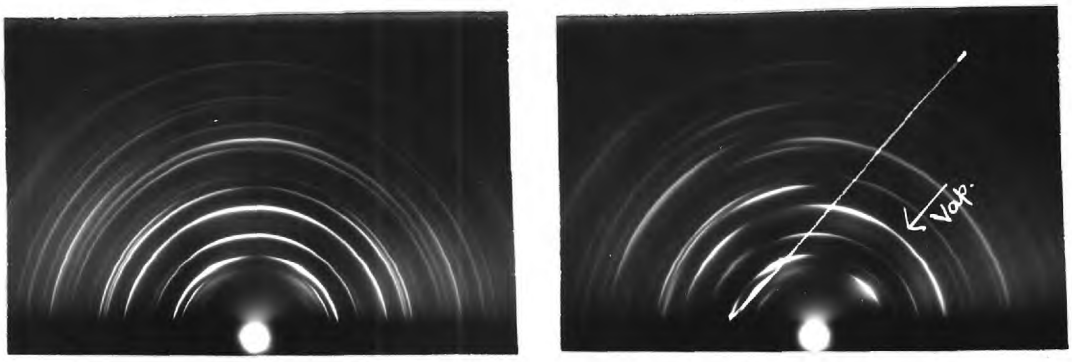

(a) (b)

Figs.45(a)&(b). Electron Diffraction Patterns showing Orientation between (102) and (103) from a Zinc specimen 3020 A thick prepared at 175 A/sec at $2x10^{-4}$ torr of air. (a) at i = 0^{o}. (b) at i = 45^{o}

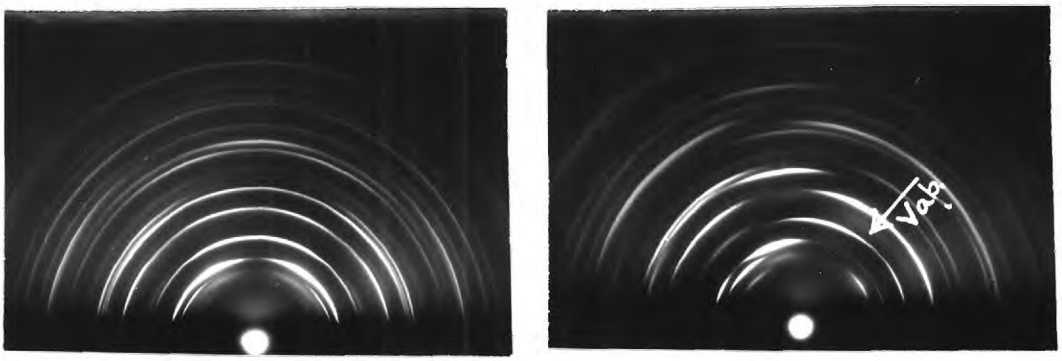

(c) (d)

Figs.45 (c) & (d). Electron Diffraction Patterns showing approximately (114) Orientation from a Zinc specimen 6368 A thick prepared at 175 A/sec at $2x10^{-4}$ torr of air. (c) at i = 0^{o}. (b) at i = 45^{o}

3.4(c). The Structure of Zinc Deposits Condensed at the Normal Incidence of the Vapour Stream at a Pressure of 1 x10^{-5} torr of Air on to Stainless Steel at Room Temperature:

A few deposits were prepared at this pressure. The minimum thickness of a deposit obtained was about 250 Å and the minimum rate used was 70 A/sec. As in the experiments at a pressure of 10^{-4} torr of air, the thinner deposits mostly showed (101) and (100) orientation for the normal incidence region of the vapour stream.

Fig.46 shows the plot of these results. Figs. 47(a-d) show some of the diffraction patterns obtained from these specimens.

Fig.47(a) from the $i = 0^{\circ}$ region of a 300 Å thick specimen prepared at 300 A/sec. The arc positions on the 101, 102, 103, 112 rings show that this is a mixture of (100) and (101) patterns. The 101 arc on the plane of incidence of the 101 ring is extended along the ring due to considerable rocking of the [101]* axis about the mean. The angular spread of the 101 arc is about $\pm 18^{\circ}$. Such an amount of rocking is bound to bring some of the {201} planes to Bragg reflection position, as is seen from the strengthening in intensity of the 201 arc at the plane of incidence. The coalescence of the neighbouring arcs near the plane of incidence on the 201 ring due to (101) type of

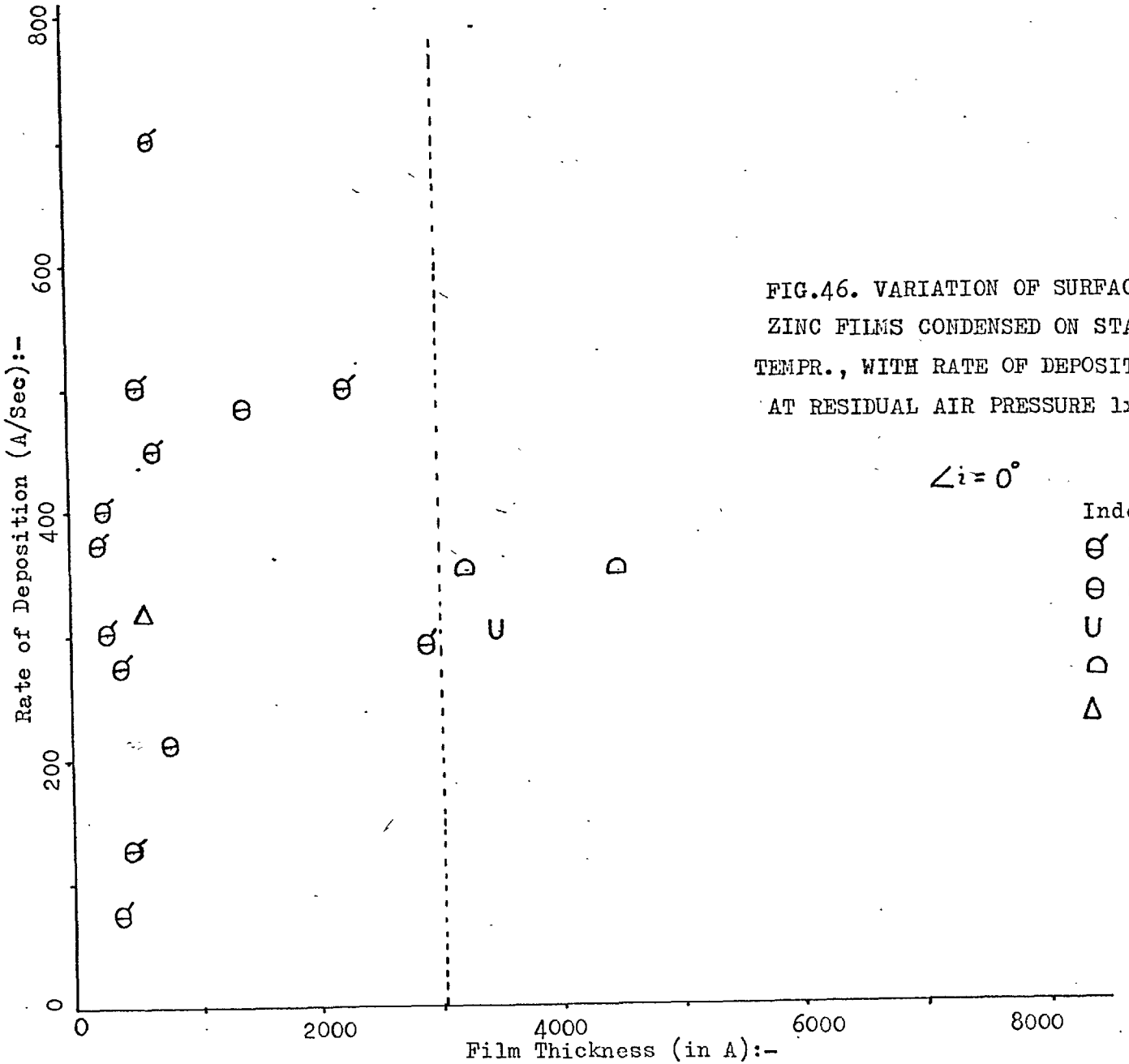

FIG.46. VARIATION OF SURFACE ORIENTATION OF THE ZINC FILMS CONDENSED ON STAINLESS-STEEL AT ROOM TEMPR., WITH RATE OF DEPOSITION & FILM THICKNESS AT RESIDUAL AIR PRESSURE 1×10^{-5} TORR.

$\angle i = 0^\circ$

Index

- (101)+(100)
- (101)
- U (135)
- (114)
- Δ approx. between (101)&(112)

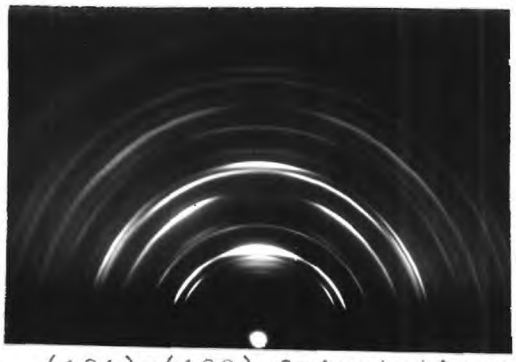

47a. (101)+(100) Orientations from a 300A thick Zinc Deposit (Rate 300A/sec; P = 1×10^{-5} torr; i=0°)

47b. Approx.(114) Orientation from a 4500A thick Zinc Deposit (Rate 350 A/sec; P=1×10^{-5} torr; i=0°)

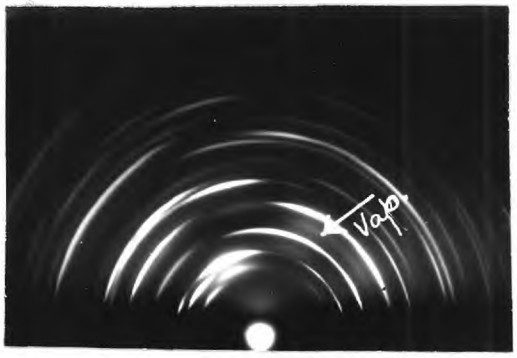

47c. As in (b) i = 45°

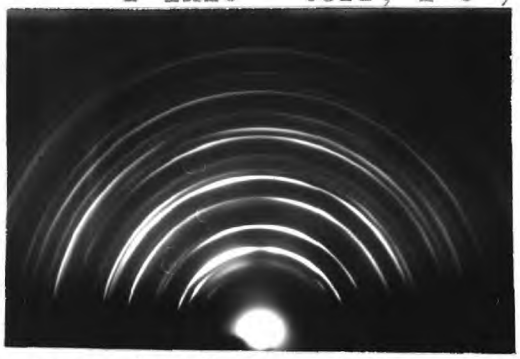

47d. (135) Orientation from a 3500A thick Zinc Deposit (Rate 300 A/sec; Angle i = 0°) P = 1×10^{-5} torr.

ZINC. (135) orientation

$R' = R + 1.4R + .433\rho.$

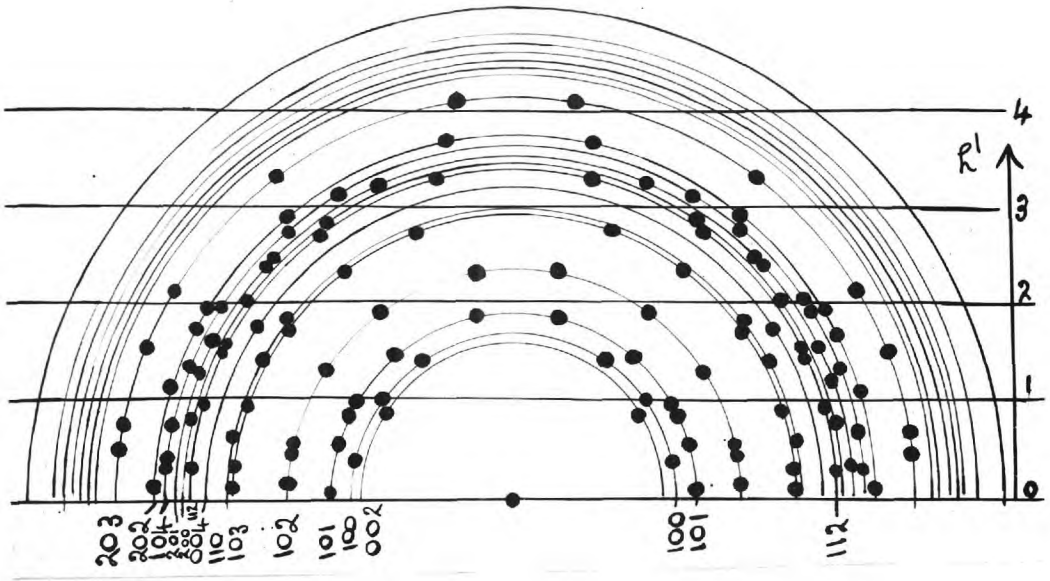

Fig. 48

orientation, is also present. The (100) orientation is also clear. The 100 arc on the plane of incidence of the 100 ring and its second order arc on the 200 ring are recognisable. The two short lateral arcs on the 100 ring near the shadow edge are clearly visible. The refraction effect on the arcings of the 101 ring indicate stronger development of {101} planes than {100} ones.

Fig.47(d) is from the i = 0° region of a specimen ~ 3500 Å thick prepared at~300 Å/sec. It shows a roughly (135) type of orientation as can be seen from a comparison with the theoretical pattern Fig.48. The lateral arcs on the 101 ring are well recognisable; the lateral arcs near the plane of incidence of the 112 ring are also in positions required by the (135) type of orientation. There is a little asymmetry in intensity and positions of the arcings showing that the vapour stream is not exactly normal to the specimen surface at the point considered.

Fig.49(a-d) are the optical micrographs of some of the deposits prepared at 1 x10^{-5} torr of air.

Fig.49(a) is the optical micrograph of a deposit ~700 Å thick whose diffraction pattern gave a (101) + (100) type of orientations. The visible striations are due to the abraded surface of the stainless-steel substrate.

Fig.49(c) is an optical micrograph of a~10,000 Å

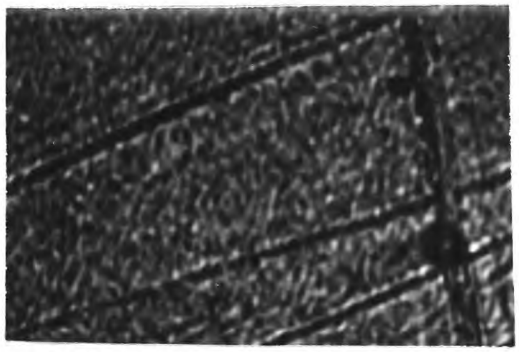

(a) Thickness = 700 A
at 700 A/sec.
Angle i = 0^{o}

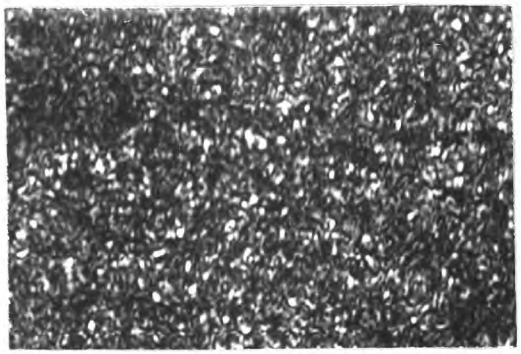

(b) Thickness = 5065A
at 248 A/sec.
Angle i = 0^{o}

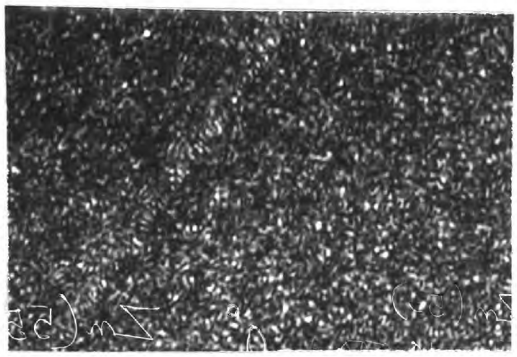

(c) Thickness = 10000 A
at 350 A/sec.
Angle i = 0^{o}

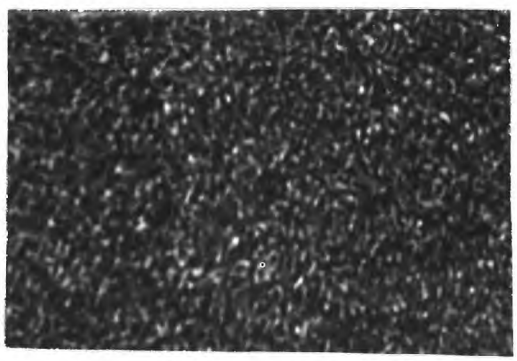

(d) Thickness = 1100 A
at 210 A/sec.
Angle i = 0^{o}

Fig.49. Optical Micrographs from the Surfaces of the Zinc Deposits prepared at 1 x10^{-5} torr.
Magnification 1220 X.

thick specimen prepared at 350 A/sec. The crystals show a discontinuous surface with crystal size much smaller than that of a thin deposit.

Figs.49(b and d) are the optical micrographs from deposits prepared on glass substrates. Fig.49(b) showed (101) type of orientation and Fig.49(d) showed (114) type of orientation. The crystal size is relatively larger than in the 10,000 A thick deposit.

3.4(d) The Structure of Zinc Deposits Condensed at Oblique Incidence of the Vapour Stream:

As has been mentioned earlier, the substrate was placed below the source in such a way that one end of it received the metal vapour at oblique incidence. For comparison of the surface orientation at the oblique end with that of the normal end, the diffraction photographs obtained from these two regions have been presented at the same place.

For thin deposits no azimuthal limitation of the crystals were observed. But for thicker deposits (~5000 A and above) crystals were in a limited range of azimuth about the specimen normal. Many of the deposits showed variation in the surface orientations at oblique incidence relative to that at normal incidence.

Figs.40(a and b) are at $i = 0^{\circ}$ and $i = 45^{\circ}$

respectively for a specimen 3206 A thick. While the pattern at the normal-incidence region shows a mixture of (101) and (112) orientations, the one at 45° incidence shows only (101). Figs.36(c and d) show that at normal incidence of the vapour stream the deposit has developed (100) + (101) orientations but at oblique incidence it has also developed (001) along with (100) and (101). Similar results are seen from Figs.36(e and f). At i = 45°, the deposit is only about 1/3 of the i = 0° thickness (and the rate of deposition also 1/3) and this leads to the difference in the orientation.

Figs.41(a and b) show another example of change of orientation from (112) at i = 0° to a mixture of (112) and (101) at i = 45°. There is no visible asymmetry of intensity or arc positions in this pattern (Fig.41(b)).

For thick specimens asymmetry in arc positions and their relative intensities have been observed.

Fig.47(c) is such a one from the i = 45° region of a 4500 A thick specimen. The asymmetry of the arc positions along with the intensity distribution is prominent. A prominent series of 10ℓ diffractions is distinctly visible with an inclination towards the vapour stream direction. This indicates strong development of $\{001\}$ faces at the oblique incidence end of the specimen, the preferred azimuth

being that at which the (001) face is facing the vapour stream most nearly normally. The strong refraction caused by the crystal plane faces further supports the evidence of the growth of {001} faces nearly perpendicular to the oblique vapour beam direction.

3.5. The Structure of Cadmium Deposits Condensed at a Pressure of 5 x10^{-3} torr of Air on to Stainless Steel Substrates at Room Temperature:

A few deposits of cadmium were prepared at this pressure. Various rates of deposition starting from about 150 A/sec up to about 975 A/sec were tried. The film thicknesses at the normal incidence of the vapour stream varied roughly between 175 A and 6750 A.

The results obtained from these deposits are plotted in Fig.50. Most of the deposits showed (like zinc had done) either one-degree (101) or a mixture of (101) and (100) orientation. Out of 21 experiments 8 showed one-degree (101), 10 showed a mixture of (101) and (100), 1 showed a mixture of (101), (100) and (001), and one showed one-degree (112) and the last one showed approximately (102) orientation. The type of orientation appears again to be systematically dependent on the film thickness.

A line of demarcation can loosely be fitted between the two regions I and II in Fig.50. The region I extends

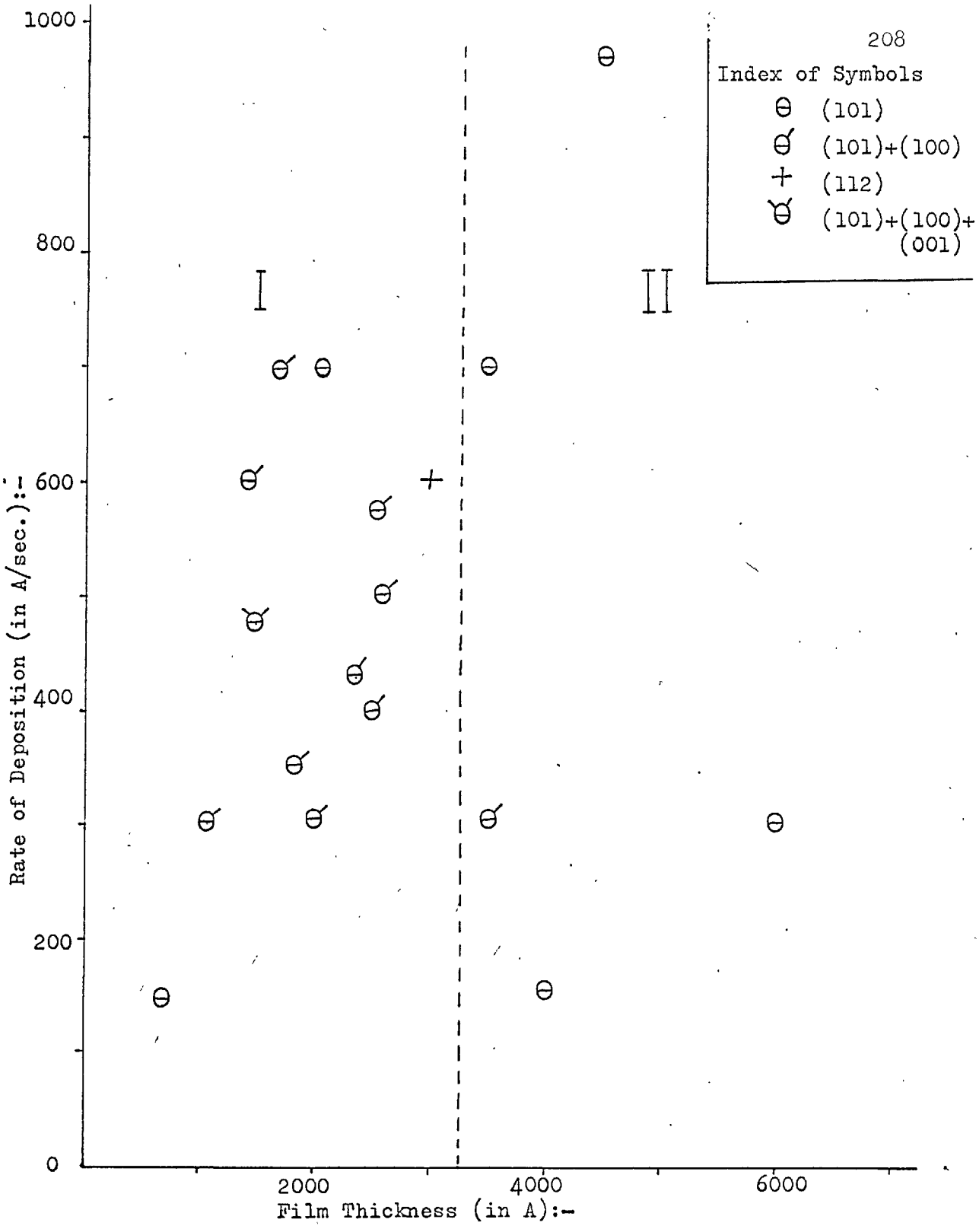

FIG.50. VARIATION OF SURFACE ORIENTATION OF CADMIUM FILMS CONDENSED ON STAINLESS STEEL AT ROOM TEMPERATURE, WITH RATE OF DEPOSITION AND FILM THICKNESS, AT RESIDUAL AIR PRESSURE 5×10^{-3} TORR.

$\angle i = 0^{\circ}$

from a thickness of~750 Å to about 3250 Å and the region II extends beyond 3250 Å.

Region I :- Results of the deposits of this region mostly show a mixture of (101) and (100) orientations. Out of 13 results coming within this region only one showed one-degree (101), one (112) and one a mixture of (101), (100) and (001). All these three results were obtained at rates of deposition higher than 450 Å/sec.

Some of the electron diffraction patterns from the deposits of this region are presented in Figs.51(a-e). Fig.51(a) is from the $i = 0^{\circ}$ region of a specimen 3007 Å thick prepared at 600 Å/sec. Referring to the theoretical pattern Fig.37(d) for (112) oriented zinc (Cd has the axial ratio $c/a \sim 1.88$) it is confirmed to be one-degree (112). The 101 arcs about the plane of incidence are separated by a fall of intensity in between them. The two short lateral arcs just above the shadow edge on the 100 ring are also in agreement with a (112) pattern. The 112 arc on the 112 ring is distinct although it has a long spread of $\pm 20^{\circ}$. Some of the rings show spottiness in them, indicating the formation of large crystals on the growing deposits.

Fig.51(b) is from the $i = 0^{\circ}$ region of a 1500 Å thick specimen prepared at 475 Å/sec. The short and sharp arcs on the plane of incidence on the 101, 100 and 001 rings

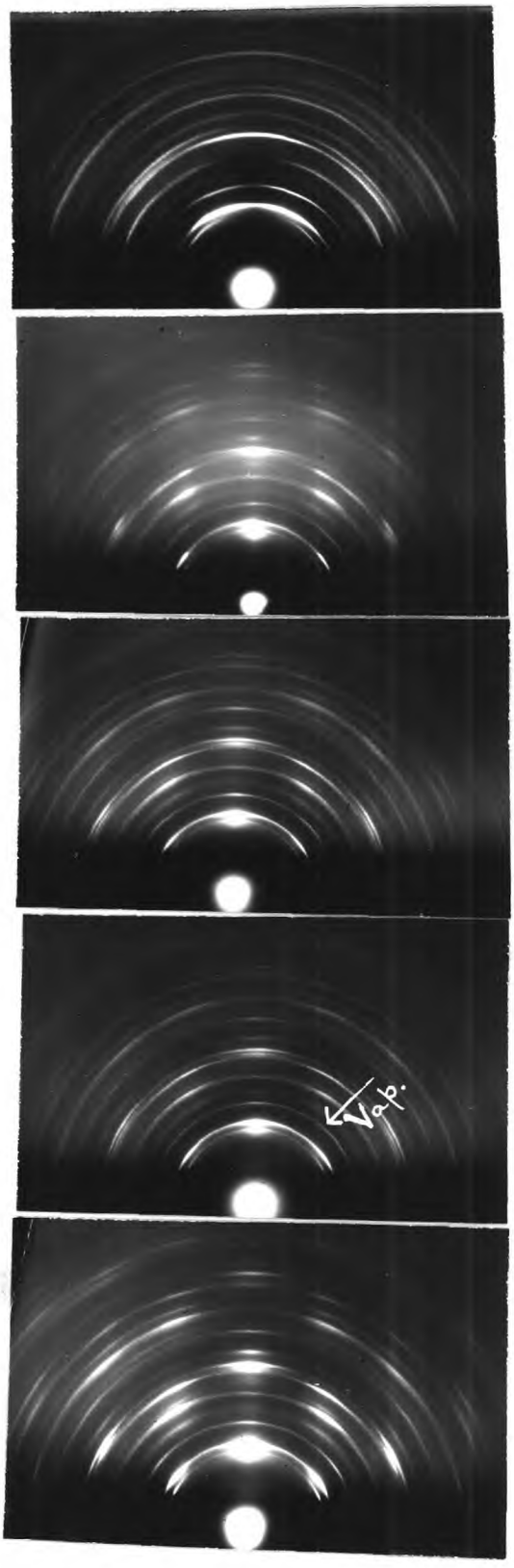

(a) (112) Orientation from a Cadmium Deposit 3007A thick (Rate 600A/sec; i = 0^{o})

(b) (100)+(001)+(101) Orientations from a Cadmium Deposit 1500A thick (Rate 475A/sec; i = 0^{o})

(c) (100)+(101) Orientations from a Cadmium Deposit 1700A thick (Rate 700A/sec; i = 0^{o})

(d) As in (c); i = 45^{o}

(e) (100)+(101) Orientations from a 1850A thick Cadmium Deposit. (Rate 350A/sec; i = 0^{o})

Fig.51. Diffraction Patterns from Cadmium Deposits prepared at 5×10^{-3} torr of Air.

are clearly visible. The second order arcs on the 200 and 004 rings on the plane of incidence are also visible. The slight strengthening in intensity of the arcs at the plane of incidence region of 102 and 103 rings may indicate the preferential development of some crystals in (102) and (103) orientation along with the main (101), (100) and (001) orientations. In the main, however, it is a pattern showing a mixture of (101), (100) and (001) orientations.

Figs.51(c and d) are from the $i = 0^{\circ}$ and $i = 45^{\circ}$ regions respectively from a 1700 A thick specimen prepared at 700 A/sec. Both these patterns show strong (100) orientation mixed with (101). Here also, a short and faint arc at the plane of incidence of the 102 ring is visible. The other arc positions of the pattern do not allow it to be interpreted as a (102) type of orientation. It may be that due to the rocking of the [101]* axis about its mean direction (as is evident from the relatively long arcing on the 101 ring) some of the {102} planes might have come to the Bragg-reflection position. Fig.51(d) does not show any change relative to Fig.51(c), indicating that the crystal habit is not sufficiently well-defined to be coming into play at oblique incidence of the vapour stream.

Region II :- Results of the deposits of this region mostly show one-degree (101) type of orientation. Only one

specimen about 6750 Å thick prepared at a rate of 300 Å/sec showed a slight deviation from the (101) towards (102), which, however, was not very perfect.

The electron diffraction patterns of some of these deposits are shown in Figs.52(a-d). Fig.52(a) is from a ~6000 Å thick specimen prepared at~300 Å/sec. The central arc at the plane of incidence of the 101 ring is distinctly visible along with the two lateral arcs on it. The two side arcs just above the shadow edge on the 100 ring are visible with a clear long gap in between. The slight strengthening in intensity in the plane of incidence region on the 112 and 102 rings is due to coalescence of two neighbouring arcs on each of them. The spread of the 101 arc is about $\pm$ 12°, indicating a corresponding spread of the {101} planes.

Fig.52(b) is from the only specimen in this region which gave a mixture of (100) and (101) orientations. This was a 3530 Å thick specimen prepared at 300 Å/sec. The arc positions on the rings show it to have a mixture of (100) and (101) orientations. The spread of the 101 arc is about $\pm$ 16°. Such a long range of rocking of the [101]* axis can bring some of the {102} and {103} planes to the Bragg-reflection position. In fact, there is a short intense arc at the plane of incidence region of the 102 ring. The arc

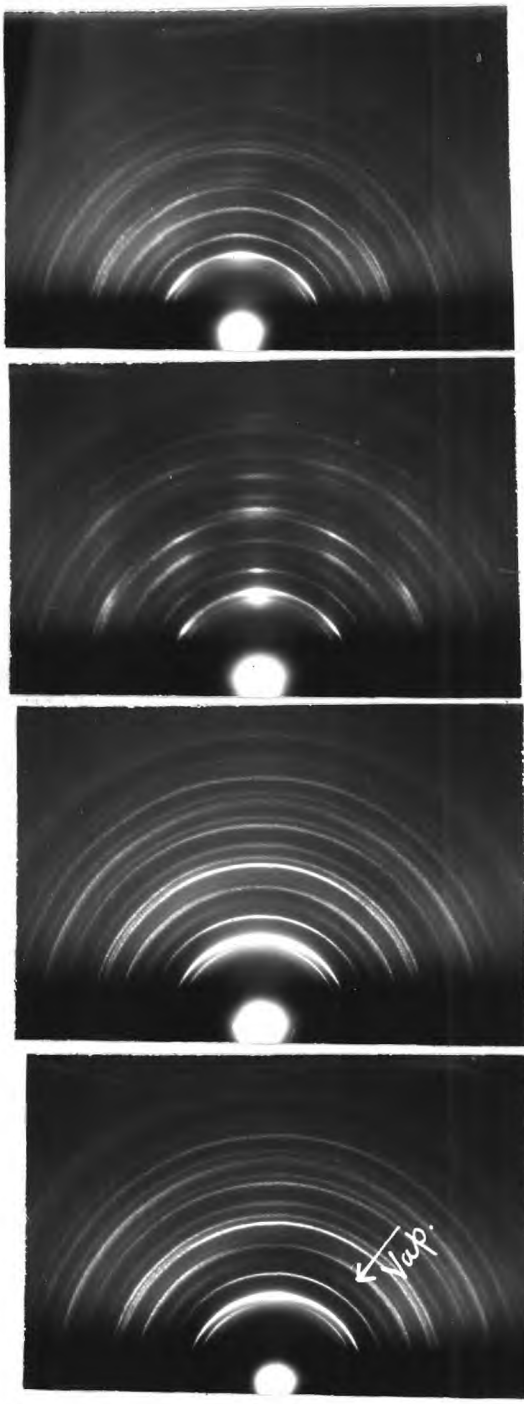

(a) (101) Orientation.
Thickness = 6000A at i=0°
Rate = 300 A/sec
Angle i = 0°

(b) (100)+(101) Orientations
Thickness = 3530A at i=0°
Rate = 300 A/sec
Angle i = 0°

(c) (101) Orientation
Thickness = 4527A at i=0°
Rate = 1000A/sec
Angle i = 0°

(d) As in (c)
Angle i = 45°

Fig.52. Electron Diffraction Patterns from the Cadmium Deposits prepared at 5×10^{-3} torr of Air.

at the plane of incidence on the 201 ring is mainly due to the coalescence of the two neighbouring lateral arcs expected due to (101) type of orientation. The pattern shows spottiness of the rings, indicating the large size of the crystals (~500 A diameter) on the growing deposit.

Figs.52(c and d) are from the $i = 0^{\circ}$ and $i = 45^{\circ}$ regions of a specimen 4527 A thick prepared at 1000 A/sec. These show weak (101) orientation, indicated by the arc positions on the different rings. The central arc on the 101 ring in Fig.52(c) is long, but still can be distinguished from the side arcs. Fig.52(d) does not show any appreciable difference in orientation. There is, however, a very little asymmetry in the intensity distribution among the similar arcs on the same ring, indicating very little azimuthal limitation of the crystals around the vapour-stream direction. The spottiness of the rings again indicates the presence of large crystals on the surface of the deposit.

SECTION 4.

DISCUSSION.

4.1. The Results for Gold, Silver and Copper:

4.1(a). The Origin and Development of the Preferred Orientations in the Gold, Silver and Copper Deposits:

The results obtained from these deposits and described in 3.1, 3.2 and 3.3 are self-consistent and reproducible. It was concluded that for all the three metals, at all the air pressures investigated, the sequence of orientations observed as the deposit thickness increased was the same (apart from additional development of some hexagonal silver lattice at pressures near 10^{-2} torr).

The sequence of different orientations in these metals was:- random, (111), (111) + {111} twinning, followed by (211) and/or (110), ((211) mixed with (111) in the case of gold). In the case of silver, after the random stage, (111) orientation was observed up to a thickness of about 15,000 A at the ultra-high vacuum region. At higher pressures Dutta (1968) observed the next stage as a mixture of (111) orientation and {111} twinning, which was followed by (110) and (110) + (211). This new orientation (110) was not observed in gold and copper and also not in the silver deposited in ultra-high vacuum.

The origins of the different orientations in these deposits are discussed in detail in the following sub-sections.

4.1a(i). The Origin of the Random Orientation in the Initial Stage:

In silver and copper deposits, the upper limit of the thickness up to which random polycrystalline orientation was observed, was found to increase as the residual air pressure decreased from 10^{-2} torr. In the gold deposits, however, this thickness decreased with decreasing pressure (cf. Figs. 4, 19 and 25). In fact, the general nature of all the three metals is concluded to be the same. The thickness before the initial (111) orientation is developed decreases on both the sides of a peak value corresponding to a particular residual air pressure.

The surface of an amorphous substrate is presumably rough on the atomic scale. When the atom-pairs or the three-dimensional crystal nuclei are formed from the metal atoms deposited from the oncoming vapour on to such an atomically rough surface at room temperature, the mobility of the metal atoms is so small that although the atoms pack closely into a crystalline aggregate, the nuclei do not take up any preferred orientation of lowest potential energy relative to the mean substrate plane surface. Further, the presence of the gas molecules in the system may reduce the

mobility of these already low-mobility atoms, thereby decreasing the migration effect of the atoms at this early stage. This may also hinder any preferential growth of the nuclei.

4.1a(ii). The Origin and Development of the (111) Orientation:

In all these three metals the next stage was the development of one-degree (111) orientation. The upper limit of this stage also varied systematically with pressure. Evidently, at a particular pressure, different for the three different metals, the thickness of the deposit at which (111) orientation begins to develop, reaches a maximum and gradually falls on either side of it (Figs. 4 and 19). Although copper did not show such a peak down to the lowest pressure investigated, it can be assumed that at a still lower pressure the loci I, II and III in Fig.25 would have attained peak values and thereafter decreased to lower values as in the cases of gold and silver.

As a deposit, at first made up of randomly oriented crystals, increases in thickness, the mobility of the metal atoms after arrival on the surface evidently increases - in effect there is a rise in temperature due to the receipt of energy by radiant heat and kinetic energy of the metal atoms (Evans and Wilman 1952, Murbach and Wilman 1953, Wilman 1955).

This raised mobility evidently leads to the development of plane faces on the growing crystals. In the case of the f.c.cubic metals the (111) faces are formed, and these are the most densely populated ones, having lowest surface energy. Once the plane crystal faces are formed, it is clear that those crystals having orientations with such a face normal to the vapour stream will receive the largest number of atoms per unit area of faces. These atoms migrate to the edges and are retained there, thus prolonging the face sideways most rapidly, and such crystals receiving more and more metal atoms will predominate in the upper region of the deposit. The strong refraction effect in the diffraction patterns shows clearly the development of the {111} faces. Evans and Wilman (1952) and Ramos and Wilman (1962) also pointed out such growth process of crystal faces on a growing deposit leading to preferred orientation.

4.1a(iii). <u>The Origin of the Octahedral Twinning</u>:

The third stage of growth consists of (111) orientation along with its {111} twinning.

Once the metal atoms have started forming the octahedral faces, the mobility of the incoming vapour atoms may be hindered by the gas molecules present in the system. This reduces the migration rate and the probability of nucleation of a new layer of atoms is more. Presumably,

it is the presence of these adsorbed gas molecules which occasionally leads to the initiation of a new sequence of stacking on the (111) planes. For example, if the initial crystal has the packing sequence ABCABCABC ... ... , the next layer may develop as ABCABACBACBA ... ... which is the reflexion twin structure of the original octahedral structure. In the low-pressure regions, this irregularity in packing may have been initiated more by stress in the deposits or occasional dislocation in the crystal formation or presence of foreign particles as impurities in the system, than by the very low number of gas molecules present. This seems to fit in with the observation that in the silver deposits up to a thickness of about 16,000 A, octahedral twinning was not observed in the ultra-high vacua.

On the other hand, twinning occurred appreciably in gold at about 1000 A thickness in the U.H.V. region of pressure (and later led to (211) orientation in further deposition (cf. Fig.4)). This difference between the silver and gold must be associated with the more extensive chemisorption of the oxygen on the silver than on the gold.

4.1a(iv). <u>The Origin of the (211) Orientation:</u>

The next stage was the one where a mixture of (111) and a new orientation (211) was found to occur, which mainly very quickly changed to the stable (211) type of orientation.

In the case of silver, however, the region beyond 16,500 A (at 2×10^{-7} torr of air) and 8,600 A (at 1×10^{-6} torr of air) was not investigated. In the case of this metal in the ultra-high-vacuum (111) type of orientation seemed to be the stable form of orientation.

This new orientation is concluded to result from the secondary twinning of the primary twin about a $[\bar{1}1\bar{1}]$ axis of the primary twin (Figs. 11(a) and (b) and 53(a),(b) and (c)). Referring to Fig.53(c), it is seen that in the secondary twin a (211) type of plane will be nearly parallel to the substrate.

The angle between the (211) plane and the substrate can be shown to be of the order of 5° as follows:-

Let the secondary twinned cube have a $[u''v''w'']$ axis perpendicular to the substrate, and let its indices in relation to the primary twinned lattice be $[u'v'w']$. Let the twinning axis $[UVW]$ be $[\bar{1}1\bar{1}]$.

Then from equation (3.3) we have

$$\begin{aligned} u' &= -u + \tfrac{2}{3}(u - v + w) \\ v' &= -v + \tfrac{2}{3}(u - v + w) \\ w' &= -w + \tfrac{2}{3}(u - v + w) \end{aligned} \qquad (4.1)$$

Solving these equations we get,

$$\begin{aligned} u &= -\tfrac{1}{3}u' - \tfrac{2}{3}v' + \tfrac{2}{3}w' \\ v &= -\tfrac{2}{3}u' - \tfrac{1}{3}v' - \tfrac{2}{3}w' \\ w &= -\tfrac{2}{3}u' - \tfrac{2}{3}v' - \tfrac{1}{3}w' \end{aligned} \qquad (4.2)$$

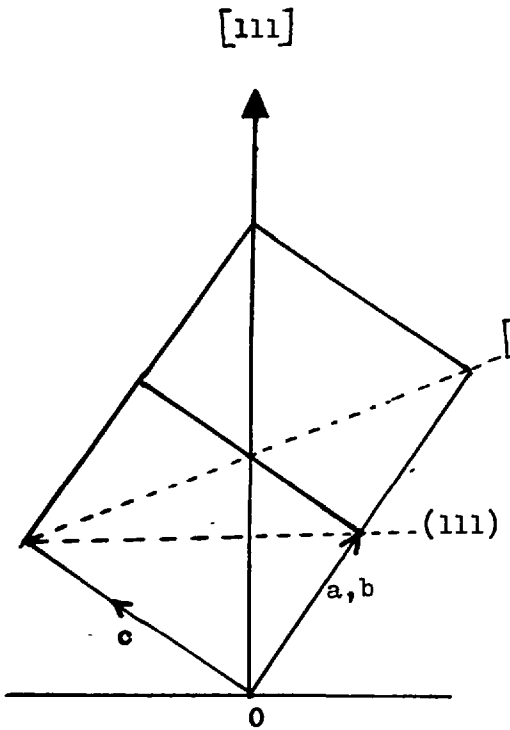

Fig.53(a). Side view of a cubic unit cell of the (111) oriented gold.

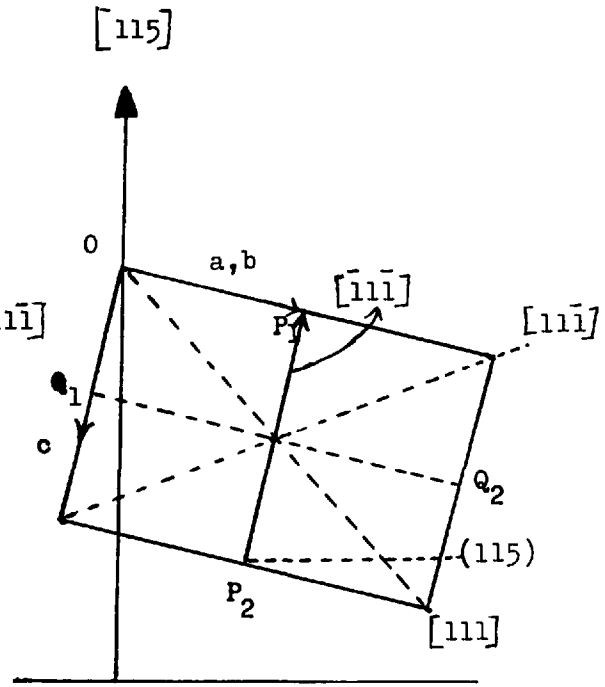

Fig.53(b). Side view of the cubic unit cell of the [11$\bar{1}$] primary twin of the (111) oriented gold.

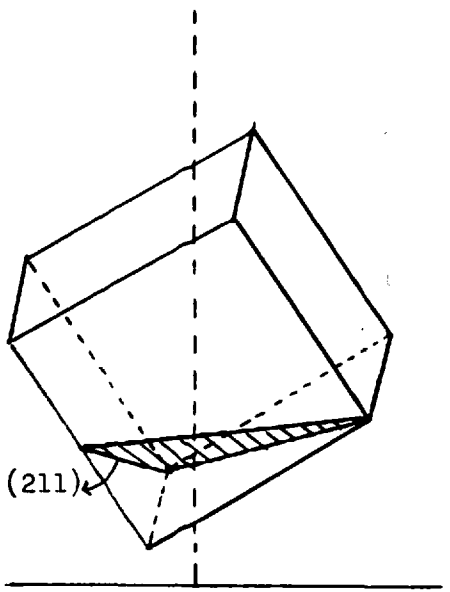

Fig.53(c). Side view of the cubic unit cell of the [$\bar{1}$1$\bar{1}$] secondary twin of the (111) oriented gold.

In this case, [u'v'w'] = [115], hence we have

$u = \frac{7}{3}$, $v = -\frac{13}{3}$ and $w = -\frac{5}{3}$

i.e. $[uvw] = [7, \bar{1}\bar{3}, \bar{5}] \simeq (1\ \bar{2}\ \bar{1})$

The angle of incidence between $[1\bar{2}\bar{1}]$ and $[7,\bar{1}\bar{3},\bar{5}]$ is obtained from the relation:

$$\cos \phi = \frac{u_1u + v_1v + w_1w}{[u_1^2 + v_1^2 + w_1^2]^{\frac{1}{2}} \cdot [u^2 + v^2 + w^2]^{\frac{1}{2}}}$$

where, $[u_1v_1w_1] = 1\bar{2}\bar{1}$ and $[uvw] = [7,\bar{1}\bar{3},\bar{5}]$.

Putting these values of u_1, v_1, w_1 and u,v,w, we have $\phi = 5^{\circ}36'$.

In comparison with the spread of the (111) orientation ($\sim \pm 10^{\circ}$) from the mean, this angle is quite small. Hence, within this spread there is a high probability of the crystals having the (211) plane normal to the vapour stream growing preferentially, if they possess a (211) face. Thus, these faces will receive more and more atoms and will grow laterally fastest, as in the previous case of the development of the {111} faces.

At the higher pressures, the abundant gas molecules lead to more extensive twinning and thus more rapid development of orientation than at the lower pressures.

4.1.(b). The Effect of the Constituent Residual Gases:

Down to a pressure of 10^{-5} torr no liquid nitrogen was used in the demountable system described in 2.4(b).

To attain a pressure lower than this, liquid nitrogen was used in the trap. In the U.H.V. system, liquid nitrogen was used for fore pumping by the sorption pumps in the beginning. The system could attain a pressure of 1×10^{-6} torr with the bell-jar and $(2-5) \times 10^{-7}$ torr with the stainless-steel tap without baking. To obtain still higher vacuum the system was baked as has been described in 2.4(c).

It thus appears that at pressures of 10^{-5} torr and higher, the partial pressure of moisture is more than at lower pressures. However, to reduce moisture in this region also, phosphorus pentoxide was used in the backing line. At lower pressures, $\sim 10^{-8}$ torr, a baking operation removed most of the water vapour from the chamber. Thus, the effect of moisture on the deposit structure seems to be not very likely. The high repeatability and self consistency in the results and the regular continuity of the loci indicating different stages of growth (Figs. 9, 19 and 25) further give support to this view. The mass spectrographic analysis (in the U.H.V. system) indicates a relatively low peak corresponding to the moisture, after baking the system.

While no mass-spectrographic analysis of the constituent gases were carried out within the demountable system, the constituent gases within the U.H.V. system were

analysed with the help of the A.E.I. "MS10" type mass spectrometer. Although a large change in the residual gas composition shown by the spectrographic analysis was observed after the system was baked, no change in the orientation of the deposits was noticed.

The mass scan of the residual gas in the unbaked U.H.V. system at 10^{-7} torr showed prominent peaks corresponding to masses 16(CH_4), 18(H_2O), 28(N_2 and CO), 32(O_2), 43(C_xH_y-hydrocarbons) and 44(CO_2). From the peak height measurements, the relative abundance of these gases were in the decreasing order of H_2O, CH_4, N_2, CO, CO_2, C_xH_y and O_2.

After baking, when the pressure was 10^{-8} torr, the relative peak heights corresponding to these gases fell appreciably, indicating the removal of most of them to a large extent. The relative abundance of the gases now were in the decreasing order of N_2(or CO), CO_2, H_2O, CH_4 and O_2. Other peaks could not, however, be interpreted very precisely.

The effect of these gases on the structure of the deposits of these three metals, as mentioned earlier, was not found to be very significant. Further work is in progress in this laboratory.

4.1c(i). The Observed Form of the Loci for the Thicknesses where Different Orientations Begin, as a Function of Pressure, and the Relationship to the Chemical Reactivity of the Metals:

Figs. 4, 19 and 25 show that the surface orientations of the deposits of these three metals show regular variation with thickness and pressure. The general nature of all the loci is the same.

As mentioned earlier, in the early stages of deposition for all the three metals no preferred orientation was observed. The lowest thickness at which gold deposits showed (111) orientation was about 250 A at 1×10^{-8} torr. Silver and copper deposits showed similar tendency of falling thickness for the development of (111) orientation as the residual air pressure was decreased.

It is concluded that at a low enough pressure, the preferred orientations in these metals set in at a very early stage of deposition i.e. at a deposit thickness of only about 250 A or less. The atomic mobility initially at room temperature is still too low to allow preferred orientation of the initial crystal nuclei, but is soon increased to the stage where octahedral faces are developed, as deposition proceeds. At these lowest pressures the mobility of the metal atoms, and the development of $\{111\}$ faces, is evidently decreased as the residual air pressure is increased,

so that the preferred orientation only sets in at higher thicknesses. However, a peak value for the thickness at which orientation develops is reached, at a pressure which presumably corresponds to a certain proportion of the deposit surface being covered by the adsorbed gas at any instant during the deposition. At still higher pressures, the adsorbed gas evidently now promotes more and more rapidly the development of octahedral faces and preferred orientation, possibly due to the increased mobility of the metal atoms on the gas-covered parts of the octahedral faces.

For different metals, the peaks can thus be expected at different pressures, this pressure being lower, the higher is the degree of adsorption (chemisorption) of the gas on the metal. The above results for gold, silver and copper can be regarded as showing the order of pressures at which the maximum occurs for metals of these respective degrees of different chemical interaction with the residual air. Copper being the most reactive, its peaks are expected at a lower pressure than those for silver and gold, which are much less reactive. Since gold adsorbs oxygen and other gases least among these three metals, it is at a relatively higher pressure that its surface mobility favours rapid growth of octahedral faces and hence (111) orientation.

Although the silver atoms have a surface mobility

and chemical reactivity comparable to those of gold, yet the chemisorption of silver may be more, oxygen atoms arising due to the probable dissociation of some of the gas molecules after evaporation.

4.1c(ii). <u>The Theoretical Consideration of the Locus for the Thickness where (111) Orientation begins</u>:

The number of metal atoms striking unit area of the substrate per unit time can be calculated from the thickness deposited per second. For example, for silver when the rate of deposition is $\sim$32 Å/sec (as in Fig.19) it is

$$N_{Ag} = \frac{32 \times 10^{-8} \times 10.50}{107.88 \times (1{,}66 \times 10^{-24})} \text{ atoms/cm}^2\text{/sec},$$

$$= 1.877 \times 10^{16} \text{ atoms/cm}^2\text{/sec}.$$

where, density of silver if 10.50 gm/cc., atomic weight is 107.88 and wt. of a hydrogen atom is 1.66×10^{-24} gm.

From the kinetic theory of gases, the number of gas molecules striking unit area of the substrate per unit time at a pressure p and temperature T, is

$$\nu = \frac{1}{m} \times p_{Torr} \left[\frac{M}{2\pi RT}\right]^{\frac{1}{2}}$$

$$= \frac{1}{m_H [2\pi RT]^{\frac{1}{2}}} \times \frac{p_{Torr}}{[MT]^{\frac{1}{2}}} = 3.51 \times 10^{22} \times \frac{p_{Torr}}{[MT]^{\frac{1}{2}}}$$

where, m_H = wt. of a H-atom,
$m = m_H M$ = mass of a gas molecule,
$R = 8.31 \times 10^7$ ergs/^oC.,
M = molecular wt. of the gas.

At p = 1 x10^{-8} torr and T = 293°K, the value of ν for oxygen is 3.629 x10^{12} molϕs/cm^2/sec. and at p = 5x10^{-3} torr and T = 293°K, it is 1.8 x10^{18}moles/cm^2/sec.

It is hence clear that while at 1 x10^{-8} torr of oxygen, for every oxygen molecule there will be about 5,000 silver atoms incident on the substrate; at 5 x10^{-3} torr, for every silver atom there will be about 100 oxygen molecules.

At low pressures $\sim 10^{-8}$ torr, the gas adsorbed by the film surface is likely to be mainly as isolated molecules, some of which may occupy some definite sites, and others be migrating over the surface of the octahedral face. In both the cases this hinders the mobility of the silver atoms i.e. lowers the rate of development (laterally) of the octahedral faces and preferred orientation, increasingly with increase in the gas pressure. This accounts for the observed increase in film thickness at which preferred (111) orientation begins as the residual gas pressure is increased from 10^{-8} torr.

However, above a certain pressure this hindrance to octahedral face development becomes evidently outweighed by a process which increasingly favours the lateral development of the octahedral faces, with further increase of the residual gas pressure. This process seems likely to be the formation of areas of close-packed adsorbed gas

molecules or atoms on the developing octahedral faces, and a reduced probability of sticking of the mobile metal atoms on these areas.

Dutta and Wilman (see Dutta, 1968), gave the following analytical treatment to explain the nature of the pressure-thickness curves for silver in this high-pressure region, which is applicable only to the right hand side of the peaks (cf. Figs. 4, 19 and 25).

Considering the stage of development of (111) faces and (111) orientation, let the octahedral faces be circular and of radius r at an instant of time t from the start of the development of (111) faces. Let the metal atoms be deposited at a rate dN_M/dt, which is the number of incident metal atoms/cm^2/sec., and let there be no re-evaporation of the metal atoms. At this instant let θ be the fraction of the total number of sites which metal atoms can occupy, occupied by the gas molecules. Therefore, the fraction of the total number of sites the condensed metal atoms can be trapped in is $(1 - \theta)$, and hence, the number of metal atoms reaching the perimeter of the face per second is proportional to θ, or more generally to a function of θ, i.e. $f''(\theta)$.

The rate of increase in area of the octahedral face is

$$\frac{dA}{dt} \propto f''(\theta)\ \pi r^2\ \frac{dN_M}{dt} \qquad (4.1)$$

Since $dA = 2\pi r.dr$, we have from equation (4.1)

$$\frac{dr}{r} \propto f''(\theta) \cdot \left(\frac{dN_M}{dt}\right) dt$$

from which on integration,

$$\log_e \left(\frac{r}{r_o}\right) = B\, f''(\theta)\, (t-t_o) \qquad (4.2)$$

where, $B = \frac{dN_M}{dt}$, a constant, and $r = r_o$ at $t = t_o$.

The thickness h of a deposit is proportional to the time t, thus from (4.2)

$$\log_e \left(\frac{r}{r_o}\right) = B\, f''(\theta)\, (h - h_o)$$

or

$$h = h_o + \frac{\log_e (r/r_o)}{B\, f''(\theta)} \qquad (4.3)$$

The rates of adsorption and desorption u and u' of gas molecules on a uniform surface are given as (Hayward and Trapnell, 1964)

$$u = \frac{\sigma p}{\sqrt{2\pi mkT}} \cdot f(\theta) \cdot e^{-E/RT} \qquad (4.4)$$

and

$$u' = K\, f'(\theta) \cdot e^{-E'/RT} \qquad (4.5)$$

where σ = condensation coefficient,

E and E' = activation energies of adsorption and desorption respectively,

K = a constant,

and the rest of the symbols have their normal significance.

For equilibrium, $u = u'$ and $E' - E = q$, and hence from equations (4.4) and (4.5) we have,

$$p = \frac{K}{\sigma} (2\pi mkT)^{\frac{1}{2}} \cdot \frac{f'(\theta)}{f(\theta)} \cdot e^{-q/RT} \qquad (4.6)$$

Putting $\frac{K}{\sigma} (2\pi mkT)^{\frac{1}{2}} e^{-q/RT} = \frac{1}{a}$, where 'a' is dependent on T alone, the isotherm becomes

$$p = \frac{1}{a} \cdot \frac{f'(\theta)}{f(\theta)} \qquad (4.7)$$

A "Langmuir isotherm" is obtained if it is assumed that $f(\theta) = 1 - \theta$ and $f'(\theta) = \theta$, and equation (4.7) then becomes, $p = \frac{\theta}{a(1-\theta)}$

$$\text{or} \quad \theta = \frac{ap}{1 + ap} \qquad (4.8)$$

Now if we put this value of θ for $f''(\theta)$ in equation (4.3) we have

$$h = h_o + \frac{\log_e(r/r_o)}{B} \left(1 + \frac{1}{ap}\right) \qquad (4.9)$$

Hence, on the above assumptions this equation represents the variation of the deposit thickness h at which the (111) faces have reached a radius r, with the gas pressure p. As p increases h decreases.

Evidently, this equation can explain to a great extent the nature of the (pressure, thickness) loci only down to a pressure near that at which the peak thickness occurs. Below that pressure this equation does not hold good.

Of the various assumptions made for deriving equation (4.9), the most doubtful one is whether u is at all

equal to u', i.e. whether an equilibrium adsorption state occurs. An ideal equilibrium state, when the rate of adsorption of gas molecules on the deposit surface is equal to that of desorption, may, however, be approximated in the range of relatively high gas pressures $\sim 10^{-5}$ to $\sim 10^{-2}$ torr.

4.1(d). The Effect of the Obliquity of the Vapour Stream:

Burgers and Dippel (1934) and Evans and Wilman (1952) found that the surface structure of deposits is affected by the obliquity of the vapour stream.

In the present work also, similar results were observed. A tilt of the orientation axis towards the direction of the vapour stream was noticed as usual. The angle of the vapour stream was kept constant ($i = 45^{\circ}$) and the variation of the tilt with the deposit thickness was studied.

At low pressures $\sim 10^{-7}$ to 10^{-8} torr, the tilt of the orientation axis was found to be practically nil for all thicknesses. At higher pressures appreciable tilts of varying degrees with varying thicknesses were observed.

Figs.18(a,b,c) and Figs.34(a,b) show that the general nature of the thickness-tilt (t, δ) plots is more or less similar for gold and copper. The maximum tilt observed for gold is about 26° corresponding to a deposit thickness 1200 Å (at $i = 45^{\circ}$) at 2×10^{-3} torr and the minimum is about 19° corresponding to a thickness ~ 1700 Å (at $i = 45^{\circ}$) at

5×10^{-5} torr. For copper, the graphs (Figs.34(a,b)) show flat peaks around 27° (at $p = 3 \times 10^{-5}$ torr) and around 23° (at $p = 5 \times 10^{-6}$ torr) corresponding to the same sort of thickness ($\sim$1500 A at $i = 45^{\circ}$).

It is seen from these graphs that in (211)-oriented films there is a relatively large tilt of the orientation axis. The (211) orientation develops due to the secondary twinning of the primary {111} twin. The twinned nuclei make the deposit surface rough. As Evans and Wilman (1952) pointed out, the tilt of the orientation axis is mainly attributable to the roughness of the deposit surface. As the deposition process continues, due to the rise in the surface energy the mobility of the incident atoms progressively increases, which promotes rapid lateral growth of the {211} faces. This in turn tends to make the deposit surface gradually smoother which consequently leads to a gradual fall in the tilt angle

At low pressures, the atomic mobility is high and hence the tilt angle before reaching a relatively high value begins to fall down. At higher pressures, in addition to having a more favourable growth of (211) oriented crystals by the secondary twin of the primary {111} twin, atoms are also less mobile. Both these factors contribute to a rougher surface, the consequence of which is more tilt of the orientation axis. This explains clearly the larger

tilt angles of the gold deposits at lower pressures than at the higher pressures.

The comparatively lower values of δ for the [111] axis is attributable to less rough deposit surface. (111) orientation arises due to the strong development of the smooth octahedral faces, as was discussed already. This makes the deposit surface less rough than the surface with (211) oriented crystals.

That at lower pressures (lower than 5 $x10^{-5}$ torr for gold, 5 $x10^{-6}$ torr for copper and 1 $x10^{-6}$ torr for silver) $\delta = 0$ for all thicknesses, further supports the validity of the above reasoning. When the number of gas molecules incident on the surface is small compared with the number of metal atoms incident (per unit area), the mobility of the atoms is high enough to promote rapid growth of smooth {111} or {211} faces. This contributes to the quick development of smooth deposit surfaces, a consequence of which is the negligible tilt of the orientation axis.

The extended nature of the peaks (Figs.34(a) and (b)) for copper relative to those of gold (Figs.18(a),(b), (c)) may again be attributed to their different chemical natures. Although both the metals have almost comparable melting points (1063°C for gold, 1083°C for copper), yet due to much higher chemisorption of oxygen on copper, the copper atoms are less mobile under identical conditions. As a

result, the copper deposit surface becomes smooth more slowly with increasing thickness, relative to a gold deposit surface. This explains the extended nature of the peaks of the (δ,t) graphs for copper.

4.2. The Origin of the Preferred Orientations in the Zinc and Cadmium Deposits.

4.2a. General Introduction:

Much work on the structure of thin films of hexagonal metals has been done by early workers. In most of these cases no extensive systematic results have been reported, particularly in relation to thickness and pressures. In the present work, particular care was taken to estimate the thickness of the deposits, as mentioned in detail in 2.5(a). With the precautions adopted, the mean film thicknesses were found to agree within about 10 or 20% with the values expected from assumption of 100% condensation and spherical symmetry of vapour from a point source.

The results obtained in the present work from the zinc and cadmium films deposited at various rates and pressures were reasonably self consistent and reproducible under similar conditions. Zinc was deposited at residual air pressures 5 $\times 10^{-3}$, 2 $\times 10^{-4}$ and 1 $\times 10^{-5}$ torr, and cadmium only at 5 $\times 10^{-3}$ torr. As mentioned in 3.4, due to the

highly gettering action of these metals, the partial pressure of the oxygen inside the system must fall rapidly during deposition and the effect becomes still more when thick deposits are prepared.

Further, as these metals have low melting points, they have a high degree of atomic mobility when condensed even at room temperature. Due to their high atomic mobility, the deposits showed relatively large isolated crystals at the early stages and also in films a few thousand Å thick, as revealed by even the optical micrographs (Figs.49(a-d)).

Consider first, the relative numbers of metal atoms and gas molecules incident initially on the specimen surface at the start of the metal deposition. The number of Zn atoms striking unit area of the substrate per second when the rate of deposition is 100 Å/sec. is

$$\frac{100 \times 10^{-8} \times 7.14}{65.38 \times (1.66 \times 10^{-24})} = 6.58 \times 10^{16} \text{ atoms/cm}^2\text{/sec}$$

where the atomic weight of Zn is 65.38, the density of Zn = 7.14 gm/cc. and the weight of a hydrogen atom is 1.66×10^{-24} gm.

The number of oxygen molecules striking unit area of the substrate per second when the initial oxygen partial pressure is 1×10^{-3} torr and T = 293°K is

$$3.51 \times 10^{22} \times \frac{1 \times 10^{-3}}{(32 \times 293)^{\frac{1}{2}}} = 3.624 \times 10^{17} \text{ mols/cm}^2\text{/sec.}$$

and at 1×10^{-5} torr and $T = 293^{\circ}K$, it is 3.624×10^{15} mols/cm^2/sec.

Thus, when the rate of deposition of Zn is 100 Å/sec. at an initial oxygen partial pressure of 1×10^{-3} torr, for every Zn atom arriving on the substrate there are initially about 6 oxygen molecules; and at 1×10^{-5} torr for every oxygen molecule there are about 18 zinc atoms.

Considering the maximum rate at which the oxygen molecules may be removed by reaction with the zinc atoms to form ZnO, it appears clear that at pressures as low as about 5×10^{-5} torr (when the partial pressure of O_2 is about 1×10^{-5} torr) nearly all oxygen molecules are removed and thereafter hardly any zinc atoms are oxidised during the further deposition.

Considering the approximate volume of the deposition chamber as 5300 cc, and a partial pressure of oxygen 1×10^{-3} torr at $20^{\circ}C$, this amount of oxygen weighs 9.96×10^{-6} gm. (22.4×10^{3} cc of O_2 weighs 32 gms at 760 mm of Hg at N.T.P.). The amount of zinc required to react with this oxygen is

$$\frac{(65.38 \times 2)}{32} \times (9.96 \times 10^{-6}) \text{ gm.} = 4.06 \times 10^{-5} \text{ gm.}$$

where the atomic weights of Zn and O are 65.38 and 16 respectively.

At 100 Å/sec., when the film thickness is about 300 Å, the amount of zinc evaporated(in air at p = 5 $x10^{-3}$ torr) is about 2 $x10^{-3}$ gm, of which only about 1/50th is likely to be required to remove all the oxygen molecules within the bell-jar. Thus the deposit must clearly be mostly zinc containing only a small amount of zinc oxide, except for extremely thin deposits.

It is clear that there is a relatively rapid removal of most of the oxygen molecules from the chamber, so that when the deposition is long (say, about 5 min. or more), the later stages of the deposition are in almost complete absence of oxygen.

In view of the progressive decrease in the partial pressure of the oxygen, it is necessary to consider only the initial orientation observed in very thin deposits ($\sim$200 Å) as corresponding to deposition of the metal in gas at the stated initial pressure. The orientation observed in the surface regions of the thicker deposits are modified as a result of the then lower oxygen pressure leading to development of different crystal faces than are at first formed, so that crystals having those faces more nearly normal to the vapour stream grow laterally most rapidly and soon predominate.

4.2 a(i). <u>The Origin of the Initial (001) Orientation in Thin Deposits</u>.

At very high rates of deposition (above 700 A/sec) in the very thin zinc deposits, (001) orientation was observed. At such a high rate of deposition, the interference with other foreign molecules was least and the probability of a metal-metal atom impact to form crystal nuclei on the initial substrate was higher than that of a metal-gas collision. Because of the very high mobility of the zinc atoms even at room temperature, the crystal nuclei grow with a definite crystallographic plane parallel to and in contact with the substrate. All these factors favoured the growth of at least some of the crystals with the most densely populated {001} atomic planes, (which are obviously the planes of least potential energy) normal to the vapour stream. The rate of arrival of the metal atoms being very high, the growth of the basal planes were thus preferred at the very early stage of the deposits. The sheet of metal atoms then grew laterally quickly due to the speedy migration of the highly mobile atoms. This preferred development of the {001} faces at the initial stage ~~which~~ was indicated by considerable refraction on the arcs in the diffraction patterns.

The heat energy radiated from the filament presumably contributed considerably to the surface mobility of the zinc, and consequently also promoted the initiation of the (001) orientation.

4.2a(ii). The Origin of the (100) Orientation.

The (100) orientation was also observed at the same high rates of deposition of both zinc and cadmium. {100} planes being the next most densely populated to (001) planes, the metal atoms may tend to form initial nuclei with these planes in contact with the substrate, even in absence of gas. It is hence not difficult to realise why (001) orientation tends to develop earlier than (100). In most of the experiments a mixture of (100) and (001) was noticed. Once the initial crystals are developed they may tend to develop with plane faces which may be of this type or other types.

4.2a(iii). The Origin of the (101) Orientation.

At rates lower than about 750 A/sec down to 25 A/sec, one-degree (101) orientation was observed for even the thinnest zinc deposits examined, prepared at 5 $x10^{-3}$ torr. At pressures of 2 $x10^{-4}$ and 1 $x10^{-5}$ torr, (101) was mostly found to be associated with (100) (Figs. 35, 42, 46). The maximum thickness showing the one-degree (101) orientation was 3850 A (in region III in Fig.35). At sufficiently high rates (above 750 A/sec) also, a few of the thicker deposits ($\sim$4000 A) showed (101) orientation.

In the case of the cadmium deposits (Fig.50), however, it is the thicker deposits that showed (101), and the thinner ones showed mostly a mixture of (100) and (101)

in the same specimen.

At such lower rates of deposition of these crystals, the interference of adsorbed gas molecules with the deposited migrating metal atoms is high, particularly at high gas pressures. As a result the gas molecules may remain as island structures on it which may partly hinder the continuity of the hexagonal close-packed (001) sheets of metal atoms and lead to the preferential growth of the (101)-oriented initial nuclei.

In a (101) plane there is very nearly a close-packed array of the metal atoms. The plan view of the atomic arrangements in or nearly in the (101) plane is shown in Fig.54. The alternate dotted circles in the plan view represent the positions of the atoms based on $[[\ \frac{1}{3},\ \frac{2}{3},\ \frac{1}{2}]]$ in the three-dimensional lattice. The plane of the atoms represented by the dotted circles is slightly above that of the atoms represented by solid circles. The metal atoms evidently tend to form such a close-packed strip with a probability next to that for $\{001\}$ and $\{100\}$.

It may be mentioned that Stranski (1949) investigating the growth of Zn and Cd single crystals from the vapour found that they developed (001), (101), (100), (110), (102) faces, (101) being the most likely to be formed after the (001).

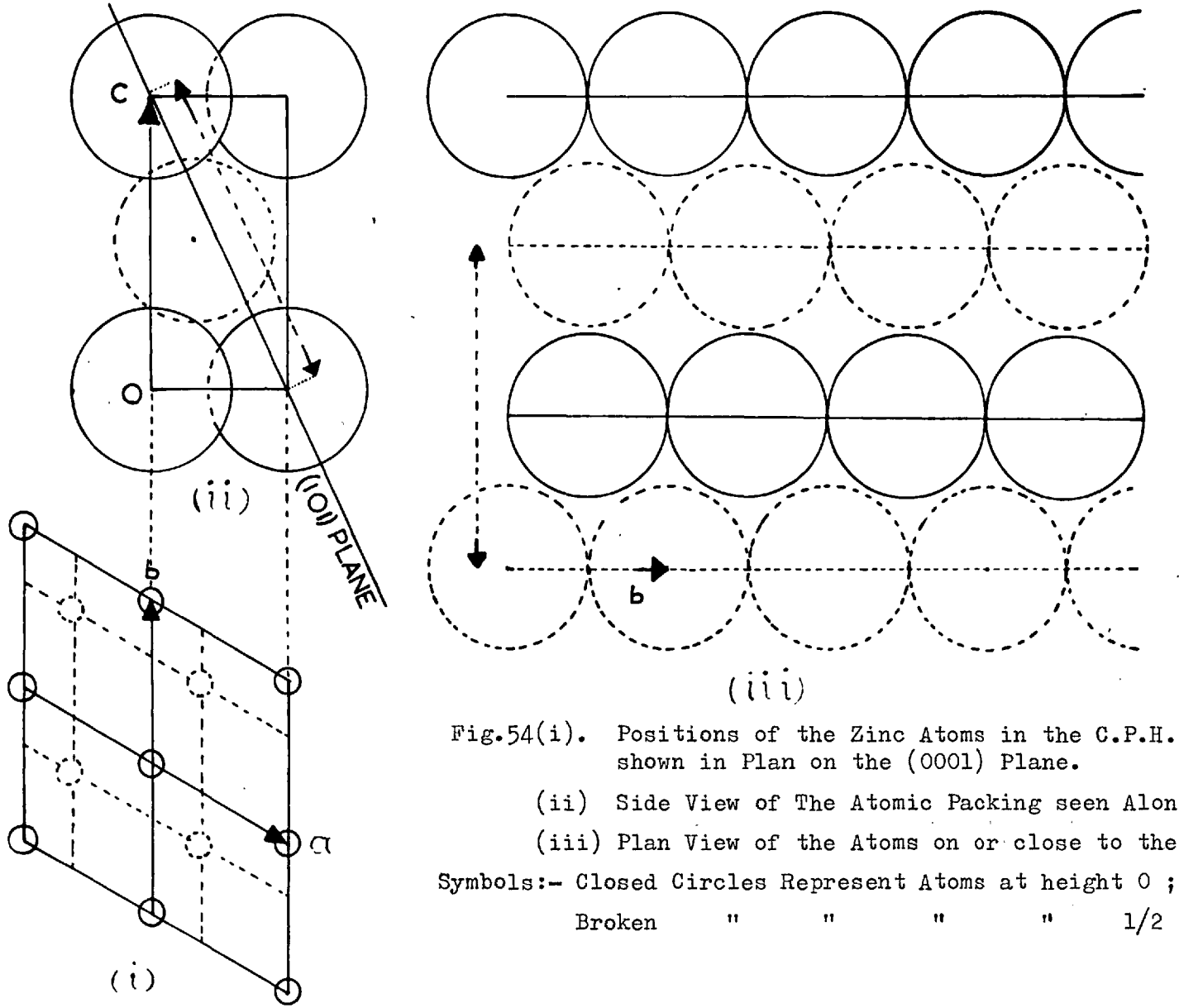

Fig.54(i). Positions of the Zinc Atoms in the C.P.H. Lattice shown in Plan on the (0001) Plane.

(ii) Side View of The Atomic Packing seen Along the b-Axis.

(iii) Plan View of the Atoms on or close to the (101) Plane.

Symbols:- Closed Circles Represent Atoms at height 0 ;

Broken " " " " 1/2 .

4.2a(iv). The Origin of the (112) Orientation.

At higher thicknesses, at 5 x10^{-3} torr, (112) orientation was most common. As the deposits grow more and more in thickness, the surface becomes atomically rough. Those faces which receive the metal atoms most (i.e. the crystals oriented with a face normal to the vapour or nearly so) will grow laterally more and more and these crystals will grow preferentially and predominate. The angle between the (101) and (112) planes being not too large the early (101) orientation may give place to (112)-oriented crystals due to the development of {112} faces. As the deposit becomes thicker the (112) orientation is eventually developed.

4.2a(v). Nature and Origin of the Surface Orientation on Thick Zn Deposits:

In the data of Figs. 42 and 46 for Zn condensed at initial air pressures of 2 x10^{-4} torr and 1 x10^{-5} torr respectively, it is seen that (101) orientation (or in Fig.42 mixed (101) + (112)) extends up to film thicknesses ~2000 - 2500 Å. At larger thicknesses (up to at least 8250 Å in Fig.42) the orientation of the Zn crystals on the surface region is modified towards but not yet as far as a preferred (001) orientation, evidently due to the {001} faces now predominating on the growing crystals. This is made clear from the nature of the orientation and from the

supporting evidence (3.4(b)) showing that at oblique vapour incidence the crystals develop with a common orientation axis which is practically along the direction of the vapour stream.

This development of {001} faces is presumably at a stage when the oxygen partial pressure has fallen to a very low value, so that there is negligible adsorption of oxygen on the growing crystal surfaces. It may be concluded that still thicker Zn deposits will increasingly approximate to (001) orientation, this axis tending to be directed along the incident vapour stream.

SECTION 5.

CONCLUSION.

The grazing incidence electron diffraction investigation of the surface structure of the thin deposits of gold, silver, copper, zinc and cadmium condensed in vacuum on inert substrates at room temperature revealed many new interesting results and confirmed some old ones.

It is established that the surface orientation is not only dependent on the film thickness, but it is also systematically dependent on the pressure of the residual air. For a f.c.c. metal deposit the thickness at which a transition to a different orientation occurs is maximum at a certain pressure of the residual air. This pressure is related to the chemical reactivity of the metal. The higher the chemical reactivity, the lower is the pressure at which the peak thickness occurs.

The sequence of orientations for Au, Ag and Cu deposits is the same throughout the range of pressures investigated. In the first stage, due to initial nucleation under conditions of low atomic mobility (i.e. at room temperature), they all show random orientation of the crystals but on increasing thickness, the surface region shows strong development of octahedral faces and a resulting preferred (111) orientation. The thickness at which this

orientation begins to set in is different for different metals depending upon their chemical reactivity with the residual air, as mentioned above. The other orientations, viz (110) and (211), follow from primary and secondary twinning of the crystals on the octahedral planes.

For the Zn and Cd deposits, even the crystal nuclei grow in preferred orientation on the substrate due to the very high atomic mobility of these metals on substrates at room temperature, and so there is no random orientation of the crystals even at the thinnest stage (~100 A).

At very high rate of deposition (~1000 A/sec), i.e. where the effect of the residual air is least, the Zn and Cd crystals are initially formed, at least in parts, with the most densely populated atomic planes in contact with the substrate. At lower rates, very thin deposits (~120 A) show mainly strong (101) orientation and refraction effect in the pattern indicate the presence of {101} boundary faces on the crystals parallel to the substrate. With increasing thickness, the surface regions of these deposits show new orientations (especially (112)) which evidently arise due to faces of other types becoming predominant on the surface of the growing crystals.

Very thick films (~6000 A) of Zn and Cd tend to show a preferred orientation with the [001] axis

approximately normal to the vapour stream, evidently due to {001} faces then predominating, the oxygen in the residual air by this time being gettered almost completely by the metal.

It is difficult to draw a unifying picture for all the metals giving the relationship between the structure of the deposit and the many variable parameters. The present work has provided some fundamental basis for future work on the effects of the residual air on the film structure. Further investigations are desirable, with other metals of different degrees of chemical reactivity with the residual air, or oxygen, nitrogen, etc., and deposited on inert and active substrates at room temperature and also at raised temperatures.

REFERENCES.

Acharya, H.K., 1948, Ph.D.Thesis, University of London.

Aminoff, G. and Broome, B., 1936, Nature, 137, 995.

Andrade, E.N.daC. and Martindale, J.G., 1936, Phil.Trans.Roy.Soc., 235, 69.

Baltz, A., 1963, J.Appl.Phys., 34, 1575.

Barker, T.V., 1908, Z.Krist., 45, 2.

Bannon, J. and Coogan, C.K., 1949, Nature, 163, 62.

Bassett, G.A., 1958, Phil.Mag., 3, 1042.

Bassett, G.A., Menter, J.W. and Pashley, D.W., 1959, "Structure and Properties of Thin Films", Proceedings of an International Conference held at Bolton Landing, New York . (John Wiley and Sons, Inc., N.Y.).

Bassett, G.A., 1961, Proc. of the European Regional Conf. on Electron Microscopy, Delft, Vol.I, 270.

Bauer, E., 1956, Z.Krist., 107, 72.

Bauer, E., 1961, Proc. Amer. Vac. Soc., Pergamon Press, N.Y., p.35.

Bauer, E., 1966, J.Appl.Phys., 37, 917(c).

Beeching, R., 1936, Phil.Mag., 22, 938.

Behrndt, K.H., 1961, Proc. Amer. Vac. Soc., Pergamon Press, p.912.

Bicknell, R.W., Joyce, B.A., Neare, J.H. and Smith, G.V., 1966, Phil.Mag., 14, 31.

Bruck, L., 1936, Ann.Phys., 26, 233.

Bryant, G.W., Hallett, J. and Mason, B.J., 1959, J.Phys. Chem. Solids, 12, (2), 189.

Buckel, W., 1959, "Structure and Properties of Thin Films" (cf. Bassett, Menter and Pashley, 1959).

Burton, W.K., Cabrera, N. and Frank, F.C., 1951, Phil.Trans.Roy.Soc., A243, 299.

Burgers, W.G. and Dippel, C.J., 1934, Physica, 1, 549.

Campbell, D.S., 1962, Trans.Nat. Vac. Symp. (Macmillan), p.29

Caswell, H.L., 1961, J.Appl.Phys., 32, 105 and 2641.

Cockcroft, J.D., 1928, Proc. Roy. Soc., A119, 293.

Cochrane, W., 1936, Proc. Phys. Soc. (London), 48, 723.

Chirigos, J.N., 1957, Ph.D.Thesis, Carnegie Institute of Technology, Pittsburgh.

Davey, J.E., 1961, J.Appl.Phys., 32, 877.

Drabble, J.D., 1949, Ph.D.Thesis, Univ. of London.

Dixit, K.R., 1933, Phil. Mag., 16, 1049.

Dutta, P.K., 1968, Ph.D.Thesis, Univ. of London.

Elleman, A.J. and Wilman, H., 1948, Proc.Phys.Soc., 61, 164.

Elleman, A.J. and Wilman, H., 1949, Proc.Phys.Soc., A62, 344

Evans, D.M., 1950, Ph.D.Thesis, Univ. of London.

Evans, D.M. and Wilman, H., 1952, Acta Cryst., 5, 731.

Evans, D.M. and Wilman, H., 1950. Proc.Phys.Soc., A63, 298.

Esterman, J., 1925, Z.Phys., 33, 320.

Finch, G.I. and Quarrell, A.G., 1933, Proc.Roy.Soc., A141, 398.

Finch, G.I. and Ikin, A.W., 1934, Proc.Roy.Soc., A145, 551.

Finch, G.I. and Wilman, H., 1936, Trans.Farad. Soc., 32, 1539.

Finch, G.I. and Wilman, H., 1936, Proc.Roy.Soc., A155, 345.

" " 1937, Ergebn. exakten Naturwiss, 16, 353.

Finch, G.I., 1937, Proc. Phys. Soc., 49, 113.

Finch, G.I. and Quarrell, A.G., 1934, Proc.Phys.Soc., London, 46, 148.

Frank, F.C. and Van der Merwe, J.H., 1949(a), Proc.Roy.Soc., London, A198, 205.

Frank, F.C. and Van der Merwe, J.H., 1949(b), Proc.Roy.Soc., London, A198, 216.

Frank, F.C. and Van der Merwe, J.H., 1949(c), Proc.Roy.Soc., London, A200, 125.

Fray, A.F. and Nielsen, S., 1961, Brit.J.Appl.Phys., 12, 603

Frenkel, J., 1924, Z.Phys., 26, 117.

Gottecke, H., 1956, Z.Naturforch., 11a, 55.

Goche, O. and Wilman, H., 1939, Proc.Phys.Soc., 51, 625.

Gen, M.I., Zelmanoff, I. and Schalkinoff, A.I., 1933, Phys. Zeits. Sowjet., 4, 825.

Geiling, S. and Ritcher, T., 1949, Acta Cryst., 2, 305.

Gunther, K.G., 1957, Z.Phys., 149, 538.

Hass, G., 1938, Ann. Phys., 31, 245.

Hass, G., 1942, Kolloidzehr., 100. 230.

Hayward, D.O. and Trapnell, B.M.W., 1964, "Chemisorption", (Butterworths, London).

Herbstein, F.H., 1957, Proc. Phys. Soc., B70, 251.

Holland, L., 1953, J.Opt.Soc. Amer., 43, 376.

Holland, L., 1958, "Vacuum Deposition of Thin Films", Chapman and Hall Ltd., London.

Hirth, J.P. and Pound, G.M., 1963, "Progress in Material Science", Pergamon Press.

Hunt, P.G., 1961, B.S.I.R.A. Res. Report.

Ino, S. and Ogawa, S., 1966, "Sixth Int. Congress for Electron Microscopy, Kyoto".

Ino, S. and Ogawa, S., 1967, J.Phys.Soc. Japan, 22, 1365.

Ino, S., 1966, J.Phys.Soc. Japan, 21, 346.

Kehoe, R.B., 1957, Phil. Mag., 2, 455.

Keith, H.D., 1956, Proc. Phys. Soc., B69, 180.

Kirchner, F. and Lassen, H., 1935, Ann. Phys., 24, 173.

Kirchner, F., 1932, Z. Phys., 76, 576.

Knudsen, M., 1907, Ann. Phys., Leipzig, 28, 999.

Konozenke, I.D., 1954, Uspekhi. Fiz. Nauk, 52, 561.

Lassen, H., 1934, Z. Phys., 35, 172.

Langmuir, I., 1917, Proc. Nat. Acad. Sci. Wash., 3, 141.

Levinstein, H., 1949, J.Appl. Phys., 20, 306.

Matthews, H.I. and Wronski, K.R., 1962, 5th Int. Conf. Electron Microscopy, Philadelphia, Academic Press, New York.

Matthews, J.W., 1959, Phil. Mag., 4, 1017.

Matthews, J.W., 1961, Phil. Mag., 6, 1347.

Matthews, J.W., 1962, Phil. Mag., 7, 915.

Matthews, J.W., 1965, Phil. Mag., 12, 1143.

Matthews, J.W., 1966, J.Vac.Sc. and Tech., 3, 133.

Matthews, J.W., 1967, "Physics of Thin Films", Vol. 4, Academic Press, New York and London.

Mayer, H., 1955, "Physik dunner Schichten", Vol.II, Stuttgart.

Mayer, H. and Gohre, H., 1963, Z. Physik.,

Melmed, A.J., 1965, J.Appl.Phys., 36, 3585.

McGee, J.D. and Lubszynski, H.G., 1939, J.I.E.E., 84, 468.

Moazed, K.L. and Pound, G.M., 1960, Thesis, Carnegie Inst. of Technology.

Murbach, H.P. and Wilman, H., 1953, Proc. Phys. Soc., B66, 905.

Murr, L.E. and Inman, M.C., 1966, Phil. Mag., 14, 135.

Mugge, O., 1903, Jahrbuch Mineralogie Beil. Bd., 16, 335.

Nelson, H.R., 1937, J. Chem. Phys., 5, 252.

Newman, R.C., 1957, Phil. Mag., 2, 750.

Newman, R.C. and Pashley, D.W., 1955, Phil. Mag., 46, 927.

Nolder, R. and Cadoff, J., 1965, Trans.A.I.M.E., 233, 549.

Ogawa, S., Ino, S., Kato, T. and Ota, H., 1966, J.Phys.Soc. Japan, 21, 1963.

Palatnik, L.S. and Komnik , Y.F., 1959, Soviet Phys.Doklady, 4, 196.

Palatnik, L.S. and Fedorenko, A.S., 1967, Fiz.Metallvedanik (USSR), 22

Pashley, D.W., 1956, Advanc. Phys., 5, 173.

Pashley, D.W., 1959, Phil. Mag., 4, 316 and 324.

Pashley, D.W., Stowell, M.J., Jacobs, M.H. and Law, T.J., 1964, Phil. Mag., 10, 127.

Pashley, D.W. and Stowell, M.J., 1966, J.Vac.Sc. & Tech., 3, 156.

Pashley, D.W. and Stowell, M.J., 1962, Proc. of the 5th Int. Congr. for Electron Microscopy, Philadelphia, edited by S.S.Breese (Academic Press, London and New York).

Preece, J.B., 1966, Ph.D. Thesis, Univ. of London.

Preece, J.B., Wilman, H. and Stoddart, C.T.H., 1967, Phil. Mag., 16, 447.

Preece, J.B. and Wilman, H., 1968, "Contribution to Symposium on Crystal Growth", 7th International Congr. of Crystallography, Moscow, July,1966.

Poppa, H., 1965, J.Vac. Sc. and Tech., 2, 42.

Ptushinskii, I.G., 1958, Zhur. Tech. Fiz., 28, 1402.

Picard, R.G. and Duffendack, O.S., 1943, J.Appl. Phys., 14, 291.

Pound, G.M., Simnad, M.T. and Yang, L., 1954, J.Chem.Phys., 22, 1215.

Quarrell, A.G., 1937, Proc. Phys. Soc., 49, 279.

Ramos, F., 1961, D.I.C. Thesis, Imperial College, London.

Ramos, F. and Wilman, H., 1962, An. Real Soc. Espan. Fis. Quim., 58, 51.

Royer, L., 1928, Bull. Soc. Franc. Mineral., 51, 7.

Royer, L., 1936, Compt. Rend., 202, 1687.

Rozenberg, G.V., 1952, Uspekhi Fiz. Nauk., 47, 3.

Rozenberg, G.V., 1958, "Optics of Thin Films" (in Russian).

Rudiger, O., 1937, Ann. Physik, 30, 505.

Sancho, J., Ramos, F. and Bru, L., 1966, An. Real Soc. Espan. Fis. Quim., A62, 363.

Saikia, B.N., 1961, Ph.D. Thesis, Univ. of London.

Sachtler, W.M.H., 1954, J. Chem. Phys., 51, 491.

Seifert, H., 1937, Fortsch. Mineral., 22, 185.

Seifert, H., 1935, Fortsch. Mineral., 13, 102.

Seifert, H., 1953, "Structure and Properties of Solid Surfaces", edited by R.Gomer and C.S.Smith (Chicago), p. 340.

Schulz, L.G., 1949, J.Chem. Phys., 17, 1153.

Schulz, L.G., 1952, Acta Cryst., 5, 130.

Semenoff, M.N. and Chariton, J.B., 1924, Z. Phys., 25, 287.

Semenoff, M.N., 1930, Zhur. Russ. Fiz. Khim. Obshchestra, 62, 33.

Sella, C., Conjeaud, P. and Trillat, J.J., 1959, Comptes Rendus Acad. Sci. (Paris), 249, 1987.

Sella, C., Conjeaud, P. and Trillat, J.J., 1958, Int. Congress of Electron Microscopy, Berlin, (Sept. 1958), Communication No. 12-02.

Sennett, R.S. and Scott, G.D., 1950, J.Opt.Soc.Amer., 40, 203.

Sennett, R.S., MacLauchlan, T.A. and Scott, G.D., 1952, Canadian J. Phys., 30, 370.

Shirai, S., 1943(a), Proc. Phys-Maths. Soc. Japan, 25, 163.

Shirai, S., 1943(b), Proc. Phys-Maths, Soc. Japan, 25, 633.

Sloope, B.W. and Tiller, C.O., 1961, J.Appl.Phys., 32, 1331.

Sloope, B.W. and Tiller, C.O., 1962, J.Appl.Phys., 33, 3458.

Smollett, M. and Blackman, M., 1951, Proc. Phys. Soc., A64, 683.

Stahl, H.A., 1949, J. Appl. Phys., 20, 1.

Stranski, J.N., 1949, Disc. Faraday Soc., No.5, 13.

Thomson, G.P., 1927, Nature, 120, 802.

Thomson, G.P., 1948, Proc. Phys. Soc., 61, 403.

Thun, R.E., 1963, "Physics of Thin Films", Vol.I, Academic Press, p.216.

Turnbull, D. and Vannegut, B., 1952, Ind. Eng. Chem., 44, 1292.

Umanskii, M.M. and Krylov, V.A., 1936, Zhur. eksptl. teoret. Fiz., 6, 691.

Van der Merwe, J.H., 1949, Disc. Faraday Soc., 5, 201.

Via, G.G. and Thun, R.E., 1961, Proc. Amer. Vac. Soc., Pergamon Press, p.250.

Vook, R.W., 1961, J. Appl. Phys., 32, 1557.

Volmer, H., 1921, Z. Phys., 5, 188.

Walton, D., 1962, Phil. Mag., 7, 1671.

Was, D.A., 1939, Physica, 6, 390.

Weaver, C., 1960, Proc. Roy. Soc., A254, 1631.

Wilman, H., 1940, Proc. Phys. Soc., 52, 323.

Wilman, H., 1948(a), Proc. Phys. Soc., 60, 341.

Wilman, H., 1948(b), Proc. Phys. Soc., 61, 416.

Wilman, H., 1949, Research (London), 2, 352.

Wilman, H., 1950, Nature, 165, 321.

Wilman, H., 1951, Proc. Phys. Soc., A64, 329.

Wilman, H., 1952, Acta Cryst., 5, 782.

Wilman, H., 1955, Proc. Phys. Soc., B68, 474.

Willems, J., 1943, Naturwissen, 31, 232.

Willems, J., 1944, Naturwissen, 32, 324.

Willems, J., 1948, Naturwissen, 38, 211.

Wood, R.W., 1916, Phil. Mag., 32, 365.

Yang, L., Birchenall, G.E., Pound, G.M. and Simnad, M.T., 1954, Acta Met., 2, 463.

Zehender, E., 1950, Optik, 7, 200.